Class VI Injection Well Application

Contains proprietary business information.

Attachment 01: Narrative

40 CFR §146.82(A)

Maple Project
Putnam County, Ohio

16 January 2026

Table of Contents

List of Figures

List of Tables

List of Acronyms and Abbreviations

1D	one-dimensional
2D	two-dimensional
3D	three-dimensional
13Cr	13-Chrome
13Cr80	13-Chrome, minimum yield strength of 80,000 pounds per square inch
25Cr	25-Chrome
25Cr125	25-Chrome, minimum yield strength of 125,000 pounds per square inch
ACZ	above confining zone
AMPP	Association for Materials Protection and Performance
AoR	Area of Review
APT	annulus pressure test
BHP	bottomhole pressure
BS	bow spring
BTC	buttress thread casing
CAA	Clean Air Act
CCS	carbon capture and sequestration
CCS1	Archer Daniels Midland Company Injection Well #1 drilled for the IBDP
CFR	Code of Federal Regulations
CO_2	carbon dioxide
CWA	Clean Water Act
DOE	Department of Energy
ECRS	Eastern Continental Rift Basin
EGRP	Eastern Granite-Rhyolite Province
EPA	Environmental Protection Agency
EPSG	European Petroleum Survey Group
ERRP	Emergency and Remedial Response Plan
EUE	external upset end
fbgl	feet below ground level
fbsl	feet below sea level
FEMA	Federal Emergency Management Agency
FWR	Fort Wayne Rift
GSDT	Geologic Sequestration Data Tool
h	Thickness
HCl	hydrochloric
IBDP	Illinois Basin–Decatur Project
k	permeability
ktpa	kilotonnes per annum
ksi	kilopounds per square inch
LAS	log ascii standard
LTC	long thread coupling
MAIP	maximum allowable injection pressure
mD	millidarcy
MD	measured depth

MEM	mechanical earth model
MPL ACZ1	Maple Above Confining Zone Monitoring Well 1
MPL INJ1	Maple Injection Well 1
MPL OBS1	Maple Deep Observation Well 1
MPL USDW1	Maple USDW Monitoring Well 1
mg/L	milligrams per liter
Mt	million tonnes
N/A	not applicable
NAD	North American Datum
NOV	National Oilwell Varco
NPDES	National Pollution Discharge Elimination System
NRI	Nationwide Rivers Inventory
O&G	oil and gas
ODNR	Ohio Department of Natural Resources
PBI	proprietary business information
pH	acidity or alkalinity measurement
PISC	post-injection site care
PNL	pulsed neutron logging
psi	pound-force per square inch
SHPO	State Historic Preservation Office
STC	short thread coupling
SU	standard units
T&E	threatened or endangered
TBD	to be determined
TCS	total closure stress
TDS	total dissolved solids
TWT	two-way-time
UIC	Underground Injection Control
US	United States
USDW	underground source of drinking water
USFWS	United States Fish and Wildlife Service
USGS	United States Geological Survey
UTM	Universal Transverse Mercator
XRD	x-ray diffraction

1. Project Contact Information, Location, and Background [40 CFR §146.82(a)(1)]

1.1. Project Contact Information

Project Name: Maple

Project Operator: Vault GSL CCS LP

Project Contact: Mark Piercey, Project Manager
Vault GSL CCS LP
1125-17th Street, Suite 1275
Denver, Colorado 80202
Email: maple@vault4401.com
Phone: 713-930-4401

Claimed as PBI

1.2. Project Background

The objective of the Maple Project is to effectively capture carbon dioxide (CO_2) produced at a nearby ethanol facility, and safely and permanently sequester approximately 4.3 million tonnes (Mt) of CO_2 over 12 years in the Mt. Simon Sandstone. One well is expected to be sufficient for injection of the project's intended mass flow rate of 359 kilotonnes per annum (ktpa) of CO_2 into the Mt. Simon Sandstone. This Underground Injection Control (UIC) Class VI application describes and supports this effort in accordance with the United States (US) Environmental Protection Agency's (EPA's) Class VI regulations in Title 40 of the Code of Federal Regulations (40 CFR §146.81).

Vault GSL CCS LP will be the owner, operator, and permit holder for the injection well MPL INJ1 and the transport pipeline. A stratigraphic well (Maple / INJ1, API #: 34-137-2-0064-00-00) will be drilled under an Ohio Department of Natural Resources (ODNR) Division of Oil and Gas Resources Management Permit to Drill a Stratigraphic Well. This stratigraphic well is intended to be used as the Maple Injection Well 1 (MPL INJ1) upon the final Class VI authorization to inject and will be constructed to meet Class VI specifications (40 CFR §146.86). Neither an injection depth waiver nor an aquifer exemption is being requested for this project.

The injection zone, which comprises the Mt. Simon Sandstone and the Rome Silt, is of sufficient depth and temperature at the site to maintain the injected CO_2 in a supercritical state. The Mt. Simon Sandstone has served as a suitable injection interval for Class I, II and VI wells in the region for multiple decades. The Rome Formation and Conasauga Formation together form the

primary confining zone. Other strata including the Glenwood Shale, the Utica Shale, and the Queenston Formation/Maquoketa Group will serve as additional confining layers between the primary confining zone and the lowermost USDW.

Figure 1 and Figure 2 show the locations of the four primary wells associated with the project: Maple Deep Observation Well 1 (MPL OBS1), Maple USDW Monitoring Well 1 (MPL USDW1), Maple Above Confining Zone Monitoring Well 1 (MPL ACZ1), and Maple Injection Well 1 (MPL INJ1). Table 1 shows the coordinates and depth for each well.

Within the Area of Review (AoR) there are currently no deep stratigraphic boreholes, State or Federal EPA approved subsurface clean-up sites, mines, quarries, State, Tribal, or Territory boundaries. Surface bodies of water within the AoR include Brush Creek, Little Yellow Creek, Hammer Creek, unnamed intermittent canals and ditches, small unnamed ponds, and several unnamed wetlands (Attachment 09: Emergency and Remedial Response Plan, 2025). The state-permitted stratigraphic well (Maple / INJ1), which the applicant intends to use as the injection well (MPL INJ1) upon the final Class VI authorization to inject, will be drilled, as permitted by the state, prior to issuance of the draft Class VI permit, and will be constructed to meet Class VI specifications (40 CFR §146.86). Information on oil and gas wells (O&G) and water wells within the AoR can be found in Section 4.1 *Tabulation of Wells Within the AoR* of Attachment 02: AoR and Corrective Action Plan (2025).

The state-permitted stratigraphic well (Maple / INJ1) will be the first project-related well drilled and will be used to collect site-specific data consistent with the specifications of 40 CFR §146.86 and §146.87 (Attachment 05: Pre-operational Testing Program, 2025). Subsequent project wells, including MPL OBS1, MPL ACZ1, and MPL USDW1, will collect additional site-specific data for the project (Attachment 05: Pre-operational Testing Program, 2025). The data gathered will be processed and analyzed to confirm or re-assess the project modeling efforts and current understanding.

Claimed as PBI


Claimed as PBI

1.3. Local, State, and Federal Emergency Contacts [40 CFR §146.82(a)(20)]

Table 2 provides emergency contact information in the event of an emergency at the project site.

Table 2: Local, state, and federal emergency contacts

Agency	Phone Number
Emergency Dispatch – Police, Fire, or Medical Emergency	911
Leipsic Fire Department	419-943-2009
Putnam County Sheriff's Office	419-523-3208
Putnam County Office of Public Safety (Emergency Management Agency / Emergency Medical Services)	419-538-7315
Ohio State Highway Patrol – Lima Patrol Post	419-228-7072
Environmental services contractor to be determined (TBD)	TBD
US EPA Region 5 UIC Program Director	312-353-7648 (UIC Region 5 Director)
US EPA Region 5 UIC Class VI Wells/Carbon Sequestration	312-353-3944 (Class VI UIC Wells/Carbon Sequestration)
EPA National Response Center (24 hours)	800-424-8802
Ohio Environmental Protection Agency	800-282-9378 (Emergency Spill Hotline)
ODNR Division of O&G Resources	844-642-2551 (Emergency Response)

1.4. Summary of Other Permits Required

Maple Project activities associated with development of the Class VI injection well include construction of well pads, access roads, and site infrastructure. Table 3 provides a summary of federal permits, under programs listed in 40 CFR §144.31(e)(6), and their applicability for the Maple Project. Except for this Class VI application, no other permits or construction approvals have been applied for or received.

Table 3: Federal permit applicability under 40 CFR §144.31(e)(6) listed programs for the Maple Project.

Program	Activity	Permit(s) Required
Hazardous Waste Management program under Resource Conservation and Recovery Act (RCRA)	CO_2 injection	Not applicable (N/A), injected CO_2 is a non-hazardous waste under 40 CFR §261.4(h).
UIC program under Safe Drinking Water Act (SDWA)	CO_2 injection	Class VI UIC permit.
National Pollutant Discharge Elimination System (NPDES) program under Clean Water Act (CWA)	Well pad construction Access road construction	Coverage under Construction Site Stormwater - General Permit NPDES program administered by the state of Ohio.
Prevention of Significant Deterioration (PSD) program under Clean Air Act (CAA)	CO_2 injection	N/A, CO_2 injection facility is not a major source, as defined in the CAA. CCS is considered a "best available control" technology for major sources.
Nonattainment program under CAA	CO_2 injection	N/A, Putnam County is currently in attainment for all criteria pollutants.
National Emission Standards for Hazardous Air Pollutants (NESHAP) pre-construction approval under the CAA	CO_2 injection	N/A, CO_2 injection is not considered a NESHAP source of hazardous air pollutants (HAPs).
Ocean dumping permits under Marine Protection Research and Sanctuaries Act	Well pad construction Access road construction	N/A, onshore project with no proposed ocean dumping.
Section 404 of CWA	Well pad construction Access road construction	N/A, construction activities are planned outside of waters of the U.S. No dredge or fill material into waters of the U.S. is anticipated.
State or Other relevant environmental permits 40 CFR §144.31 (e)(6)(ix)		
Ohio Environmental Protection Agency Stormwater Program	Well pad construction Access road construction	Coverage under Construction Site Stormwater - General Permit, administered by Ohio EPA.
ODNR Division of Oil and Gas Resources Management	Drilling of stratigraphic well (Maple / INJ1)	Permit to Drill a Stratigraphic Well (API #: 34-137-2-0064-00-00)

1.5. Landowners Within the AoR

A list of names and addresses of all owners of record of land within the AoR of the Maple Project can be found in PBI Appendix 1A – List of Landowners Within the AoR.

2. Site Characterization [49 CFR §126.82(a)(2), (3), (5) and (6)]

Unless otherwise stated, all depths are in reference to feet below ground level (fbgl).

2.1. Regional Geology, Hydrogeology, and Local Structural Geology [40 CFR §146.82(a)(3)(vi)]

The Maple Project site is in northeastern Putnam County, Ohio, U.S.A and is located within the Arches Province (Figure 3). This region has a basement primarily composed of crystalline Precambrian rocks that are unconformably overlain by Paleozoic sedimentary rocks (Figure 4). These Paleozoic strata overlay three broad Precambrian arches, which are the Findlay, Kankakee, and Cincinnati, that divide the Michigan, Appalachian, and Illinois Paleozoic basins (Figure 3 and Figure 4). The project site is on the west limb of the Findlay Arch and has approximately 3,000 feet of Cambrian through Silurian strata (Figure 4).

The Cambrian Mt. Simon Sandstone and the Arches Province have been the focus of research into geological carbon sequestration due to the intersection of reservoir thickness, permeability, and depth. Previously conducted computational modeling of the Mt. Simon Sandstone in the Arches Province concluded that large-scale injection into the Mt. Simon Sandstone reservoir may be achieved in the region (Sminchak, 2012). The Mt. Simon Sandstone has served as a suitable injection interval in the province for Class I wells in the region for decades (INEOS Nitriles, 2016; Vickery Environmental Inc., 2020). In the adjacent Illinois Basin, the Mt. Simon Sandstone has been investigated and used for carbon sequestration for over two decades through the Midwest Regional Carbon Sequestration Partnership's Illinois Basin–Decatur Project (IBDP) (Wickstrom et al., 2005; Greenberg, 2021), CarbonSAFE programs (Leetaru et al., 2019; Korose, 2022; Whittaker, 2022; Whittaker and Carman, 2022), and the commercial Illinois Industrial Carbon Capture and Storage Project at Decatur Illinois (Gollakota and McDonald, 2014).

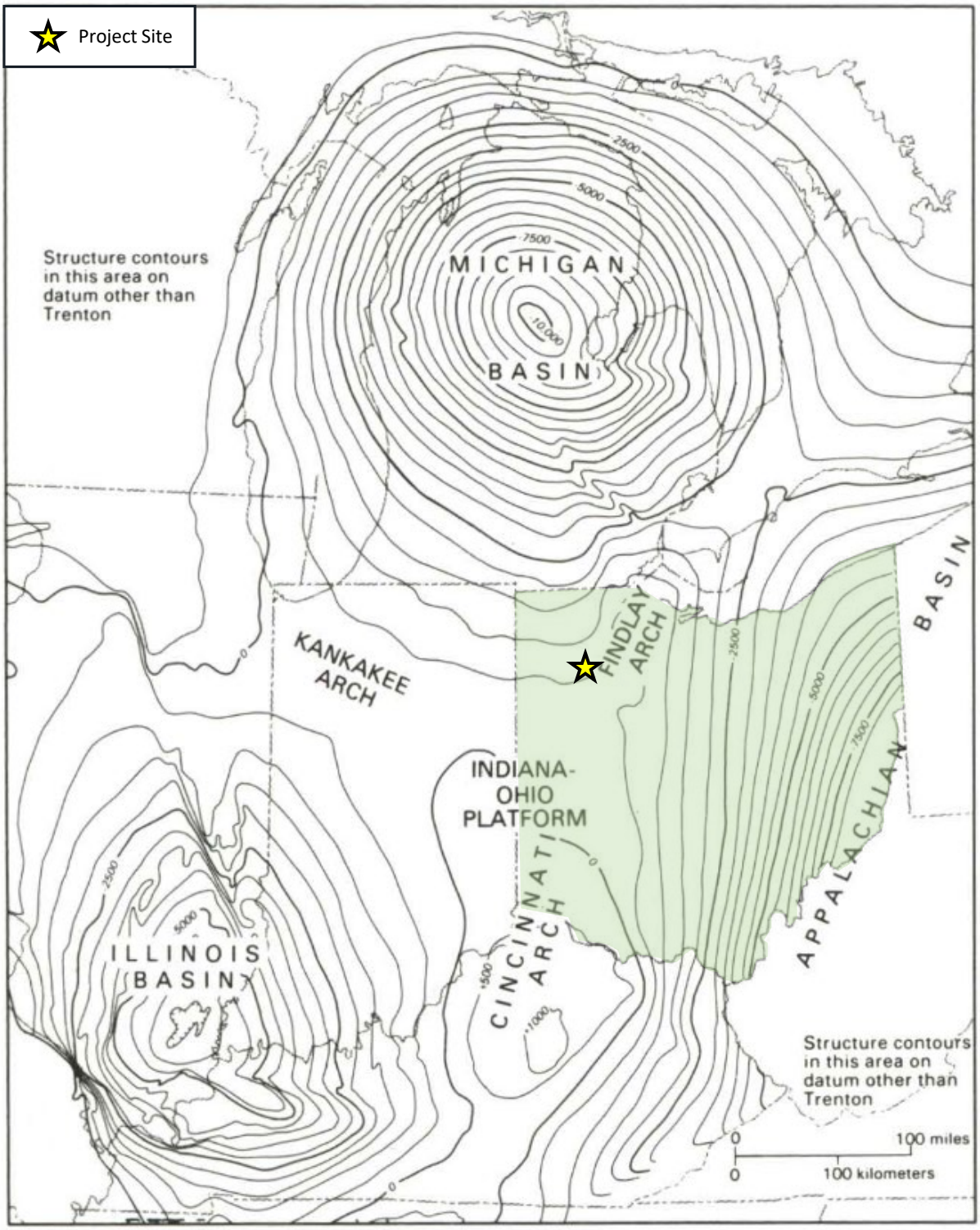

Figure 3: Regional structural contour map (top of Trenton Limestone) showing the location of the Arches Province, the arches within the province, and surrounding sedimentary basins. The state of Ohio is shaded green, and the Maple Project site is a yellow star. Modified from Wickstrom et al. (1992).

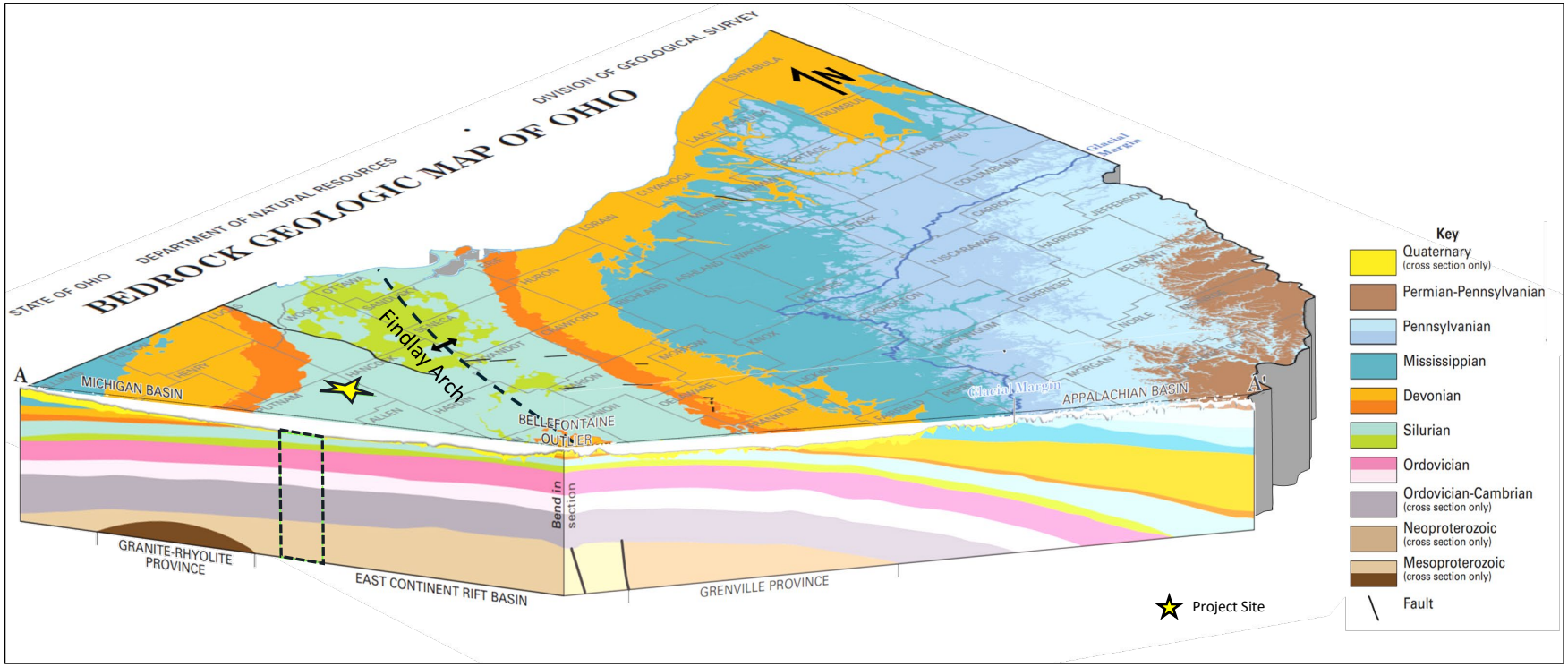

Figure 4: Vertical section through bedrock geology of Ohio showing broad nature of Findlay Arch, and the structural position of Maple Project site on the west limb of the arch. The approximate surface location of Maple Project site (yellow star) and underlying geology (black dashed rectangle) are shown. Modified from the Ohio Department of Natural Resources (2006).

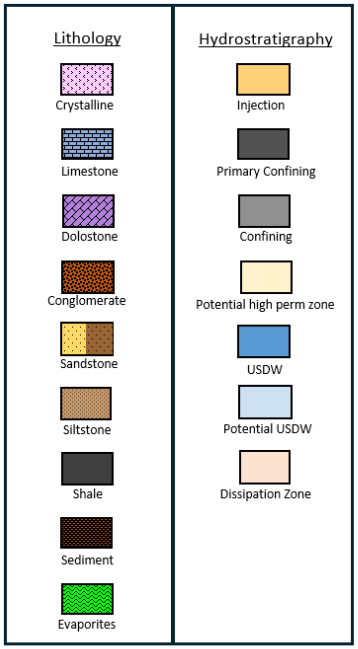

Age	Group	Nomenclature	Lithology	Hydrostratigraphy	~ Depth at Project Site (fbgl)
Quaternary		Undifferentiated		USDW	~60
Silurian	Salina	Salina		USDW	493
	Lockport	Lockport Dolomite		Lowermost USDW	632
	Clinton Group	Dayton/Packer Shell/Rochester Shale			
	Medina	Clinton Formation/Cabot Head Shale			
Ordovician	Queenston	Queenston/Maquoketa			
		Utica Shale			
	Galena	Trenton Limestone			
	Black River	Black River			
		Gull River			
	Wells Creek	Glenwood Shale			
	Knox	Knox Dolomite/ Copper Ridge Dolomite/Trempealeau			2,499
Cambrian	Potsdam	Kerbel		ACZ Monitoring	2,549
		Conasauga		Primary Confining	
		Rome			2,811
		Rome Silt		Injection	
		Mt. Simon Sandstone			3,044
Precambrian		Precambrian			

Figure 5: Maple Project site-specific stratigraphic column with age, nomenclature, generalized lithology, and formation depths at the injection well.

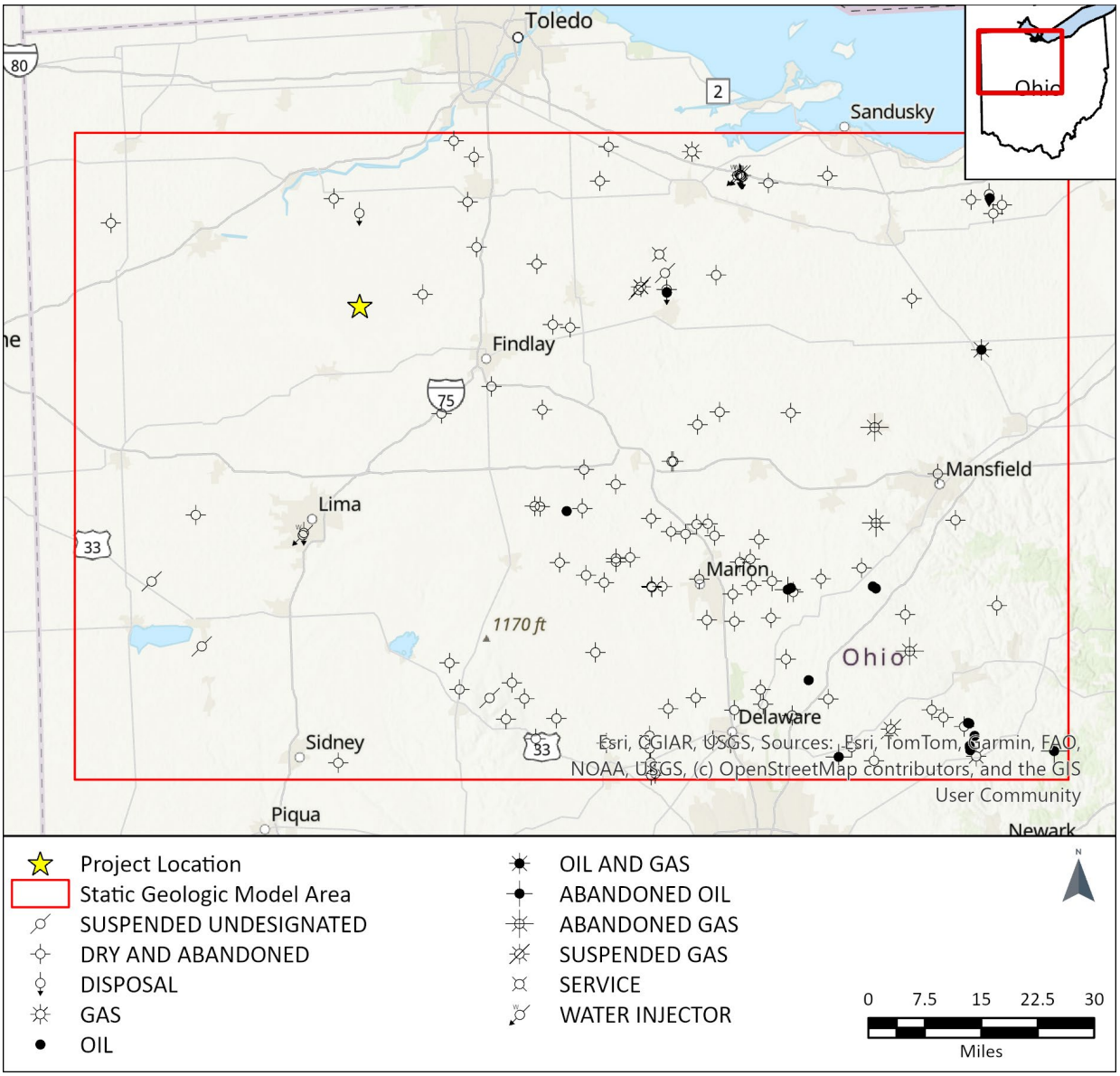

Figure 6 Map shows the wells that were used to develop the static geologic model.


Claimed as PBI

Eustatic sea level fluctuations coupled with tectonics allowed for the accumulation of both marine and terrestrial sediments in the Arches Province and surrounding basins. At the project site, the Precambrian Basement is composed of crystalline rocks of varying origins and ages. The thickness and depth of the Paleozoic strata in the Ohio portion of the Arches Province are relatively shallow and thin (less than 4,000 feet) compared the thickness of strata in the surrounding sedimentary basins (Baranoski, 2002). In contrast, up to 18,000 feet of Paleozoic strata accumulated in the Reelfoot Rift and Rough Creek Graben, which are significant features within the southern portion of the Illinois Basin related to processes linked to subsidence (Kolata and Nimz, 2010). In portions of western Ohio, clastics of the Neoproterozoic Middle Run Formation were deposited on the crystalline basement and are unconformably overlain by the Cambrian Mt. Simon Sandstone (Drahovzal et al., 1992). However, it is uncertain whether the Middle Run Formation will be found at the project site.

The Cambrian Mt. Simon Sandstone, Rome Formation, and Conasauga Formation are among the oldest and deepest Paleozoic strata in Ohio (Figure 5). The Mt. Simon Sandstone and Rome Silt will serve as the injection zone, and the Rome Formation and Conasauga Formation will be the primary confining zone for the Maple Project. These sediments were deposited in a near shore environment fed by drainage systems that transgressed to a shallow shelf/pro-delta depositional environment (Freeman, 1953; Janssens, 1973; Green, 2018).

By late Cambrian, much of Ohio was covered by a shallow sea. This sea regressed in the Ordovician due to both eustatic and tectonic forces, which resulted in the Knox Unconformity (Figure 5; Janssens, 1973). The Arches Province was near the wave-base in the Middle Silurian and much of the sediment deposition during this time was diverted to the surrounding basins. During the Devonian, the sea regressed, and uplift occurred due to the Acadian Orogeny, which allowed for non-deposition and erosion along the arches. Following this, sea level transgressed into parts of Ohio during the Devonian-Mississippian, depositing marine sediments. Ohio was a low-relief coastal plain swamp in the Pennsylvanian and was filled with deltaic sediments related to the Alleghenian Orogeny during the Permian. This uplift during the late Paleozoic to early Mesozoic further separated the surrounding sedimentary basins from the Arches Province and eroded previously deposited sediment (Ohio Division of Geological Survey, 2014).

Erosion and/or nondeposition prevailed along the arches throughout the Mesozoic and Cenozoic. During the Pleistocene Epoch, the region was covered by continental ice sheets that deposited hundreds of feet of glacial sediment in the region, some of which now serve as shallow groundwater aquifers (Ohio Division of Geological Survey, 2014).

2.2. Regional Stratigraphy

Figure 5 is a site-specific stratigraphic column for the Maple Project and will be referred to throughout this Narrative.

To develop a comprehensive understanding of the site-specific geology for this project, a database of publicly available geophysical well logs from Ohio and Indiana was compiled. The well logs were interpreted and used to develop a static model for the project site. The wells that were used to construct the static model are presented in Appendix 1B – *Wells used for Geologic Evaluation* and shown in Figure 6.

Geophysical logs from regional wells were used to construct the static model (Figure 7, Figure 8, and Figure 9). The regional continuity of the Paleozoic strata in the vicinity of the project site [40 CFR §146.82(a)(3)(i)] is demonstrated through cross sections of the site model (Figure 7 and Figure 9). Quaternary glacial sediments overlie the bedrock (Figure 5) and are discussed further in Section 2.9. *Hydrologic and Hydrogeologic Information.*

Within 50 miles of the Maple Project, 56 wells penetrate the Precambrian Basement, and 73 wells penetrate the Mt. Simon Sandstone. Area wells were used to assess the site-specific geology. The Ohio Liquids Disposal well (UWI 34143202370000) is located approximately 54 miles northeast of the project site and is part of a field that contains nine Mt. Simon Sandstone Class I injection wells, some of which have been plugged and abandoned (Figure 8). These wells penetrate the Precambrian Basement and use the Mt. Simon Sandstone as an injection zone. The Rome Formation and the Conasauga Formation are the primary confining zone, and the Kerbel Formation is a monitoring zone (Vickery Environmental Inc., 2020). This site will be discussed more in Section 2.6.2. *Mineralogy, Diagenesis, Porosity, and Permeability*. Approximately 30 miles south in Lima, Ohio, the BP Chemical 2 Class I injection well (UWI 34003200670000) is part of a field that also utilizes the Mt. Simon Sandstone for wastewater storage. The wells in this field penetrate through the entire Mt. Simon Sandstone into the Precambrian Middle Run Formation (Figure 8). It is uncertain whether the Middle Run Formation will be present at the Maple Project site.

Figure 9 shows the closest wells to the Maple Project that penetrate the Mt. Simon Sandstone. The Barlage Louis well (UWI 34137200310000) is approximately seven miles southwest of the site and does not have geophysical logs. The Knox High well (UWI 34063203600000) is approximately nine miles east-northeast of the project site, but it does not penetrate the Precambrian Basement. The Shidler James 2 well (UWI 34069201390000) is approximately 13 miles north of the Maple Project site and is the closest well with geophysical logs to penetrate the entire thickness of the Mt. Simon Sandstone. (Figure 9).


Claimed as PBI


Claimed as PBI

2.2.1. Precambrian Basement Complex

In western Ohio, the Precambrian Basement is divided into three provinces: 1) the Eastern Granite-Rhyolite Province (EGRP), 2) the East Continent Rift System (ECRS), and 3) the Grenville Province (Figure 10). The precise boundary among these provinces is difficult to determine (Baranoski et al., 2009). The EGRP is a large Precambrian autochthonous terrain composed of primarily unmetamorphosed igneous and felsic volcanic rocks (Figure 10; Denison et al., 1984; Wickstrom et al., 1992). It is likely the oldest of the Precambrian provinces in the project region with the ECRS faulting through and the Grenville thrusting over the EGRP rocks.

The ECRS is a mid-Proterozoic rift system that cross-cuts and is partially overlying the EGRP, and the Fort Wayne Rift (FWR) is a part of this rift system. A boundary between the EGRP and the ECRS exists west of the project site (Figure 10; Baranoski et al., 2002). In the Arches Province, the ECRS contains intrabasinal volcanic rocks and sandstones of the Neoproterozoic Middle Run Formation.

The Middle Run Formation was first recognized in the ODNR Division of Geological Survey #2627 core located in Warren County approximately 111 miles south of the project (Figure 11). Sediments of the Middle Run Formation were deposited in the ECRS, and seismic, magnetic, and gravity data suggest a genetic relationship between the ECRS, the FWR, and flanking clastic rift basins that contain the Middle Run Formation (Figure 10; Dickas et al., 1992; Drahovzal et al., 1992; Baranoski et al., 2009). The Middle Run Formation has been identified in portions of Ohio, Kentucky, and Indiana, and it may be present at the Maple Project site (Drahovzal et al., 1992). Specific to the Maple Project, the FWR is located to the west of the site (Figure 10), though the exact boundary is unknown, and is discussed in more detail in Section 2.3. *Regional Structure*.

The Grenville Province in the region is an allochthonous terrain composed of metamorphic rocks intruded by igneous rocks (Figure 10). These rocks have been thrust over the existing terrains to the (present-day) west during the Proterozoic Grenville Orogeny when Laurentia collided with other continents and created the supercontinent Rodinia (Baranoski et al., 2009). The Grenville Province extends across eastern Canada, the eastern United States and into Central America and contributed to the source of Early Cambrian siliciclastic strata in the Arches Province and Appalachian Basin (Bickford et al., 1986).

The Grenville Front is a geomagnetic anomaly approximately 15 miles east of the project site and is used as the boundary between the Grenville Province and the Precambrian provinces to the west (Figure 10). The anomaly is correlated to the erosional edge of the Grenville Province rocks that were thrust over older Precambrian rocks during the Grenville Orogeny (Bickford et al., 1986; Drahovzal et al., 1992; Atekwana, 1996; Lidiak, 1996; Baranoski et al., 2009; Green, 2018). The Grenville Front will be discussed in more detail in Section 2.3. *Regional Structure*.

The Precambrian Basement underlying the project site is located where the ECRS and Grenville Province meet (Figure 10).


Claimed as PBI

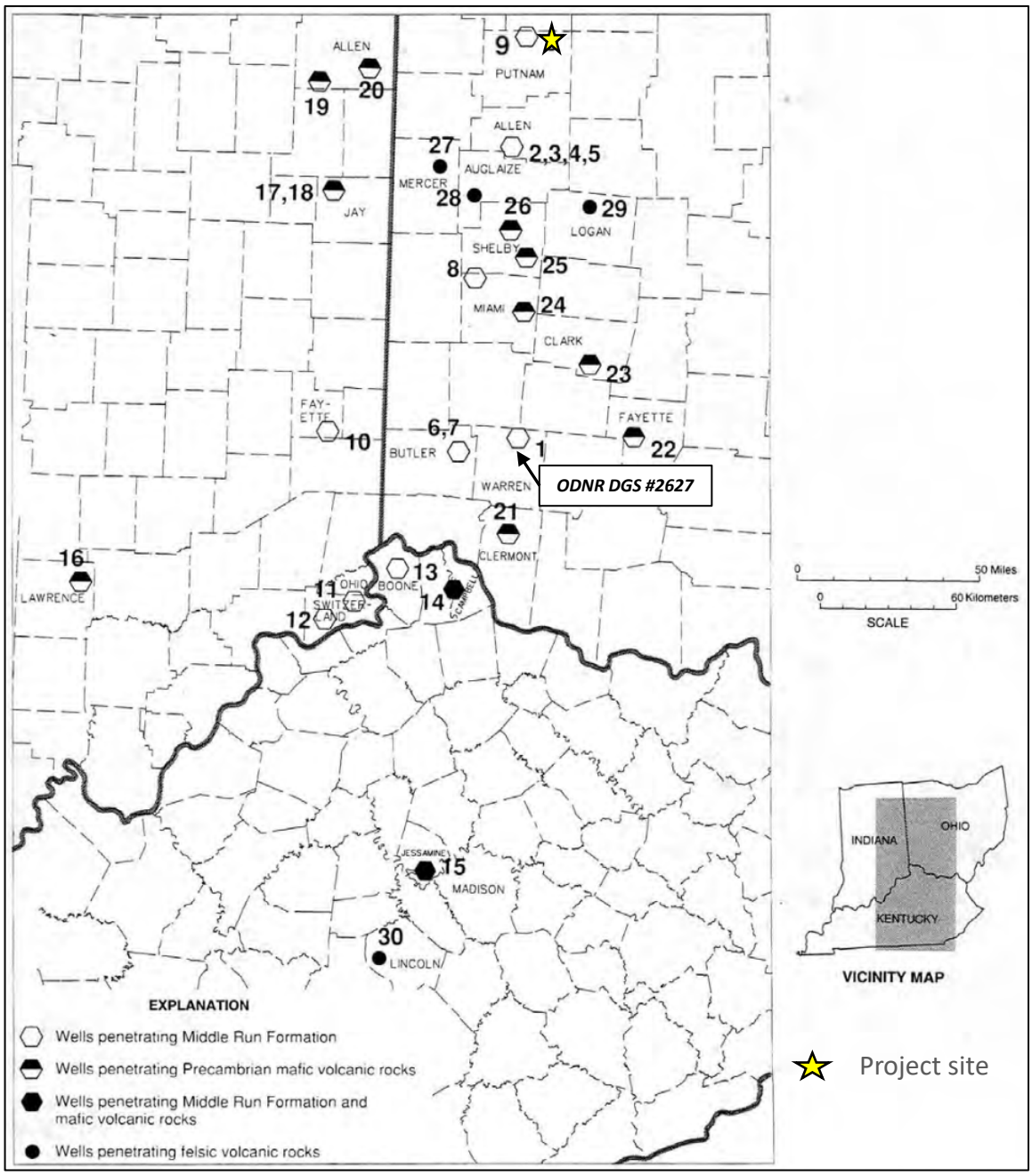

Figure 11: Map of wells identifying Precambrian rock type in the Arches Province. Modified from (Drahovzal et al., 1992).

Figure 12 shows that the Precambrian Basement deepens from approximately 1,800 to 2,200 feet below sea level (fbsl) in the eastern mapped area to more than 3,100 fbsl in the northwest portion of the map.

2.2.2. Mt. Simon Sandstone (Injection Zone) (Cambrian)

The Potsdam Supergroup of the Cambro-Ordovician Sauk sequence unconformably overlies Precambrian rock in the Arches Province and includes the Mt. Simon Sandstone, the Rome Formation (including the Rome Silt), the Conasauga Formation, and the Kerbel Formation (Figure 5, Figure 7 and Figure 9). Specific to this project, the Mt. Simon Sandstone and the Rome Silt form the injection zone, and the rest of the Rome Formation and Conasauga Formation form the primary confining zone (Figure 5).

The Mt. Simon Sandstone is a transgressive terrestrial to shallow marine sequence that is a laterally extensive deposit throughout the Arches Province, the Illinois Basin, and the Michigan Basin (Janssens, 1973; Kolata and Nelson, 1990). It is thickest in northeastern and east-central Illinois (Janssens, 1973; Leetaru and McBride, 2009). Throughout the Midwest, the Mt. Simon Sandstone sedimentology was impacted by a wide range of depositional environments including shallow marine, deltaic, fluvial, eolian, and coastal (Janssens, 1973; Bowen et al., 2011; Saeed and Evans, 2012; Baranoski, 2013; Freiburg et al., 2016). The Mt. Simon Sandstone is interpreted to primarily be a laterally extensive transgressive terrestrial sequence that was reworked (Janssens, 1973; Kolata and Nelson, 1990).

In western Ohio, the Mt. Simon Sandstone is composed of friable, fine-grained to conglomeratic quartz and arkosic sandstone that generally fine upwards (Janssens, 1973). Much of the Mt. Simon Sandstone in this region is poorly consolidated, though some intervals have siliceous cement. The Mt. Simon Sandstone grades into the overlying Rome Formation, and portions of the Mt. Simon Sandstone may be dolomitic and oolitic. The rock is generally frosted, mostly rounded, and poorly sorted, though individual beds may be well sorted. Glauconite and fossils are not present in the Ohio portion of the Mt. Simon Sandstone (Janssens, 1973), though trace fossils have been identified (Saeed and Evans, 2012).

As previously mentioned, the Mt. Simon Sandstone has been the focus of numerous studies and has served as the injection interval in the Arches Province for Class I UIC wells for multiple decades, which will be discussed more in Section *2.6.2. Mineralogy, Diagenesis, Porosity, and Permeability* (Vickery Environmental, Inc., 1989; INEOS Nitriles, 2016; Vickery Environmental Inc., 2020). The Mt. Simon Sandstone is also the injection interval in the adjacent Illinois Basin through a number of US Department of Energy (DOE) funded projects including the Regional Carbon Sequestration Partnerships' IBDP's CCS1 well (Greenberg, 2021) and the CarbonSAFE program (Leetaru et al., 2019; Korose, 2022; Whittaker and Carman, 2022). In the Illinois Basin, the Mt. Simon Sandstone is relatively thick and subdivided into Lower, Middle, and Upper intervals. Due to the relatively thin nature of the Mt. Simon Sandstone at the project site, it has not been subdivided (Figure 5).

The elevation map of the Mt. Simon Sandstone, which represents the top of the planned injection zone, shows the continuity of the unit across a wide region and that it deepens to nearly [redacted] fbsl to the northwest toward the Michigan Basin center (Figure 13). It also deepens eastward toward the Appalachian Basin. Figure 14 shows the thickness of the Mt. Simon Sandstone, which is estimated to be [redacted] feet thick around the project site, and it thins eastward towards the Appalachian Basin.


Claimed as PBI

2.2.3. Rome Formation (Primary Confining Zone) (Cambrian)

The Rome Formation conformably overlies the Mt. Simon Sandstone. Throughout portions of the Arches Province and Appalachian Basin, the Rome Formation is a complex sequence of carbonates, shales, siltstones, and sandstones (Figure 15; Harris and Baranoski, 1997). These strata formed as a result of the transgression that deposited the Mt. Simon Sandstone that continued throughout the Cambrian period (Saeed and Evans, 2012).

Specific to western Ohio, the Rome Formation is primarily composed of microcrystalline dolomite with interbedded fine-grained clastics. Ooids, peloids, and pyrite are found throughout the formation (Calvert, 1962). It thickens eastward across Ohio and develops a sandy interval in west-central Ohio that is sandwiched between upper and lower dolomitic intervals (Janssens, 1973). Thin intervals of bioturbated shale and siltstone are also found within the Rome Formation (Saeed and Evans, 2012). The horizontal transition from the fine-grained clastics of the Eau Claire Shale to the dolomitic clastics of the Rome Formation and overlying Conasauga Formation occurs just west and south of the Maple Project site (Figure 15; Janssens, 1973; Hansen, 1998b).

At the base of the Rome Formation is the Rome Silt, a siltstone lithofacies predicted to be about 27 feet thick at the project site. The Rome Silt forms the upper part of the injection zone (Figure 5).

Above the silt, the Rome Formation is a low porosity, tight microcrystalline dolostone. This lithofacies serves as a confining zone at the Ohio Liquids Disposal well (Vickery Environmental, Inc., 1989; Vickery Environmental Inc., 2020) and will also form the lower part of the primary confining zone at the Maple Project site (Figure 5, Figure 7, and Figure 9).

Figure 16 shows that the Rome Formation deepens from [redacted] feet in the southeast to over [redacted] feet in the northwest. Figure 17 is a regional thickness map of the Rome Formation and shows that the rock is between [redacted] and [redacted] feet thick in the mapped area. At the Maple Project site, the Rome Formation portion of the primary confining zone (above the Rome Silt) is expected to be about [redacted] feet thick and is described in more detail in Section 2.6.2. *Mineralogy, Diagenesis, Porosity, and Permeability.*

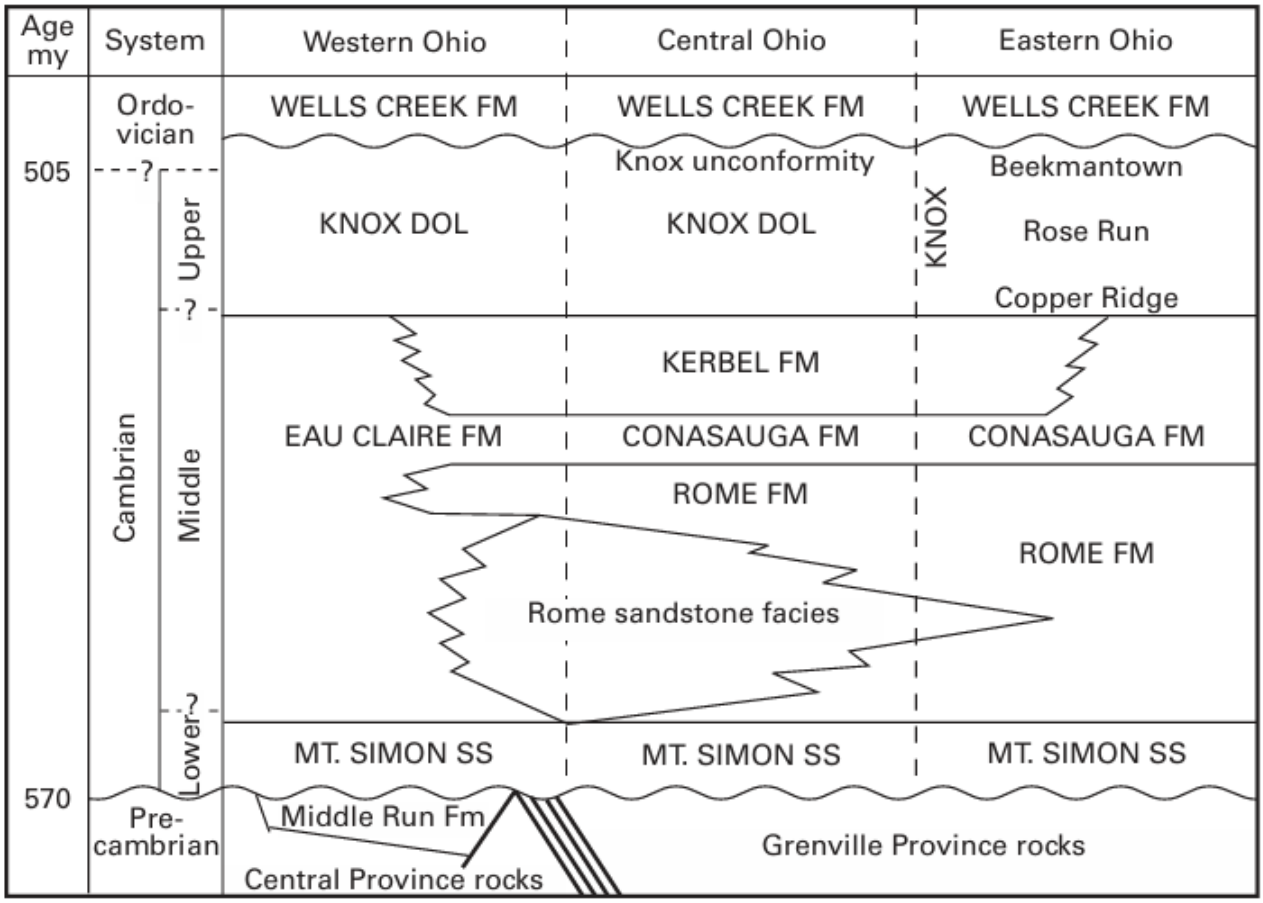

Figure 15: Relationships of Cambro-Ordovician rocks of Ohio. The project site is just east of where the Eau Claire Shale grades into the Rome Formation and Conasauga Formation. Modified from Janssens (1973).


Claimed as PBI


Claimed as PBI

2.2.4. Conasauga Formation (Primary Confining Zone) (Cambrian)

The Conasauga Formation conformably overlies the Rome Formation and is the upper unit of the primary confining zone at the Maple Project site. In west-central Ohio the contact between the formations (Figure 15) is observed where microcrystalline dolomite of the Rome Formation transitions into interbedded, fine-grained glauconitic clastics of the Conasauga Formation (Janssens, 1973). In north-central Ohio the Conasagua Formation was deposited in a more proximal environment, and Banjade (2011) describes its lithology as mixed siliclastic and carbonate sediments based on core from the Ohio Liquids Disposal Well (54 miles northeast of the Maple Project site; Figure 8). In this well, the formation generally has an upward coarsening and thickening sequence of clastic beds with planar laminations, cross beds, flaser beds, massive beds, hummocky cross stratification, and ripple marks (Banjade, 2011). Banjade (2011) interprets shallow marine sedimentary structures and trace fossils of the lower Conasauga Formation to be consistent of an offshore, shallow shelf and pro-delta depositional environment. The sediment was sourced from the northwest and the lack of marine fossils in the upper section of the formation suggests that the depositional environment shallowed to a marginal marine setting (Janssens, 1973; Michael C. Hansen, 1998; Saeed and Evans, 2012).

The transition from the Eau Claire Shale to the Conasauga and Rome formations occurs just west and south of the Maple Project site (Figure 15; Janssens, 1973; Hansen, 1998b). Section 2.6. *Injection and Confining Zone Details* describes the gradational sequence of the Conasauga Formation/Rome Formation/Eau Claire Shale primary confining zone at the BP Chemical 2 well in Richland Country, Ohio (29 miles south-southwest of the project site; Figure 8). This well is situated where the Eau Claire Shale of the Illinois Basin grades into the Rome and Conasauga formations, with the top of the Conasauga Formation being equivalent to the top of the Eau Claire Shale (Figure 15). The gamma-ray signature of the Conasauga Formation increases from the northeast (Ohio Liquids Disposal well) to the southwest (BP Chemical 2), and the bulk density logs decrease from northeast to southwest (Figure 9). The well log character in the Shidler James 2 and Knox High wells indicates that the Conasauga Formation at the Maple Project site is similar to that of the BP Chemical 2 well, and with higher clay content relative to the Ohio Liquids Disposal well (Figure 9).

Regionally, the Conasauga Formation deepens from less than [redacted] feet in the southeast to more than [redacted] feet in the northwest (Figure 18). The regional thickness of the Conasauga Formation shows that the rock thickens from less than [redacted] feet in the southeast to more than [redacted] feet in the west and southwest (Figure 19). At the Maple Project site, the Conasauga Formation is expected to be [redacted] feet thick and will be described in more detail in Section 2.6. *Injection and Confining Zone Details.*


Claimed as PBI


Claimed as PBI

2.2.5. Kerbel Formation (ACZ Monitoring) (Cambrian)

The Kerbel Formation is an upward coarsening deltaic sandstone that conformably overlies the Conasauga Formation and will serve as the above confining zone (ACZ) monitoring interval for the Maple Project (Figure 5). This rock was sourced from the north and forms a north-south oriented deltaic lobe (Kerbel Delta) throughout central Ohio that reaches a maximum thickness of [redacted] feet in north-central Ohio (Janssens, 1973). The Kerbel Formation is absent in southern, extreme western, and eastern Ohio and dolomite content increases upward (Hansen, 1998). Gupta et al. (2017) determined that the Kerbel Formation has reservoir potential in northcentral Ohio where it is primarily a clean sandstone and correlates to the Gatesville Formation in western Pennsylvania (Janssens, 1973). The Kerbel Formation is prognosed to be [redacted] feet thick at the Maple Project site.

2.2.6. Knox Supergroup (Trempealeau Formation/Copper Ridge Dolomite/Knox Dolomite) (Cambro-Ordovician)

Sediment deposition by the Kerbel Delta had stopped by the late Cambrian, which allowed for the deposition of carbonates of the Trempealeau Formation; this formation is also called the Copper Ridge Dolomite in portions of Ohio (Figure 5; Conner et al., 2016). The Trempealeau Formation/Copper Ridge Dolomite represents the beginning of an extensive interval of carbonate deposition across the Arches Province and adjacent areas (Wickstrom et al., 2005). These rocks are interpreted to have been deposited in a shallow marine carbonate shelf environment and are the basal strata of the Knox Supergroup (Figure 5; Komara, 2017). Carbonates and siliciclastics of the Knox Dolomite overly the Trempealeau Formation in western Ohio (Riley et al., 2002; Wickstrom et al., 2005).

The transition from passive margin deposition to the Taconic Orogeny convergent boundary created the Knox Unconformity and associated karst topography in the Early Ordovician (Figure 5). At the Maple Project site, the Knox Unconformity separates the passive margin carbonates from the overlying interbedded clastics and carbonates of the Wells Creek/Glenwood Shale/Gull River strata (Droste and Patton, 1985).

In Morrow County in central Ohio, the Trempealeau/Copper Ridge Dolomite play is one of the most prolific plays in the state's history. This play produces oil out of vugular, fractured dolomite that was created during the formation of the Knox Unconformity (Figure 5), with peak production occurring between 1963 and 1964 (Sutton, 1965). This play does not extend to Putnam County, Ohio.

2.2.7. Wells Creek Formation/Glenwood Shale (Confining) (Ordovician)

The Middle Ordovician Wells Creek Formation directly overlies the Knox Unconformity at the project site and consists of a mixture of siliciclastics and carbonates, with dolomitic shale being the primary facies (Figure 5; Droste and Patton, 1985; Wickstrom et al., 2005). This rock was deposited in a shallow sea that transgressed following the uplift associated with the Knox Unconformity and can be differentiated into several members throughout the Midwest. At the Maple Project site, the Glenwood Shale is the basal unit of the Wells Creek Formation and will serve as an additional confining zone for the Maple Project (Droste and Patton, 1985; Wickstrom et al., 2005).

2.2.8. Black River Group/Gull River Formation (Ordovician)

The micritic to finely crystalline limestone of the Black River Group was deposited in subtidal to intertidal conditions (Figure 5; Wickstrom et al., 2005). This formation consists of lithographic limestone with sandstone, chert, and brown shales. The Gull River Formation is the basal interval of the Black River Group and is described as a relatively pure limestone with lenses of brown dolomite. Thin interbedded limestone is present in the upper section of the Black River Group, and bentonites at the top of the group are evidence that the Taconic Orogeny was increasing in intensity to the east (Drahovzal et al., 1992; Wickstrom et al., 2005). These rocks may be dolomitized near faults (Wickstrom et al., 2005).

2.2.9. Galena Group/Trenton Limestone (Ordovician)

Deepening of the sea resulted in the deposition of the marginal-platform to open-shelf facies of the Ordovician Trenton Limestone of the Galena Group (Figure 5). As a result of subsidence of the proto-Appalachian Basin and the early stages of the Taconic Orogeny, the end of deposition of the basal Trenton Limestone facies is marked by a change in depositional strike. This caused shallowing of the sea to the northwest and the deposition of thick carbonate platform facies of the Trenton Limestone over the Arches Province. These carbonates are further subdivided into the Curdsville, Logana, and Lexington Members in southwestern Ohio (Wickstrom et al., 2005).

The Trenton Limestone is a common hydrocarbon-bearing unit in the Midwest. In areas of western Ohio and eastern Indiana, the Trenton has produced hydrocarbons where it is dolomitized and has fracture/vuggy porosity (Wickstrom et al., 2005; Hickman et al., 2015). The Lima-Indiana Trend was first discovered in 1884 and led to Ohio being the leading oil-producing state at the turn of the twentieth century (Division of Geologic Survey, 2004). No recoverable hydrocarbons have been observed in the Trenton strata in the area of the Maple Project site.

2.2.10. Utica Shale (Confining) (Ordovician)

The Utica Shale conformably overlies the Trenton Limestone at the project site and grades eastward into the limestone of the Point Pleasant Formation (Hickman et al., 2015). These rocks represent a regional sea level transgression that occurred across the eastern United States that resulted in a deeper, anoxic, interplatform depositional environment (Wickstrom et al., 2005; Hickman et al., 2015). The dark, organic-rich Utica Shale was deposited in a marine basin with low-energy and restricted circulation (Bergstrom and Mitchell, 1992). In the Appalachian Basin portion of eastern Ohio (Figure 3), the Utica Shale/Point Pleasant Formation are an unconventional play that produces oil and gas. This play is not found at the Maple Project site (Hickman et al., 2015).

2.2.11 Queenston Formation/Maquoketa Group (Confining) (Ordovician)

The red shale of the Queenston Formation is part of the Queenston Delta Complex, which is a regional clastic wedge that was deposited westward from the Taconic Orogeny and extends from Ontario to Alabama (Figure 5; Fisher and Nightengale, 2006; Hickman et al., 2015). This formation is the time equivalent of the Maquoketa Group in the Illinois Basin. In Ohio, it conformably overlies the Utica Shale and grades to coarser clastics of the Juniata Formation eastward in the Appalachian Basin. It is interpreted to have been deposited in a mudflat environment that was periodically flooded during a eustatic regression (Wickstrom et al., 2005). The Queenston Formation will serve as an additional confining zone at the Maple Project site (Figure 5).

2.2.12. Clinton Formation and Cabot Head Shale (Silurian)

The Clinton Formation of the Medina Group (Figure 5) is composed of interbedded clastics that were deposited in the fluvial-deltaic environment that persisted to flow westward from the Taconic Highlands (Haneberg-Diggs, 2015). The Clinton Formation interfingers with and eventually transitions to the finer-grained marine clastics of the Cabot Head Shale in western Ohio (Knight, 1969). In eastern Ohio, the underlying organic-rich Utica Shale sourced hydrocarbons that migrated into the interbedded sand layers of the Clinton Formation. More than 80,000 wells have been drilled in this play, and the Clinton Formation is also used for natural gas storage or wastewater injection in these depleted reservoirs in eastern Ohio (M.C. Hansen, 1998). The Clinton Formation is not a significant reservoir in western Ohio and is often called the “Clinton Sand” by oil and gas drillers. This terminology also includes the overlying Dayton Formation/Packer Shell and Rochester Shale (M.C. Hansen, 1998; Haneberg-Diggs, 2015).

2.2.13. Dayton Formation/Packer Shell and Rochester Shale (Silurian)

A shallow sea transgressed over the study area during the Silurian, as recorded by the depositional transition of fluvio-deltaic sands to marine carbonates of the Dayton Formation (Clinton Group; Figure 5). This strata is primarily limestone, thickens eastward across Ohio, and is also called the "Packer Shell" in eastern Ohio (Haneberg-Diggs, 2015). As previously stated, oil and gas operators often integrate the Dayton Formation with the underlying Clinton Formation and the overlying Rochester Shale into the "Clinton Sand" clastics (Hansen, 1998). The Rochester Shale is a thin, dark gray, fossiliferous shale with interbedded carbonates and serves as seal to the Clinton Sand play in eastern Ohio (M.C. Hansen, 1998; Haneberg-Diggs, 2015). Together, the Dayton Formation, Packer Shell, and Rochester Shale are part of the Clinton Group (which does not include the underlying Clinton Formation; Figure 5).

2.2.14. Lockport Dolomite (Lowermost USDW) (Silurian)

The Lockport Dolomite represents a time of extensive shallow carbonate platform reef building that extended across northern and eastern Ohio (Figure 5, Hansen, 1998a). This dolomite is fossiliferous, slightly argillaceous, and develops porosity associated with patch reefs in the basal section. At the project site, the Lockport Dolomite is the lowermost underground source of drinking water (USDW) (Riley et al., 2012), and will be further discussed in Section 2.9.4. *Determination of Lowermost USDW*.

2.2.15. Salina Group (Silurian)

The strata of the Salina Group is the bedrock at the project site (Figure 5). These strata are composed of interbedded dolomite, shale, and evaporites and subdivided into seven units based on lithology in portions of eastern Ohio. It has also been used for underground mining, salt-solution mining, and propane storage within the salt-solution mines in eastern Ohio (Janssens, 1973; Wickstrom et al., 2005). Generally, in the area of the project site the Salina Group is mapped as undifferentiated, so while there are seven distinct units recognized in eastern Ohio, in the northwestern part of the state the Salina Group is primarily microcrystalline dolomite (Janssens, A, 1977). The Salina Group will be discussed further in Section 2.9. *Hydrologic and Hydrogeologic Information*.

2.2.16. Quaternary Sediments

Ohio experienced numerous glacial intervals during the Quaternary Period, and glacial processes and post-glacial streams deposited up to 700 feet of sediment throughout northern and western Ohio with greatest thicknesses occurring in bedrock valleys (Figure 5, Division of Geologic Survey, 2017). Specifically, the Maple Project site is located on Wisconsinan Woodfordian glacial deposits composed of lake-planed moraine and associated beach sand deposits. These deposits will be discussed in detail in Section 2.9. *Hydrologic and Hydrogeologic Information*.

2.3. Regional Structure

The structural geology of the Maple Project region has been influenced by changes in tectonic regimes from the Precambrian to present times. The Maple Project site is within the Arches Province, a tectonically stable region, which is defined by three radiating Precambrian arches (Kankakee, Findlay, and Cincinnati) that divide the Michigan, Illinois, and Appalachian Basins (Figure 3). The project site is on the western flank of the Findlay Arch (Figure 3 and Figure 4). The Precambrian rocks forming the arches are separated from the overlying Paleozoic strata by an extensive unconformity.

The Precambrian Basement in western Ohio is a stable, largely crystalline, tectonic assemblage associated with the amalgamation of the proto–North American continent. In this region, the basement can be divided into three domains of differing origins: 1) the EGRP, 2) the ECRS and the FWR, and 3) the Grenville Province. See Section 2.2.1 *Precambrian Basement Complex* for a description of the Precambrian Basement in western Ohio. The Precambrian Basement underlying the Maple Project site is located where the ECRS and Grenville Province meet.

The Grenville Front is approximately 15 miles east of the Maple Project site and represents a regional, north-south oriented tectonic zone associated with the Mesoproterozoic Grenville Orogeny (Baranoski et al., 2009; Figure 10 and Figure 20). This front marks an approximate boundary of the EGRP/ECRS to the west and the Grenville Province to the east. At this boundary, the Grenville Province rocks were thrust over the EGRP and ECRS terrains in a present-day west-northwestward direction, causing the Grenville Province Basement to be found in areas west of the actual structural front (Figure 20; Wickstrom et al., 2005).

In western Ohio and southern Michigan, the Grenville Front thrust is hypothesized to be expressed at the surface by the Bowling Green Fault System. The fault system is also 15 miles east of the project site and has been mapped from surface exposures and subsurface data (Figure 10 and Figure 20; Onasch, 2007). This system is interpreted to be a series of faults that extend to the Precambrian Basement with both strike-slip and dip-slip motion (Wickstrom et al., 1992). Vertical offset varies from 400 feet in the northern extent to less than 100 feet in southern (Onasch, 2007). The Maumee Fault is a northeast-southwest trending fault that is approximately 15 miles north of the project site (Figure 20). This fault obliquely intersects the Bowling Green Fault System and is interpreted to be a left-lateral strike-slip fault associated with the Grenville Front and Bowling Green Fault System (Wickstrom et al., 1992).

The Bowling Green Fault System has likely influenced the stratigraphic evolution of western Ohio, as well as fluid flow through the strata of the region (Onasch, 2007). Solution collapse, dolomitization, and mineralization within and around the fault system suggest that it locally focused the flow of subsurface fluids (Onasch, 2007). Much of the oil produced from the Lima-Indiana Trenton Limestone play was produced from reservoirs associated with the dolomitization of the Trenton Limestone around the Bowling Green Fault System (Section 2.2.9 *Galena Group/Trenton Limestone*). Along with providing a pathway for the localized dolomitization of the Trenton Limestone reservoir, the Bowling Green Fault

System created both stratigraphic and structural trapping mechanisms (Wickstrom et al., 1992).

The Outlet Fault is a synthetic shear zone within the Bowling Green Fault System (Figure 20, Wickstrom et al., 1992). Core collected near the Outlet Fault shows that the Trenton Limestone is extensively fractured, although the core was fractured to a lesser extent than at the main branch of the Bowling Green Fault System to the west. In addition, vertical offset along the Outlet Fault is minimal and hydrocarbon trapping mechanisms along the fault are similar to that along the Bowling Green fault system (Wickstrom et al., 1992).

The Marion Fault is a northwest-southeast trending fault approximately 40 miles southeast of the project site and is also interpreted to be part of the Bowling Green Fault System (Figure 20; Onasch, 2007). The Tiffin, Crawford, and Harlem faults all have a similar northwest-southeast trend as the Marion Fault, and several other unnamed faults with similar orientations have been mapped in the area. Relatively little Precambrian offset is observed at the Crawford and Harlem faults, although the basement structure becomes complex at the intersection of the Tiffin Fault and an unnamed west-east trending fault (Figure 20).

The northeast-southwest trending Auglaize Fault is approximately 32 miles south of the project site. It is associated with the ECRS and is not exposed at the surface (Figure 20). Offset along this feature is also questionable due to data constraints, and it is not interpreted to have been active during the Paleozoic. The Auglaize Fault is mapped to crosscut the Fort Wayne Rift of the ECRS (Wickstrom et al., 1992; Baranoski et al., 2009).

The Anna-Champaign, Logan, and Bellefontaine Outlier faults, as well as numerous unnamed faults of northwest-southeast orientation, are mapped just south of the Auglaize Fault (Figure 20), though none of the faults have a clear surface expression. These faults were identified in a regional east-west Consortium for Continental Reflection Profiling (COCORP) seismic reflection profile that was collected in 1987 (Baranoski et al., 2009). This profile and additional well data demonstrate that there is up to 100 feet of vertical displacement along the faults and the Mt. Simon Sandstone is absent on individual fault blocks. These faults are interpreted to be associated with the Anna Seismic Zone, which will be discussed in Section 2.8. *Seismic History* (Ruff et al., 1994).

High density, two-dimensional (2D) surface seismic data acquired specifically for the Maple Project indicates there are no significant structural features identified within the project's AoR that would impact CO_2 sequestration and containment. The 2D surface seismic data is discussed in detail in Section 2.5. *Faults and Fractures*. The structural features listed above are significantly removed from the project area and are not considered impactful to carbon sequestration operations.


Claimed as PBI

2.4. Maps and Cross Sections of the AoR [40 CFR §146.82(a)(2), 40 CFR §146.82(a)(3)(i)]

Figure 21 shows the AoR for the Maple Project. The AoR is defined by the maximum extent of the critical delta front (151 pound-force per square inch (psi)) plus 0.25 miles, which also encompasses the maximum extent of the CO_2 plume over 62 years (12 years of injection and a 50-year post-injection site care (PISC)) (Attachment 02: AoR and Corrective Action Plan, 2025).

Figure 21 also shows known existing wells within the area. The input data and physical processes incorporated into Maple Project static and computational models, as well as methodology used to delineate the AoR, are described in the AoR and Corrective Action Plan (Attachment 02: AoR and Corrective Action Plan, 2025).

The Mt. Simon Sandstone and Rome Silt form the injection zone, and the overlying Rome Formation and the Conasauga Formation together comprise the primary confining zone. These formations extend laterally beyond the AoR limits, as demonstrated by the regional thickness maps (Figure 14, Figure 17, and Figure 19), the cross sections shown in Figure 7 and Figure 9, and 2D surface seismic data discussed below.

The strata of the Mt. Simon Sandstone, Rome Silt, Rome Formation, and Conasauga Formation are of consistent thickness with no evidence of stratigraphic pinch-out within the AoR. Claimed as PBI [redacted] Additionally, there is no indication that structural trapping by faults or domes could occur within the AoR.

2D surface seismic data (Figure 22, Figure 23, Figure 24, Figure 25, Figure 26, Figure 27, Figure 28, Figure 29, and Figure 30) acquired specifically for the Maple Project indicate the Mt. Simon Sandstone, Rome, and Conasauga strata are laterally continuous and exhibit no significant faults or structural features (Section 2.5. *Faults and Fractures*. All known faults truncate at or below or at the Precambrian unconformity. These faults are not expected to impact injection or containment (Section 2.5. *Faults and Fractures*).

The Silurian Lockport Dolomite is the lowermost USDW within the AoR. The top of the USDW is prognosed at [redacted] feet depth, and its base is more than [redacted] feet above the top of the primary confining zone at the Maple Project site (Section *2.9.4. Determination of Lowermost USDW*). There are no structural features or faults observed to intersect the Lockport Dolomite in the AoR. As described in Section 2 *Site Characterization*, there are several additional confining zones between the Conasauga Formation and the Lockport Dolomite in the AoR.

There is one record of a potential oil and gas well, recorded as “other, never completed,” in the AoR that was drilled to 62 fbgl and is plugged and abandoned (Figure 21) according to the Ohio Department of Natural Resources Division of Oil and Gas public database (Ohio Division of Geologic Survey, 2004). The latest water well data search indicates that 153 groundwater wells are located within the Maple AoR; well depths range from 45 fbgl to 535 fbgl with an average depth of 181 fbgl (Figure 21).

There are no existing wells that penetrate the primary confining zone in the AoR at the Maple Project site.

2.5. Faults and Fractures [40 CFR §146.82(A)(3)(ii)]

Figure 22 shows the seven 2D surface seismic lines and [redacted] miles of data that were acquired to characterize the subsurface within the Maple Project AoR and to provide information regarding surface structure and stratigraphy. Five of the seismic lines fully traverse the AoR (Lines 1, 2, 4, 6, and 7) and Line 5 is located fully within the AoR. The synthetic seismogram and the seismic lines used for interpretation are shown in Figure 23, Figure 24, Figure 25, Figure 26, Figure 27, Figure 28, Figure 29, and Figure 30. The vertical seismic sections are shown in two-way-time (TWT).

A high density 2D surface seismic program was acquired with a vibrator truck on roadways in March 2024 (Figure 22). The vibrator truck used a 4-120Hz broad band sweep of 20 second duration as the seismic source for these data. A source and receiver spacing of 40 feet was used to enable high density processing to identify both shallow and deep subsurface features. Long offsets were obtained to enable additional inversion work to identify any lithological changes at target.

Seismic lines 1 through 7 (Figure 22, Figure 24, Figure 25, Figure 26, Figure 27, Figure 28, Figure 29, and Figure 30) indicate the Paleozoic stratigraphy very gently dips to the west (<1 degree), which is consistent with regional interpretations from well and seismic data (Baranoski, 2002, 2013). In addition, the Paleozoic strata from the top of the Mt. Simon Sandstone reflector to reflectors above the Trenton Limestone are relatively continuous in thickness and without notable structural features (Figure 24, Figure 25, Figure 26, Figure 27, Figure 28, Figure 29, and Figure 30). The Mt. Simon Sandstone thickness varies, but this is interpreted to be due to in-filling on the Precambrian unconformity surface and not a product of structural deformation.

Six horizons were interpreted in the Maple Project seismic data: the Trenton Limestone, the Kerbel Formation, the Conasauga Formation, the Rome Formation, the Mt. Simon Sandstone, and the Precambrian Unconformity. The 2D surface seismic data was correlated to the stratigraphy using the Knox High offset well (UWI 34063203600000; Figure 8 and Figure 23). Line 1 was extended to the Knox High well in order to have a direct well-to-seismic data tie. A synthetic seismogram was generated for the Knox High well from bulk density and synthetic sonic data available for this well, and calibrated with checkshot and sonic data from the Shidler James 2 well (Figure 8). The synthetic seismograph display shows a good match between the synthetic seismic traces for the main interpreted horizons, and the actual trace in Line 1 at the location of the Knox High well (Figure 23).

The Precambrian pick was based upon three factors: 1) the Knox High well tie, 2) interval velocities from the Knox High well in conjunction with Mt. Simon Sandstone thickness values for the well in the area, and 3) the identification of a reflector at about the predicted two-way travel time that showed a subtle but clear angular unconformity visible at the Precambrian reflector on all of the interpreted seismic lines (Figure 24, Figure 25, Figure 26, Figure 27, Figure 28, Figure 29, and Figure 30).

In all acquired seismic lines, the Precambrian unconformity is identified as the first (shallowest) strong positive reflector below the Mt. Simon Sandstone and has variable relief due to erosion along the unconformable surface. The erosional relief on the Precambrian unconformity results in small variations in thickness in the Mt. Simon Sandstone, as the sand initially filled topographic lows. This is demonstrated by the onlapping of Mt. Simon Sandstone reflectors to the Precambrian surface. All of the seismic lines also show that seismic reflectors above the Mt. Simon Sandstone are relatively parallel and continuous until approximately 75 ms (TWT) where more variability in the strata is observed. Lateral discontinuities are not observed in the Paleozoic reflectors, which indicates that the Paleozoic strata have not been faulted.

Several high angle faults in the Precambrian Basement were interpreted by breaks and/or small offsets in the reflectors in lines 1, 7, 4, 6, and 2 (Figure 24, Figure 25, Figure 26, Figure 27, and Figure 30). None of the interpreted Precambrian faults demonstrate large offsets (>5 ms) or extend above the Precambrian unconformity. The interpreted faults were also not traceable between seismic lines with any accuracy or confidence, which suggests that the identified faults are limited in lateral extension.

A small Precambrian high is observed along line 5 (just south of the line 7 intersection; Figure 29). It is observable on the Precambrian unconformity reflector. It may propagate to the Kerbel Formation based on the reduction in amplitudes. Strata within the Mt. Simon Sandstone appear to onlap the feature, and there are no breaks in the Precambrian or Paleozoic reflectors (Figure 29). As such, this feature is likely not associated with faulting.

As described in Section 2.1. *Regional Geology, Hydrogeology, and Local Structural Geology*, the Maple Project site is located within the Arches Province, which is a tectonically stable area that has little deformation visible in the Paleozoic strata. Underlying deformation in the Precambrian Basement is separated from the Paleozoic strata by a regional unconformity surface. This is supported by the seismic data which shows very little to no deformation in the Paleozoic strata (Figure 24, Figure 25, Figure 26, Figure 27, Figure 28, Figure 29, and Figure 30). The seismic data also shows relative consistency in the amplitude of the interpreted formations along both axes acquired (N/S lines and E/W lines). This suggests that the rock is relatively consistent and features such as fractures are not affecting the seismic response. While this is not conclusive proof of sparse natural fractures in the rocks at the project site, the limited strain observed in the Paleozoic section suggests that the Maple Project site will be minimally influenced by natural fractures.


Claimed as PBI


Claimed as PBI


Claimed as PBI


Claimed as PBI


Claimed as PBI


Claimed as PBI


Claimed as PBI


Claimed as PBI


Claimed as PBI


Claimed as PBI


Claimed as PBI

2.5.1. Fault Slip Analysis

Fault slip analyses were performed to evaluate the potential for failure of the Precambrian faults (mapped with 2D surface seismic data) during injection operations and post-injection. In western Ohio, the Cambrian strata and Precambrian rocks are separated by an unconformity that spans hundreds of millions of years, and the topography observed on the Precambrian Unconformity is a result of erosion when the basement was exposed. The extent of mapped faults and the nature of seismic reflectors indicate that the Precambrian faults are decoupled from the Cambrian and younger strata and have not been active for over 500 million years, since the onset of Mt. Simon Sandstone deposition.

The extended time of inactivity would lend itself to diagenetic alteration (mineralization, etc.) that would increase fault strength (differential stress required to slip pre-existing parallel surfaces) of Precambrian faults beyond simple parallel plates. Whereas diagenetic cementation along fault planes is considered likely, there is no direct evidence in the area, and all fault slip potential calculations on possible faults assume the most conservative view that any faults are simple parallel plates.

All faults interpreted in the seven 2D surface seismic lines of this project area (Figure 33) were confined to the uppermost Precambrian section and could not be traced upward through the Mt. Simon Sandstone or downward into the deeper Precambrian section. Claimed as PBI [redacted]


Claimed as PBI

A one-dimensional (1D) mechanical earth model (MEM) was developed to characterize the mechanical properties of rocks and faults, as well as the pressures and stresses acting at depth. The project area is in a strike-slip domain (Hurd and Zoback, 2012), where:

$$SHmax > Sv > Shmin \quad (1)$$

$SHmax$ is the maximum horizontal stress, Sv is the vertical stress, and $Shmin$ is the minimum horizontal stress. The orientation of the localized stress components are $SHmax$ (s_1) =65° / 245°, Sv (s_2) is vertical, and $Shmin$ (s_3) = 155° / 335° (Hurd and Zoback, 2012; Heidbach et al., 2016).

Principal stress (Sv, Shmin, and SHmax) values, ranges, and orientations were calculated using log data from the Knox High and Shidler James 2 wells (Figure 9 and Figure 35) and are reported in Figure 34

Table 4. Pore pressure was determined using an average calculated pore pressure gradient from wells in the region, and the values indicate the Mt. Simon Sandstone is normal to slightly under-pressured.

Vertical stress is calculated in two parts for this analysis. The vertical stress for the overburden (ground surface to the top of Trenton Limestone) was from two wells in the region resulting in gradients from 1.14 to 1.15 psi/ft (Table 4). This gradient was used to calculate the vertical stress at the top of the Trenton Limestone (Svo). The vertical stress for the interval from the top of the Trenton Limestone to the well total depth was calculated by integrating the rock density (from geophysical logs) using equation 2,

$$Svz = (Svo) + \left(\int_n^z \rho\,(z) g dz\right) \sim (\overline{\rho} g z) \quad (2)$$

where Svz is the vertical component of stress at depth z, Svo is the vertical component of stress at depth n (bottom of the overburden), $\rho(z)$ is the density as a function of depth, g is the gravitational acceleration and $\overline{\rho}$ is the mean overburden density (Jaeger and Cook, 1971). The resultant stress and gradient values are presented in Table 4**.** The Mt. Simon Sandstone vertical stress gradient of 1.14575 psi/ft to the Mt. Simon Sandstone with a range of 0.0056 psi/ft.

Minimum horizontal stress calculations utilized closure stress calculated for the Knox High and Shidler James 2 wells (Figure 35) and normalized the stress values to a gradient at the Mt. Simon Sandstone level. Lacy's equation (Lacy, 1997) was used to convert dynamic Young's modulus to

a static modulus and a modified uniaxial strain equation (Barree and Conway, 2009) to determine closure stress. From these results, a minimum stress gradient and deviation was calculated at the Mt. Simon Sandstone interval for the Knox High and Shidler James 2 wells (Figure 35) providing an average and range for the minimum horizontal stress gradient in the region (Table 4).

The Mohr Coulomb theory is used assuming a critically stressed crust to determine an upper limit for the maximum horizontal stress using the methodology outlined in (Zoback, 2010). This methodology builds on Jaeger and Cook (1971) that demonstrates that where a critically stressed fault is at its frictional limit:

$$\frac{\sigma_1}{o_3} = \frac{S1-P_P}{s_3-P_p} = \left[(\mu^2+1)^{\frac{1}{2}} + \mu\right]^2 \quad (3)$$

where s_1 is the maximum effective stress, s_3 is the minimum effective stress, S_1 is the maximum stress, S_3 is the minimum stress, Pp is the pore pressure, and m is the coefficient of friction. From the World Stress Map Data (2016) and (Hurd and Zoback, 2012) the region is a strike-slip fault regime (Anderson's faulting theory) so that $S_1 = S_{Hmax}$, $S_2 = S_v$, and $S_3 = S_{hmin}$. Equation 3 can then be written as a limit for SHmax where:

$$\frac{SHmax-Pp}{Shmin-Pp} \leq \left[(\mu^2+1)^{\frac{1}{2}} + \mu\right]^2 \quad (4)$$

If we assume a conservative value for the coefficient of friction (m = 0.6) and the value for Shmin as calculated for the region, the equation can be simplified as a maximum value for SHmax:

$$SHmax = 3.1(Shmin - Pp) + Pp \quad (5)$$

Using this equation, an SHmax upper limit was calculated, and a maximum stress gradient and deviation was calculated at the Mt. Simon Sandstone interval for each well (Figure 35) providing an average and range for the minimum horizontal stress gradient in the region (Table 4).


Claimed as PBI

Claimed as PBI


Claimed as PBI

To determine the potential for a fault to fail, the assumption of a critically stressed crust was made such that at an optimal angle, any increase in pore pressure will result in fault slip. Of the twenty possible basement faults interpreted on the 2D surface seismic lines within the project area, four of these faults provide sufficient detail to analyze for fault slip potential under the proposed injection scheme. The remaining faults were also analyzed using regional data to infer fault orientations (Figure 34).

Table 4 shows the list of values from the 1D MEM used in the fault slip analysis. Along with the calculated values for Sv, SHmax and Shmin, the friction angle was set to $\mu = 0.6$ based on Byerlee's law ($0.6 \leq \mu \leq 1.0$) to introduce slip at the lowest increase in pore pressure. Cohesion was assigned a value of zero, which is a conservative approach that does not allow for any increase in fault strength due to alteration of the fault plane. Fault orientations were taken from seismic interpretations for the four faults that intersect at least two seismic lines and given a range in the sensitivity analysis to account for uncertainty regarding fault orientation. Data for the remaining faults observed in the 2D surface seismic lines was not sufficient to determine orientation, so regional values were used (Figure 34). Pore pressure was determined in the 1D MEM to be 0.415 psi/ft +-0.21 and is within the range or values expected for normally to slightly under-pressured reservoirs (hydrostatic pore pressure ~ 0.44 psi/ft). Thermal variations were not considered.

FSP 2.0 is peer-reviewed, industry and academically recognized software used extensively in determining fault slip potential (Walsh et al., 2018). It was used to transform the 3D stress tensor field defined by the 1D MEM to shear and normal stress on individual fault plane orientations. It was also used to calculate the increase in pore pressure required to critically stress a fault plane. This software uses Monte Carlo analysis of the parameters and range of values for the parameters to determine probability cases for the slip potential and the sensitivity of pore pressure to changes in the individual parameters. One thousand cases were run, and Figure 36 is a display of the results of the fault slip analysis showing the probability of a range of pore pressures determined by the variability in the input parameters. Sensitivity to the individual parameters for each fault is also shown in Figure 36 with the difference between fault strike and maximum stress direction having the largest influence on pore pressure.

For the 16 faults that only intersect one seismic line, the regional analysis of fault orientations (Figure 34) was used to assign fault orientation and dip and a probability model was used with the variance of the regional fault orientations used for the sensitivity analysis. As with the four faults having known orientations, fault strike has the greatest influence on pore pressure for these 16 faults.


Claimed as PBI

Profiles of the change in pressure (delta pressure) at the top of the Mt. Simon Sandstone from the injector to mapped faults were extracted from the computational model (Attachment 02, AoR and Corrective Action Plan) for Years 12 (end of injection) and Years 13, 14, and 15 (one to three years post-injection) and are shown in Figure 37. Delta pressure at the top of the Mt. Simon Sandstone (top of perforations) was used rather than the top of the Rome Silt (top of injection zone). Maximum delta pressure occurs at the top of the Mt. Simon Sandstone; the Rome Silt has similar to slightly lower delta pressures due to decreased permeability along with irregular pressure. As such, the top of the Mt. Simon Sandstone with the most continuous and highest delta pressures was used in the fault slip analysis. Figure 37 Reduction in delta pressure (DeltaP) at the bottom of the Mt. Simon Sandstone near the injector is due to buoyancy effects of the CO2 versus water. Note the maximum pressure seen is below the P1 cases for increase in pressure to fail faults on the seismic or regional fault orientations. The black arrows show the calculated increase in pressure expected at the closest interpreted fault to the injector. Claimed as PBI

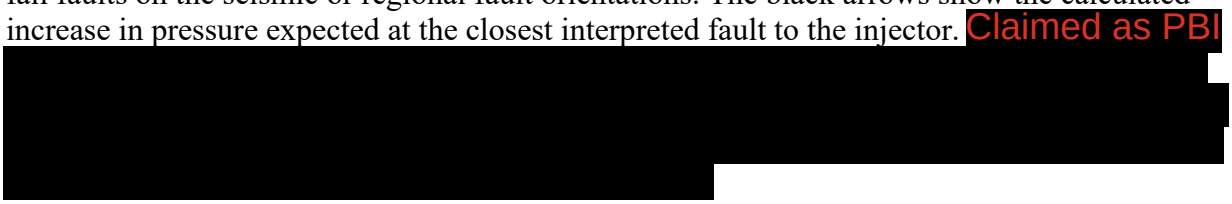

Claimed as PBI

2.5.2. Impact on Containment

Based on the analysis and interpretation of the seismic data, faults are not observed within the injection or primary confining zones at the Maple Project site. This is supported by the consistency of the stratigraphic thickness, the low and consistent dip of the stratigraphy, and the consistent amplitude of individual reflectors within the Paleozoic strata. Regionally, identified faults in Paleozoic strata have thickness variations and offset on formation tops (Vickery Environmental, Inc., 1989; Onasch, 2007) and the lack of these features in the Maple Project seismic data supports the interpretation that faults do not penetrate the injection zone and primary confining zone. The small high in the early Paleozoic strata observed on Line 5 (Figure 29) is not associated with a break in the Precambrian Basement or Paleozoic strata reflectors, and as such is not associated with faults.

Limited faulting is observed in the Precambrian Basement and all interpreted faults terminate below or at the Precambrian unconformity. As no offset or continuation of the faults are observed within the injection or primary confining zones, these faults are not expected to impact containment per 40 CFR §146.82(a)(3)(ii). Minor faults identified in surface seismic data collected for other CO_2 sequestration projects in the Midwest suggest that minor faults in the Precambrian and Mt. Simon Sandstone strata are not expected to act as conduits through the confining zone (Greenberg, 2021) and present no endangerment to USDWs.

Vault GSL CCS LP intends to acquire a baseline three-dimensional (3D) surface seismic survey at the Maple Project site during the Pre-operational Testing Program and any identified structural features or faults will be mapped and assessed to determine if there is any potential impact to storage or containment. The data gathered during the pre-operational phase of the project will be used for geomechanical modeling to evaluate whether any minor faults identified in the surface seismic data are stable or whether they could become critically stressed during the injection phase of the project (Attachment 05: Pre-operational Testing Program, 2025)

2.5.3. Tectonic Stability

The Maple Project site is within an intraplate setting several thousands of miles distant from a plate boundary. It is located in the Arches Province, which is a tectonically stable region that has a low probability of seismic activity or earthquakes above M 2.5. Section 2.8. *Seismic History* includes a detailed discussion about earthquakes near the Maple Project site. In addition, fault slip analyses conclude that there is a very low probability of the Precambrian Basement slipping in the AoR due to the planned injection operations.

The 2D surface seismic data acquired for the project demonstrate that all of the identified faults truncate at or below or at the Precambrian unconformity (Section 2.5. *Faults and Fractures*) and do not extend into the Mt. Simon Sandstone. In addition, though the Maple Project site is located where the Grenville Province and ECRS meet (Figure 10), the Precambrian Basement and associated faults are separated from the Paleozoic strata by a regional unconformity surface, and the seismic data show very little to no deformation in the Paleozoic strata. As such, the basement faults identified are not expected to impact the injection and primary confining zones.

2.5.4. Addressing Uncertainty

A 3D surface seismic survey will be acquired for the project prior to submitting the Pre-Operational Narrative to evaluate injection and primary confining zone properties, map Precambrian Basement topography, and characterize any identifiable basin fill or basement faults. Detailed mapping and attribute analysis using this dataset is expected to confirm the lack of large-scale faulting. The 3D surface seismic survey will be designed to obtain full fold data over the predicted extent of the CO_2 plume after 12 years of injection and proposed 50-year PISC period to provide an indirect measurement of CO_2 plume migration over time (Attachment 06: Testing and Monitoring, 2025; Attachment 08: Post-injection Site Care and Site Closure, 2025).

As detailed in Attachment 05: Pre-operational Testing Program, (2025), 4-inch core and geophysical logs, which include sonic and image logs, will be acquired while drilling the MPL INJ1 well. These will be used to assess the nature of identifiable fractures and their impact on long-term integrity of the primary confining and injection zones.

The static model will be updated with the 3D surface seismic data and well analyses, and a Pre-operational Narrative will be submitted to the EPA that will provide the new data and updated static and computational models. Narrative text, maps, and cross sections related to faults and fractures will be updated with the new data.

2.6. Injection and Confining Zone Details [40 CFR §146.82 (a)(3)(iii)]

2.6.1. Injection Zone and Confining Zone Extent and Thickness

The Mt. Simon Sandstone and the Rome Silt form the injection zone for the Maple Project. Computational modeling indicates that most of the injected CO_2 will remain in the Mt. Simon Sandstone, and the Rome Silt portion of the injection zone will provide minimal storage as described in Attachment 02: AoR and Corrective Action Plan, (2025). Above the Rome Silt, the Rome Formation and the Conasauga Formation will comprise the primary confining zone for the Maple Project (Figure 5). Regional characteristics of the injection and confining zones are also described in Section 2.2. *Regional Stratigraphy*.

Available public data were collected and integrated to develop site-specific subsurface maps, petrophysical relationships, and a static model of the Maple Project site. Within the Maple Project AoR, there are minor elevation and thickness variations of the injection interval. The primary confining zone does not exhibit significant elevation and thickness variations.

Claimed as PBI [redacted] Site specific 2D surface seismic data confirms the lateral continuity and structural integrity of these strata across the AoR (Section 2.5. *Faults and*

Fractures). The primary confining zone will provide a thick, laterally extensive barrier to prevent upward migration of injection zone fluids over time.

CO_2 plume development is expected to be controlled dominantly by porosity and permeability distribution influenced by heterogeneities within the injection zone resulting from lithological variations and diagenetic processes; structural features will have minimal influence on CO_2 plume development at this site (Attachment 02: AoR and Corrective Action Plan, 2025). Analysis of geophysical log response and core descriptions and mineralogy of Ohio Liquid Disposal and BP Chemical 2 wells (Section 2.6.2. *Mineralogy, Diagenesis, Porosity, and Permeability*) confirmed that the most significant controls on lithofacies variation and heterogeneity for the Mt. Simon Sandstone, Rome Formation, and Conasauga Formation were compaction, dolomitization, feldspar dissolution and consequent creation of secondary porosity. These processes are discussed in detail in Section 2.6.2. *Mineralogy, Diagenesis, Porosity, and Permeability*. Density logs and the resulting effective porosity logs (Section 2.7.2. *Petrophysics*) best capture lithofacies variations in the injection and primary confining zones. Six clastic to dolomitic facies (dolomite, shale, tight dolomitic clastics, tight siltstone/sandstone, quartz sandstone, and arkosic sandstone) were defined for the key petrophysical wells. Effective porosity logs of nearby wells were the input for the geostatistical property modeling described in Attachment 02: AoR and Corrective Action Plan, (2025), which adequately captures depositional and diagenetic facies variations (Section 2.6.2. *Mineralogy, Diagenesis, Porosity, and Permeability*).

2.6.2. Mineralogy, Diagenesis, Porosity, and Permeability

Public log and core information from four key wells in Ohio provide significant data that has been used to characterize the injection and primary confining zones at the Maple Project site. Available wells that penetrate the Mt. Simon Sandstone or deeper are from UIC Class I sites and O&G wells that have well logs, core, and fluid injection data from the Mt. Simon Sandstone, Rome Silt, Rome Formation and Conasauga Formation (Figure 38). The four key wells that are considered geologic analogs to the Maple Project site are the: 1) Knox High (UWI 34063203600000), 2) Shidler James 2 (UWI 34069201390000), 3) Ohio Liquids Disposal (UWI 34143202370000), and 4) the BP Chemical 2 (UWI 34003200670000).

The Knox High well (UWI 34063203600000) is approximately 9 miles east-northeast of the Maple Project site and represents the closest analog for the injection and confining zones; although, it does not penetrate the entire thickness of the Mt. Simon Sandstone. The Shidler James 2 well (UWI 34069201390000) is approximately 13 miles north of the site and also serves as a geologic analog for the injection and primary confining zones (Figure 38).

Additional wells used for characterization are the Ohio Liquids Disposal well (UWI 34143202370000) and the BP Chemical 2 well (UWI 34003200670000); both are UIC Class I wells that use the Mt. Simon Sandstone for injection. The Ohio Liquids Disposal well is in Sandusky County, Ohio, about 54 miles northeast of the project site, and the confining zone strata are the Rome and Conasauga Formations as well as beds within the Knox Group. The BP Chemical 2 well is in Richland Country, Ohio, about 30 miles south of the project site. This well is situated where the Eau Claire Shale of the Illinois Basin begins grading into the Rome and

Conasauga Formations, and this gradational sequence is the primary confining zone at the BP Chemical site. For the purposes of this project, the top of the Conasauga Formation is equivalent to the top of the Eau Claire Shale at the BP Chemical 2 well.

The Ohio Liquids Disposal well is one of nine wells within a field that has been injecting fluid into the Mt. Simon Sandstone since the 1970s. Vickery Environmental Inc. performed an extensive study that examined mineralogy, porosity, permeability, and diagenesis in core samples collected from the disposal wells (Vickery Environmental, Inc., 1989; Vickery Environmental Inc., 2020). Vickery Environmental, Inc (1989) provides thin section descriptions of the Mt. Simon Sandstone, Rome, and Conasauga Formations from numerous wells located within the disposal field. The results from this study are consistent with the petrophysical results, including porosity and permeability distribution, observed in the geophysical logs from the Shidler James 2 and Knox High wells that are closer to the Maple Project site. As such, the Ohio Liquids Disposal well also serves as an analog for the Maple Project site due to extensive data and analysis (Section 2.6.2.1 *Analog Well: Ohio Liquids Disposal*). Petrophysical trends of the four key wells are further discussed in Section 2.7.2. *Petrophysics*.


Claimed as PBI

2.6.2.1. Analog Well: Ohio Liquids Disposal (UWI 34143202370000)

The Ohio Liquids Disposal well in Sandusky County, OH, was drilled in a similar geologic setting, and has correlative stratigraphy, to that expected at the Maple Project site. As such it is considered an analog well for the project site. Vickery Environmental, Inc. (1989; 2020) provides a detailed mineralogic and petrographic analysis of the injection and confining strata found in wells at the Sandusky County disposal site (Figure 39). The ranges of x-ray diffraction (XRD) mineralogy (quartz, potassium (K-) feldspar, dolomite, clay) for Mt. Simon Sandstone from all wells at the Ohio Liquids Disposal site are presented below in Table 5. The described mineralogy is also used as input for geochemical modeling (Section 2.10. *Geochemistry*).

Table 5: Mt. Simon Sandstone XRD mineralogy ranges reported from the Ohio Liquids Disposal site (Vickery Environmental, Inc., 1989; Vickery Environmental Inc., 2020).

Mineral	Formation	Composition Range
Quartz	Mt. Simon Sandstone	24% to 92%
K-feldspar	Mt. Simon Sandstone	6% to 55%
Dolomite	Mt. Simon Sandstone	2% to 36%
Clay	Mt. Simon Sandstone	< 3%

At the Ohio Liquids Disposal site, the moderately well-sorted, very fine to coarse, subangular to rounded sandstone of the Mt. Simon Sandstone is primarily composed of quartz, K-feldspar, and dolomite, with pinkish beds containing more feldspar. In general, quartz grains are larger and rounder than the feldspar grains, which show significant dissolution features and are associated with zones of slightly higher gamma API values and increased porosity (Section 2.7.2. *Petrophysics*). Clays are concentrated along laminations and are both detrital and autochthonous (Figure 39; Vickery Environmental, Inc., 1989). Quartz (including overgrowth) is the dominant cement throughout the Mt. Simon Sandstone. Dolomite cement occurs within the top half of the sandstone, is variable, and is both grain-replacing and pore-filling near the top of the formation (Vickery Environmental, Inc., 1989). The average effective porosity and permeability for the Mt. Simon Sandstone in the Ohio Liquids Disposal well are 15% and 47 millidarcy (mD), respectively.

The Rome Formation is described as a dolomitic packstone/wackestone with argillaceous laminations throughout the formation in the Ohio Liquids Disposal site. In this well, the Rome Formation has average porosity and permeability values of 5% and 0.4 mD (Figure 39). Sandy beds are more common in the middle of the formation. Thin-section analysis of the Rome Formation shows that the upper and lower intervals are composed of packstones, wackestones, and grainstones that have been pervasively dolomitized resulting in complete replacement of original carbonate grains which has significantly reduced porosity and permeability. Sandier layers in the middle of the Rome Formation also have been extensively dolomitized. Pores in the carbonate lithologies are primarily intragranular, moldic, and described as ‘very poorly connected’ with permeability values less than 1 mD (Figure 39; Vickery Environmental, Inc., 1989).

The Conasauga Formation has a range of interbedded lithologies, ranging from dolomitized, fine-grained sandstone, glauconitic sandstone and siltstone, wavy-bedded shale, and dolomitized mudstone (Vickery Environmental, Inc., 1989). In the Ohio Liquids disposal well, the Conasauga Formation has average porosity and permeability values of 12% and 13 mD, respectively. Visible porosity is negligible in the layers with dolomitic cement and clay laminations. The middle Conasauga Formation may have sandstone beds with increased porosity and permeability that are bound by tight dolomitized beds. In general, the mudstone of the Conasauga Formation is pervasively dolomitized and has very little permeability (Figure 39; Vickery Environmental, Inc., 1989).

Claimed as PBI

The mineralogic/petrographic data and cementation patterns reported by Vickery Environmental, Inc., (1989 and 2020) suggest that four distinct stages of diagenesis (following burial compaction) affected the Mt. Simon Sandstone, the Rome Formation, and the Conasauga Formation, though the extent to which the rocks were affected by diagenesis varies based on primary mineralogy:

- Grain-coating chlorite,
- Quartz/feldspar overgrowth cementation,
- Extensive dolomitization and replacement of primary carbonate grains, and
- Feldspar dissolution.

The order of diagenetic events is supported by the fact that dolomite cement envelopes the quartz/feldspar overgrowth cement, which in turn covers grains coated in chlorite (Vickery Environmental, Inc., 1989). However, the dolomitic cement is not found in beds with secondary pores created by feldspar dissolution in the Mt. Simon Sandstone and Conasauga Formation. This suggests that the dolomitization of some Mt. Simon Sandstone beds and the extensive dolomitization of the Rome and Conasauga Formations occurred after continued burial and compaction but before feldspar dissolution. The Mt. Simon Sandstone has the highest porosity in intervals that have experienced significant feldspar dissolution, as suggested by the increased gamma values and relatively high porosity and permeability values, and the lowest porosity is in thin beds that have been dolomitized near the top of the sandstone (Vickery Environmental, Inc., 1989).

The Rome Formation experienced extensive dolomitization and thus has poorly connected intragranular, moldic, and vuggy pores. The dolomitized grainstones in the upper and lower portions of the Rome Formation have less porosity than the middle, sandier interval of the Rome Formation. The Conasauga Formation at the Ohio Liquids Disposal site field also experienced extensive dolomitization, which reduced porosity.

2.6.3. Mt. Simon Sandstone (Injection Zone)

The Mt. Simon Sandstone is present across western Ohio and can be correlated regionally as shown in the cross sections in Figure 7 and Figure 9. Reservoir characteristics for the Mt. Simon Sandstone in the Knox High, Shidler James 2, BP Chemical 2, and Ohio Liquid Disposal wells are described below and their log-derived effective porosities and permeabilities are reported in Table 6. The Knox High and Shidler James 2 wells are both less than fifteen miles away from the project site. These wells have porosity and permeability trends similar to those described in the Ohio Liquids Disposal well (Section 2.6.2.1 *Analog Well: Ohio Liquids Disposal*).

The Knox High well (UWI 34063203600000) has 186 feet of excellent quality reservoir in the Mt. Simon Sandstone with average porosity and permeability values of around 17% and 65 mD as shown in Figure 40 and Table 6. The Shidler James 2 well (UWI 34069201390000) has 288 feet of Mt. Simon Sandstone reservoir with average porosity and permeability values of 15% and 48 mD (Figure 41). The BP Chemical 2 well has 321 feet of Mt. Simon Sandstone with average

porosity and permeability values of 15% and 48 mD (Figure 42). The Knox High and BP Chemical 2 wells do not penetrate all of the Mt. Simon Sandstone.

In the Knox High, Shidler James 2, and BP Chemical wells, the Mt. Simon Sandstone exhibits thin (approximately two to 10 feet thick), interbedded layers of sandstone with varying porosity and permeability values. Relatively high porosity beds (approximately 16 to 22%) contrast with average porosity beds (approximately 12 to 16%). The interbeds in the sandstone correlate to variations in the gamma ray API values: higher porosity intervals correspond to higher gamma ray values, and lower porosity intervals correspond to lower gamma ray values. The high gamma ray/ high porosity intervals suggest the presence of K-feldspar minerals. This interpretation is supported by the core description and mineralogical analysis of the Mt. Simon Sandstone in the Ohio Liquid Disposal and BP Chemical 2 wells (Vickery Environmental, Inc., 1989; INEOS Nitriles, 2016; Vickery Environmental Inc., 2020). The higher porosity of these layers is most likely associated with development of secondary porosity due to feldspar dissolution (Section 2.6.2. *Mineralogy, Diagenesis, Porosity, and Permeability*). The relationship among high gamma ray values, higher porosity, and arkosic (high K-feldspar) lithologies has been noted in other regional studies of the Mt. Simon Sandstone (e.g., Freiburg et al., 2016).

Bowen et al. (2011) concluded that porosity types in the Mt. Simon Sandstone in the Arches Province range from intergranular porosity, elongate and oversized pores, fracture porosity, and dissolution porosity. These authors also note that porosity does not necessarily decrease with depth. Rather it varies laterally and vertically depending on depositional facies, mineralogy, and diagenesis. Quartz and feldspar overgrowth cement, iron-bearing illitic clays, kaolinite, chlorite, iron oxides, and dolomite reduce porosity in the Mt. Simon Sandstone. In addition, Sminchak (2012) examined geophysical well logs, rock samples, drilling logs, and geotechnical tests collected from the Mt. Simon Sandstone in the Arches Province and concluded that the Mt. Simon Sandstone has sufficient porosity and permeability for large-scale injection of CO_2 into the Mt. Simon Sandstone.

Another source of vertical heterogeneity within the Mt. Simon Sandstone is the presence of relatively low porosity/ permeability streaks within the strata that is likely caused by a greater abundance of dolomite cement in these intervals. However, this effect is more pronounced in the eastern side of the Arches Province where the Ohio Liquid Disposal wells are located (Figure 38, Figure 40) and as described by Janssens (1973). The basal half of the Mt. Simon Sandstone in the BP Chemical 2 well also exhibits intervals of relatively low porosity/ permeability which correspond to relatively low gamma ray values in quartz sandstone beds. These intervals with poorer reservoir quality are likely attributed to the absence of porosity-creating feldspar dissolution (Figure 42).

Claimed as PBI [redacted]

Additional site specific information regarding the injection zone will be acquired when the project wells are drilled during the Pre-operational Testing Program and will include, but not

limited to, well logging, fluid sampling, and core acquisition and analysis (Attachment 05: Pre-operational Testing Program, 2025).

The baseline 3D surface seismic data will be calibrated to the well data and will be used to derive 3D seismic inversion datasets. This will allow the project to characterize variations in injection zone porosity and lithology away from the project wells over the imaging area of the 3D surface seismic data volume.

Claimed as PBI

Claimed as PBI

Claimed as PBI

2.6.4. Rome and Conasauga Formations (Primary Confining Zone)

2.6.4.1. Rome Formation

The strata of the Rome Formation that are part of the primary confining zone are those that occur above the Rome Silt, which is considered part of the injection zone as described in Section 2.6.1. *Injection Zone and Confining Zone Extent and Thickness* (Figure 5). The lithology of the confining strata of the Rome Formation at the Ohio Liquids Disposal field is a dolomitic packstone/wackestone with argillaceous laminations that act as barriers to vertical movement of fluid in the primary confining zone at this field (Figure 8; Vickery Environmental, Inc., 1989; Vickery Environmental Inc., 2020) (Section 2.6.2.1 *Analog Well: Ohio Liquids Disposal*). Pores are observed to be intragranular, moldic, and poorly connected having permeability values less than 1 mD (Vickery Environmental, Inc., 1989). Similar average porosity and permeability values of the confining beds of the Rome Formation are encountered in the Knox High (Figure 40) and Shidler James (Figure 41) wells (Table 7, Section 2.6.2. *Mineralogy, Diagenesis, Porosity, and Permeability*). All wells have average Rome Formation effective porosity and permeability values of 7% and less than 1 mD, respectively. The dolomitic lower and upper portions of the Rome Formation above the Rome Silt have lower effective porosity and permeability which will be discussed further in Section 2.7.2. *Petrophysics*.

The well logs and petrophysical analyses of the Rome Formation from the Knox High and Shidler James 2 wells suggest that the Rome Formation experienced similar extensive dolomitization as at the Ohio Liquids Disposal field (Figure 39, Section 2.6.2.1 *Analog Well: Ohio Liquids Disposal*; Section 2.7.2. *Petrophysics*). Dolomitization greatly reduced porosity in the Rome Formation confining strata and occurred prior to widespread porosity enhancing feldspar dissolution primarily within the Mt. Simon Sandstone. Figure 39 shows core photographs of the Rome Formation depicting the sporadic, isolated (unconnected) moldic pores that result in low average permeability values of less than 1 mD. Similar lithologic and petrophysical characteristics are expected to be encountered at the project site, although with greater argillaceous content and likely lower porosity and permeability values as the site is near the area of western Ohio where the Rome Formation and Conasauga Formation grade to Eau Claire Shale (Figure 9, Figure 15, and Figure 42; Table 7). This topic will be discussed further in Section 2.7.2. *Petrophysics*.

2.6.4.2. Conasauga Formation

The Conasauga Formation also forms part of the primary confining zone and has average porosity and permeability values at the Knox High and Shidler James 2 wells between 2 to 5% and less than 1 mD, respectively (Figure 40, Figure 41, Table 7). An approximately 40 foot thick sequence having low porosity and permeability is present in the lower half of the Conasauga Formation at Knox High well (Figure 40), and a 50-foot thick package of low porosity and low permeability strata is present in the top of the Conasauga Formation at the Shidler James 2 well (Figure 41).

The Conasauga Formation and Rome Formation grade to the Eau Claire Shale near the Ohio/Indiana border. Figure 9, Figure 39, Figure 40, Figure 41, and Figure 42 show that the gamma-ray signature of the Conasauga Formation increases from the northeast (Ohio Liquids Disposal well) to the southwest (BP Chemical 2) as indicated by the geophysical logs and petrophysical analysis discussed in Section 2.7.2. *Petrophysics*. The well log character in the Shidler James 2 and Knox High wells indicates that the Conasauga Formation has a higher clay content compared to the Ohio Liquids Disposal well.

2.6.5. Addressing Uncertainty

Vault GSL CCS LP will collect a 3D surface seismic survey and conduct a comprehensive core and logging program at the MPL INJ1 well prior to injection to characterize the injection and confining zones (Attachment 05: Pre-operational Testing Program, 2025). The site-specific data collected from MPL INJ1 will be used to update the injection and primary confining zone depths, thicknesses and petrophysical characteristics including capillary pressure measurements, using laboratory measurements such as mercury injection capillary pressure , and relative permeability curves for the site. The calibrated logs also will be used to update the seismic well tie for seismic interpretation. These data will be used to calibrate and reduce uncertainty within the static and computational models (Attachment 02: AoR and Corrective Action Plan, 2025).

2.7. Geomechanical and Petrophysical Information [40 CFR §146.82 (a)(3)(iv)]

2.7.1. Geomechanics

A 42-layer geomechanical model was constructed to test the integrity of the confining zone at the Maple Project site. Average values of Young's Modulus, Poisson's Ratio, and bulk compressibility were calculated for the injection zone and the lower portion of the primary confining zone, the Rome Formation, using data from the Knox High well (Figure 8, Figure 38, Figure 43, and Table 8). The Rome Formation was divided into three separate sub-units (A, B, and C) based on the petrophysical analysis (Section 2.7.2. *Petrophysics*). Average values of total closure stress (TCS) and pore pressure are shown in Table 9. The large difference between the TCS and the pore pressure indicates that there is a sufficient buffer that will allow a significant injection rate to occur without opening existing fractures. The geomechanical model predicts that fracturing will not occur in the Mt. Simon Sandstone injection zone or the Rome Formation portion of the primary confining zone at the planned injection rate of 359 ktpa. In addition, fracturing does not occur at three times the operational injection rate (1,077 ktpa). As fractures at the planned injection rate are not projected to occur in the Rome Formation, the overlying Conasauga Formation was not included in the model.

Figure 43 is a log with the calculated geomechanical properties, including bulk compressibility, Poisson's ratio, Young's modulus (dynamic and static), overburden stress, and TCS, calculated on 0.5-foot intervals, based on a log analysis using data from the Knox High well. These geomechanical data were then used to model the integrity of the Rome Formation portion of the primary confining zone with an anticipated injection rate of 359 ktpa into the Mt. Simon Sandstone.

Claimed as PBI

Claimed as PBI

During the Pre-Operational Testing program, a variety of site-specific data from the injection and primary confining zones will be acquired in the project wells to support further geomechanical modeling as per 40 CFR §146.82(a)(3)(iii) and §146.82(a)(3)(iv). Information on the core testing that will provide ductility information for the injection and confining zones are provided the Pre-Operational Testing Program (Attachment 05: Pre-operational Testing Program, 2025). These data include:

- Caliper, dipole sonic, and image logs,
- Triaxial testing to establish geomechanical parameters such as rock strength, ductility, Young's Modulus, Poisson's Ratio, and fracture gradient,
- Step-rate tests and pressure transient analyses,
- In situ stress information, including measurements or determinations of vertical stress, maximum horizontal stress, and minimum horizontal stress, and
- Capillary pressure measurements on core samples from both injection zone and confining zone strata.

2.7.2. Petrophysics

Petrophysical analysis of the Mt. Simon Sandstone, the Rome Silt, the Rome Formation, and the Conasauga Formation was completed using the four key wells in Figure 38 and Table 10. These petrophysical analyses were used to evaluate the characteristics of the primary confining and injection zones (Figure 44, Figure 45, Figure 46, Figure 47, and Figure 48). For the analyses, LAS files and routine core data were acquired from the Ohio State Geological Survey. Geophysical well logs, core plugs, and well test data were used to calibrate the petrophysical calculations to derive effective porosity and permeability (Section 2.6.2 *Mineralogy, Diagenesis, Porosity, and Permeability*). These analyses will be re-visited once the project acquires site-specific well logs and core data in the project wells (Attachment 05: Pre-operational Testing Program, 2025).

Core and log data were calibrated to well test data that was publicly available from the Ohio Liquids Disposal and BP Chemical 2 wells (Figure 39 and Figure 42; INEOS Nitriles, 2016; Vickery Environmental Inc., 2020). Porosity and permeability cross plots and histograms were made using this data which enabled better analysis of wells that did not have core data and improved the static model (Figure 44, Figure 45, and Figure 46). The Knox High and Shidler James 2 are the closest wells with geophysical logs to the project site and were the primary focus of this petrophysical analysis.

Pre-processing work on the raw log data, including depth shifting, unit conversion, and synthetic log generation, was performed prior to the petrophysical calculations. Gamma, neutron porosity, sonic, PE, and density logs were used to derive the petrophysical properties for the four key wells, which included:

- Effective porosity,
- Permeability,
- Mineralogy (where data quality was reliable),
    - Volume Shale (VSH_V),
    - Volume Quartz (Quartz_V),
    - Volume Limestone (Limestone_V),
    - Volume Dolomite (Dolomite_V),
    - Volume Sphalerite (Sphalerite_V),
    - Precambrian (Basalt_V),
    - Bound Water (BVW_V).

Table 11 and Table 12 summarize porosity and permeability values, respectively, as determined from nearby geophysical well logs (Figure 38; Section 2.6.2. *Mineralogy, Diagenesis, Porosity, and Permeability*) that were calibrated using data from core and testing in the Mt. Simon Sandstone, the Rome Formation, and the Conasauga Formation. The petrophysical values were incorporated into the static model for the Maple Project site (Attachment 02: AoR and Corrective Action Plan, 2025). For the Mt. Simon Sandstone, the four key wells all have average porosity

and average permeability values that range from 15-17% and 47-65 mD. The Knox High well has the highest Mt. Simon Sandstone porosity and permeability averages (17% and 65 mD; Table 11 and Table 12), though this well does not penetrate into the Precambrian Basement. The effective porosity/permeability cross plots (Figure 44), effective porosity histograms (Figure 45), and permeability histograms (Figure 46) indicate that Mt. Simon Sandstone and Rome Silt have higher porosity and permeability values compared to the Rome Formation and Conasauga Formation.

The resulting porosity and permeability petrophysical logs for these four key wells show that the Mt. Simon Sandstone is primarily composed of interbedded higher porosity/permeability and average porosity/permeability sandstone intervals. These porosity and permeability contrasts are likely due to the development of secondary porosity and inhibition of cementation due to the presence of K-feldspar in the beds that exhibit high gamma ray values (Figure 47 and Figure 48; Section 2.6.2. *Mineralogy, Diagenesis, Porosity, and Permeability*; Janssens, 1973; Vickery Environmental, Inc., 1989; Vickery Environmental Inc., 2020).

The Rome Formation has lower average effective porosity and permeability values compared to the Mt. Simon Sandstone and the well log signatures are more variable than in the underlying Mt. Simon Sandstone (Figure 47 and Figure 48). To investigate porosity and permeability trends in the Rome Formation, it was subdivided into three sub-units based on the Knox High and Shidler James 2 geophysical log analysis: A (base), B (middle), and C (top) (Figure 47, Figure 48, and Table 13). The A and C sub-units are heavily dolomitized and have significantly reduced porosity that is not interconnected as evidenced by permeability values of <0.1 mD. Unit B has higher clastic content and lower dolomite content, as a result it has average porosity values of 8 to 9%. However, the permeability values are < 1 mD that suggests that pores are not interconnected in the B sub-unit (Figure 47 and Figure 48).

The Rome Formation at the Knox High and Shidler James 2 wells have over 166 feet and 206 ft, respectively, of microcrystalline dolomite with permeability of generally less than 1 mD that overlies the Rome Silt (Figure 47, Figure 48, and Table 13). Though porosity values vary within the Rome Formation in relation to dolomite content, permeability values indicate pores are not connected, which is consistent with the description of the Rome Formation at the Ohio Liquids Disposal well (Vickery Environmental, Inc., 1989; Vickery Environmental Inc., 2020).

The Knox High and Shidler James 2 wells also have 115 and 192 feet, respectively, of low average permeability (<1 mD) Conasauga Formation that is the upper portion of the primary confining zone. The Conasauga Formation increases in clay content to the southwest as it grades to the Eau Claire Shale near the Ohio/Indian border. This results in lower permeabilities in the Knox High, Shidler James 2, and BP Chemical 2 wells as compared to the Ohio Liquids Disposal Well (Figure 9, Figure 39, Figure 42, Figure 47, Figure 48, and Figure 49).

Figure 49 displays the lateral continuity of the Rome Formation in the four key petrophysical wells. The transition from deeper marine clastics of the Eau Claire Shale in the west (BP Chemical 2 well) to shallower-water Conasauga Formation dolostones and tightly cemented dolomitic clastics to the east in wells on the Findlay Arch (Knox High, Shidler James 2, and Ohio Liquids Disposal wells) is also shown in Figure 49. Though shale content decreases from

west to east in Figure 49, the integrity of the Rome Formation and Conasauga Formation primary confining zone is maintained by the impermeable dolomites and dolomitic clastic facies at the project site (Figure 47 and Figure 48).

The porosity and permeability values reported for the Knox High and Shidler James 2 wells in Figure 47 and Figure 48 show that the Rome and Conasauga Formations contain impermeable dolostone and dolomitic clastics in the Rome A and Rome C subunits. The Rome B subunit is a more porous interval present between the Rome A and Rome C subunits in the middle of the Rome Formation (Figure 47, Figure 48, and Figure 49). The average Rome B permeability in both the Knox High and Shidler James 2 wells is less than 1 mD and indicates that the pores are not well connected (Figure 47 and Figure 48). The Rome and Conasauga Formations have been mapped both regionally throughout western Ohio and locally with 2D seismic profiles acquired specifically for the Maple Project. The Rome B subunit, as well as the Conasauga Formation, becomes more permeable east of the Bowling Green Fault in northern Ohio (Figure 49). Within the project area, the Rome B facies is expected to have low permeability and is bounded by the impermeable dolostones of the Rome A and Rome C, which are laterally extensive and continuous (Figure 49). At the Maple Project site, the entire thickness of the Rome Formation is prognosed to be 142 feet thick, with 69 feet of tight dolostone in the Rome A and Rome C subunits. The Rome A, B and C subunits are continuous and were mapped and incorporated into the geocellular model. This succession of impermeable Rome and Conasauga dolostones will provide a highly competent primary confining zone at the Maple project site.

The competence of the Rome Formation and Conasauga Formation primary confining zone is additionally demonstrated at the Ohio Liquids Disposal well field (Figure 39 and Figure 49) (Vickery Environmental, Inc., 1989; Vickery Environmental Inc., 2020), where fluid is injected and contained within the Mt. Simon Sandstone. In this field, there is no pressure communication between the Mt. Simon Sandstone and the top of the Kerbel Formation, as measured by a monitoring well (Vickery Environmental Inc., 2020). In the Ohio Liquids Disposal well shown in Figure 39, the combined thickness of the Rome and Conasauga formations is approximately 300 feet, and there is 64 feet of tight dolostone within the Rome A overlying the Mt. Simon Sandstone. The Rome C subunit has also been cored in this field and described in Figure 39, and the impermeable nature of the Rome and Conasauga formations is evident in core descriptions and permeability measurements.

The Precambrian Basement underlying the project site is located near to the suture between the Eastern Continental Rift System (ECRS) and the Grenville Province. In this area the basement rocks may be crystalline or the Middle Run Formation which are dominantly arkosic sands and conglomerates related to rift basins. Because of their age and depth of burial, rocks of the Middle Run Formation have low porosity and negligible permeability as reported by Shrake (1991). Neither crystalline or Middle Run basement rocks have significant porosity and permeability so that fluid flow within these units is negligible and any pressure communication with the overlying Mt. Simon Sandstone will be limited.

Cumulative shale and siltstone thickness was calculated for the Knox High well (Figure 38 and Figure 40) using a combination of gamma and Vshale geophysical log cutoffs (gamma > 60 API; Vshale > .25), and density derived facies (shale or siltstone). Average porosities were calculated

from a combination of neutron porosity, density porosity, and effective porosity logs. This method shows that there are approximately 81 feet of cumulative shale/siltstone within the primary confining zone. Above the primary confining zone, there is a cumulative shale/siltstone thickness of 750 feet.


Claimed as PBI

Claimed as PBI


Claimed as PBI


Claimed as PBI

Claimed as PBI

Claimed as PBI

Claimed as PBI

Table 14: Formation, rock type, thickness (feet), depth (feet), average porosity, average permeability, interbedded shale/siltstone thickness (feet), and cumulative shale/siltstone thickness at the Knox High well (Figure 38 and Figure 47). Shale/siltstone thickness was calculated using a combination of a gamma cutoff (>60 api), Vshale (Vshale>.25), and density derived facies (shale and siltstone).

Formation/Member	Rock Type	Thickness (feet)	Depth to top MD (feet)	Average Porosity (%)	Estimated average permeability (mD)	Interbedded Shale/Siltstone Total Thickness (feet)	Cumulative Shale/Siltstone Thickness (feet)	Characteristic
Lockport	Dolostone	128	385	31	N/A	0	0	Lowermost USDW
Packer Shell	Limestone	94	513	33	N/A	1	1	N/A
Queenston/Maquoketa/Utica	Shale	804	607	3	N/A	713	714	Confining
Trenton	Dolostone/Limestone	644	1,411	2	NA	23	737	N/A
Gull River/Glenwood Shale	Dolostone/Limestone/Shale	40	2,055	2	N/A	5	742	Confining
Trempealeau	Dolostone	332	2,095	2	N/A	5	747	N/A
Kerbel	Sandstone	78	2,427	7	0.20	3	750	ACZ Monitoring
Conasauga	Shale/Dolostone	114	2,505	4	0.08	31	781	Primary Confining
Rome	Dolostone	166	2,619	7	0.02	50	831	Primary Confining
Rome Silt	Siltstone	39	2,785	9	5.03	15	846	Injection
Mt. Simon Sandstone	Sandstone	220	2,824	15	64	11	857	Injection
Precambrian	Sedimentary/Crystalline	N/A	3,044	N/A	N/A	N/A	N/A	N/A

2.7.3. Addressing Uncertainty

The core and logging program for MPL INJ1 is designed to provide a comprehensive dataset and reduce uncertainty at the Maple Project site (Attachment 05: Pre-operational Testing Program, 2025). Triaxial compression and rock compressibility tests will be performed to characterize Young's modulus, Poisson's ratio, rock strength, compressibility, and ductility, and in-situ fluid pressures will be assessed with downhole logging. These calculations will be incorporated into existing geomechanical analyses and updates will be made as needed.

As previously stated in Section 2.5.3. *Tectonic Stability*, image logs from MPL INJ1 will be used to characterize fractures at the Maple Project site. Additionally, step rate tests will be performed to determine fracture opening pressure, fracture propagation pressure, and fracture closure pressure in the injection zone. These tests and logs will be used to update primary stress fields and fracture gradient calculations at the Maple Project site.

2.8. Seismic History [40 CFR §146.82(a)(3)(v)]

Based on Federal Emergency Management Agency (FEMA) classification the Maple Project site has a very small probability of experiencing damaging earthquake effects. The site is more than 375 miles northeast of the Strongest Shaking Zone E associated with the New Madrid Seismic Zone (Figure 50).

The project site is more than 25 miles north of the Anna Seismic Zone, which is a small seismic zone with moderately frequent though episodic earthquakes (Dart and Hansen, 2008). Some earthquakes within the Anna Seismic Zone coincide with known faults (i.e., Anna-Champaign Fault; Figure 20), and there is no paleo seismological evidence for significant post-Paleozoic activity (Dart and Hansen, 2008).

Seismic activity in Ohio is monitored and recorded by both the national Earthquake Hazard Program and the Ohio Seismic Network (OhioSeis). OhioSeis monitors seismic activity from its network of seismograph stations located throughout the state; stations are concentrated in the most seismically active areas or where conditions are best for detection of small earthquakes. The United States Geological Survey (USGS) Earthquake Hazard Program records earthquakes having a magnitude of 1.0 or greater and is augmented with OhioSeis stations.

Figure 51 displays all of the earthquakes recorded by USGS since 1800 with a magnitude of 1.0 or greater and all seismic activity recorded by OhioSeis within a 100-mile radius of the Maple Project site; these are also listed in Appendix 1C – *Seismic Events* The largest earthquake within this 100-mile radius occurred in 1937 approximately fifty miles southwest of the project site with a magnitude of 5.4 Mw (USGS, 2025). The most recent earthquake occurred on 29 December 2024 approximately 42 miles west of the project site and had a magnitude of 2.9 mb_lg (a short period surface wave) ("OhioSeis," 2025). No earthquakes have been recorded that have an epicenter within the project AoR (Appendix 1C – *Seismic Events*).

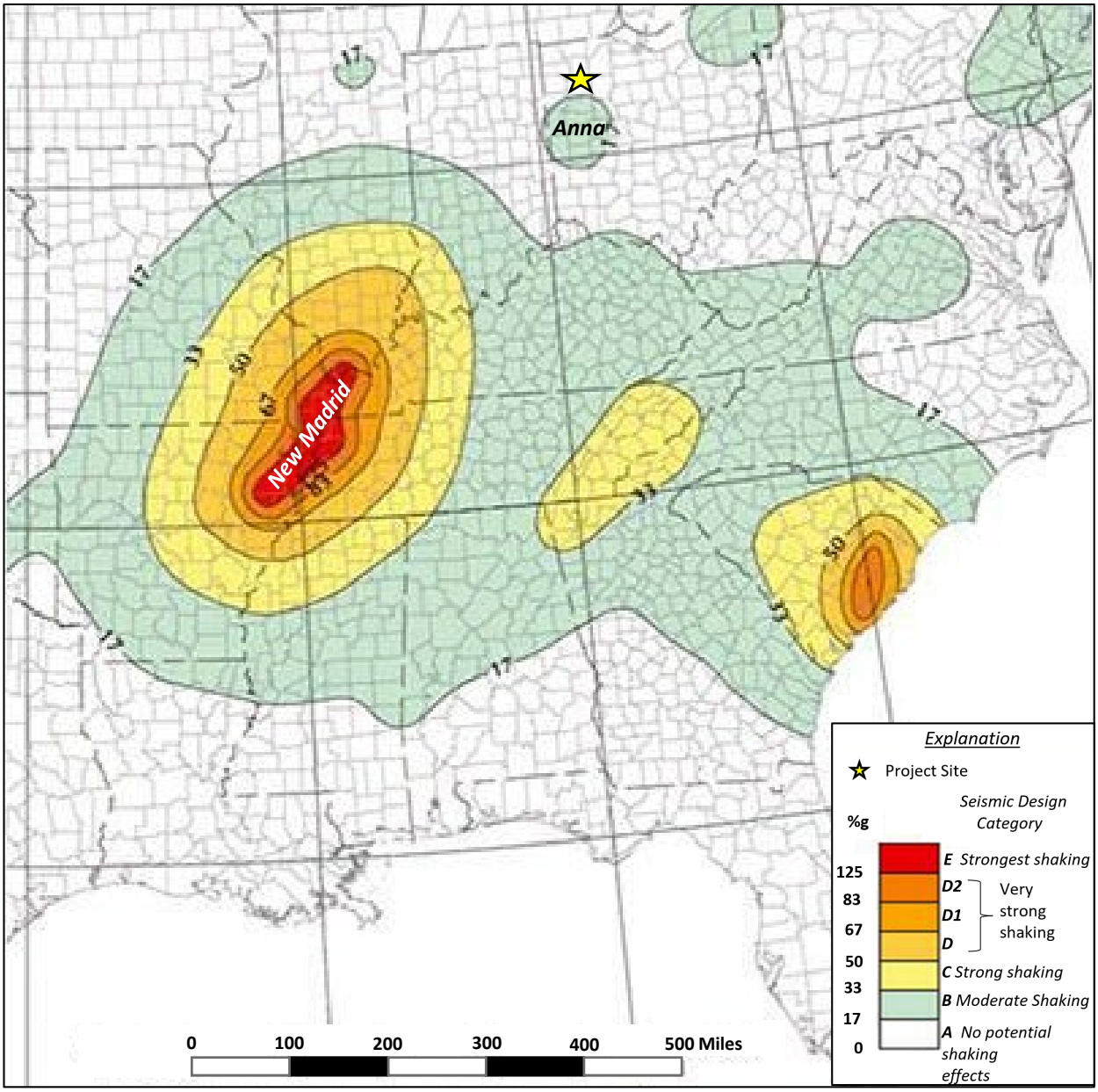

Figure 50: FEMA Earthquake Hazard Map shows that the project site (yellow star) is located in the lowest earthquake hazard category A and just north of the Anna Seismic Zone, which is in Zone B. The New Madrid Seismic Zone is in Zone E and is approximately 300 miles away from the project site.

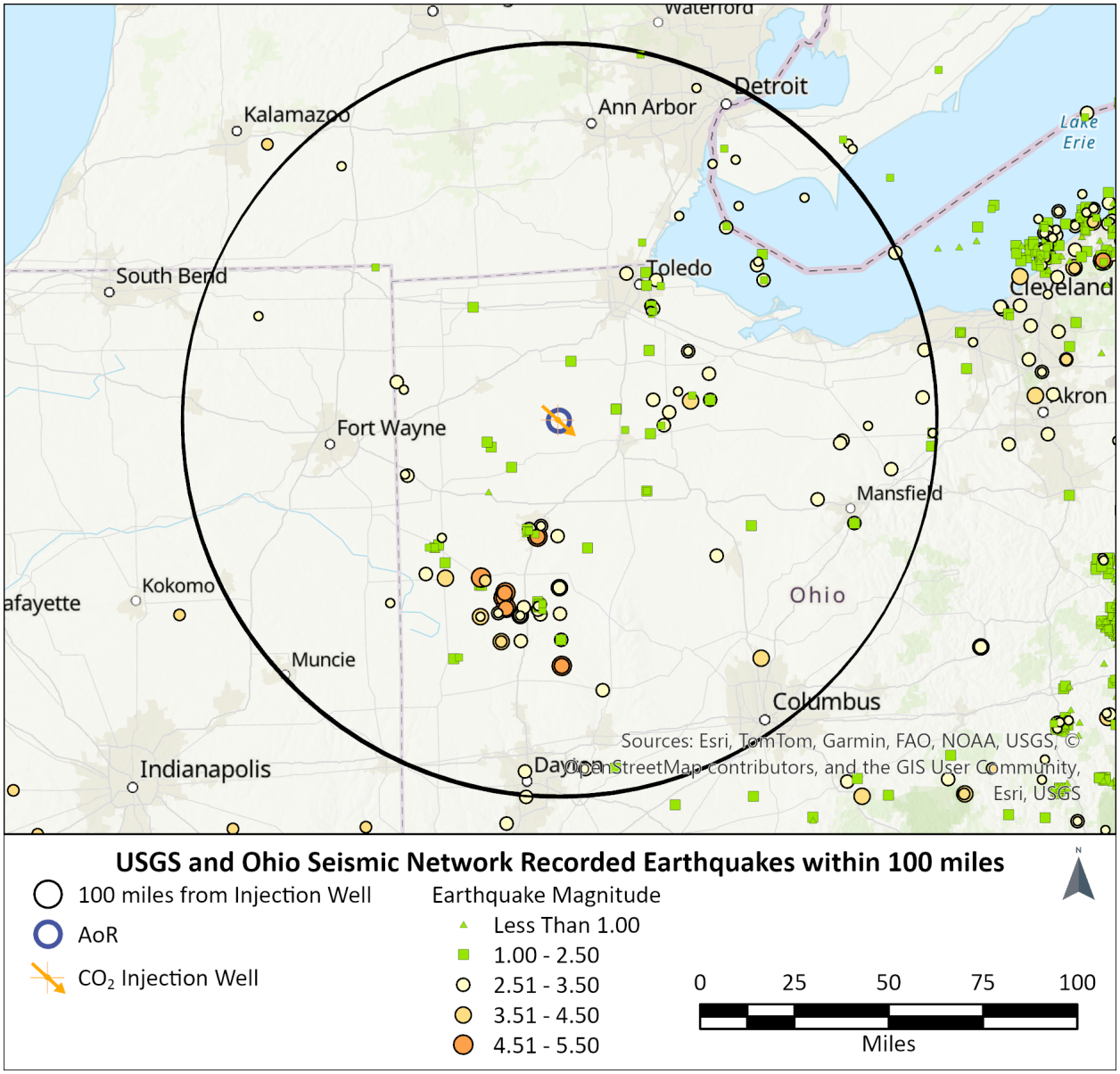

Figure 51: Map showing the epicenters of earthquakes that occurred between 1 January 1800 and 3 July 2025 within 100 miles (black circle) of the Maple AoR. (USGS, 2025; "OhioSeis," 2025).

2.9. Hydrologic and Hydrogeologic Information [40 CFR §146.82(a)(3)(vi), 40 CFR §146.82(a)(5)]

A USDW is defined by the EPA as an aquifer that (40 CFR §146.3):

- Supplies any public water system,
- Contains a sufficient quantity of groundwater to supply a public water system; and
    - Currently supplies drinking water for human consumption, or
- Contains fewer than 10,000 milligrams per liter (mg/L) total dissolved solids (TDS),
- Is not an exempted aquifer.

The following sections provide information regarding available USDW resources and delineation of the lowermost USDW, which is the base of the Silurian Lockport Dolomite at the project site. Water well, monitoring well, and dry well records were collected for the project AoR from the ODNR Division of Geological Survey.

A total of 153 shallow water wells are located within the AoR and there are no known springs within the AoR (Figure 21). Over 40 wetlands, identified through satellite imagery, are located within the AoR (Figure 60) The 153 water wells within the AoR have total depths ranging from 45 to 535 fbgl with an average depth of 181 fbgl. Shallow USDW sources occur in the unconsolidated glacial sediments overlying Silurian bedrock, but the primary shallow USDW within the AoR occurs within the Salina Group dolomites. Publicly available information does not clearly identify which formation within the Salina Group the 153 wells are drawing water from. The AoR and Corrective Action Plan includes a detailed discussion of the number and locations of the shallow groundwater wells within the AoR (Attachment 02: AoR and Corrective Action Plan, 2025).

2.9.1. Local Hydrology

The study site is located within the Lower Maumee sub-basin of the Ohio portion of the Lake Erie Watershed. This watershed drains rural, agricultural land and communities across northern Ohio (Figure 52). The study site is located near Brush Creek, which is part of the Lower Maumee sub-basin.

There are two main sources of shallow groundwater in Putnam County, Ohio:

1) Woodfordian unconsolidated valley fill, moraine, and other glacial deposits, and
2) Silurian carbonates including the Salina Group and the Lockport Dolomite of the Lockport Group (Calhoun, 1992; Figure 5 and Figure 47).

The area within and surrounding the Maple Project site primarily utilizes the aquifers of the thick, well- sorted, permeable sand and gravel of the Defiance Moraine aquifer and Silurian carbonate bedrock (Salina Group and Lockport Dolomite).

2.9.2. Near Surface Aquifers

During the Pleistocene Epoch, Ohio experienced several glacial intervals, and glacial sediments were deposited on top of the Paleozoic bedrock throughout much of the state except in the southeast portion. These glacial deposits affect surface hydrology and aquifers in the region with 600 to 700 feet of till, drift, lake, and valley fill sediment in northern areas of the state. Specifically, the Maple Project AoR is within glacial deposits composed of till, drift, loam, and outwash associated of the Wisconsinan Woodfordian lake-planed moraine and associated beach sand deposits (Figure 53 and Figure 54) where less than 100 feet of moraine deposits (Figure 55) overlie the Silurian-aged Salina Group bedrock (Figure 56).

The sand and gravel of the Defiance Moraine aquifer tend to be interbedded with glacial till, and domestic wells typically yield between 25 to 100 gallons per minute (Figure 57). Due to depositional variations within this glacial system, this aquifer is not continuous across the county and flow patterns are localized (Calhoun and Orr, 1992). If water well drillers do not penetrate a sufficient thickness of permeable unconsolidated Woodfordian aquifer in Putnam County, wells are drilled deeper into the Salina Group and the Lockport Dolomite (Calhoun,1992).

The Defiance Moraine glacial deposits are expected to be less than 100 feet thick at the Maple project site (Figure 55) These sediments are underlain by approximately 400 feet of carbonates and evaporites of the Salina Group, which in turn are underlain by 139 feet of Lockport Dolomite (Figure 56). The Maple Project site is located where water wells are drilled through the Defiance Moraine deposits and into the Silurian bedrock due to low yield (less than 10 gallons per minute). Water wells drilled into the Salina Group to depths exceeding 255 feet may produce yields in excess of 50 gallons per minute. However, hardness and sulfur content in the Silurian bedrock aquifer may deter use (Figure 57; Calhoun,1992).

The primary near surface aquifer at the Maple Project site is the Salina Group carbonates. Groundwater within the Silurian bedrock is sourced from joints, fractures, bedding planes and solution channels (Casey, G.D., 1994; Eberts, S.M. and George, L.L., 2000). The depth to water-bearing zones, even within the AoR, is highly variable.

Studies on the regional groundwater flow direction do not differentiate individual units but rather group aquifers based on rock type. The regional groundwater flow direction for carbonate aquifers, which includes the Salina Group and Lockport Dolomite, is generally from drainage divides towards the major streams and Lake Erie, with a major component of horizontal flow across surface water divides (Norris, S.E. and Fidler, R.E., 1971; Bugliosi, E.F., 1990). Near the Maple Project site area, groundwater generally flows to the north-northeast towards Lake Erie (Norris, S.E. and Fidler, R.E., 1971; Eberts, S.M. and George, L.L., 2000).

The Ohio EPA Division of Drinking and Groundwater maintains the Ambient Ground Water Monitoring Network as part of an effort to characterize general water quality conditions across Ohio (Ohio EPA). There is one monitoring well approximately 11 miles northeast of the AoR that penetrates unconsolidated sand and gravel and a total depth of 74 feet deep and has TDS concentrations of 946 mg/L.

2.9.3. Addressing Uncertainty

Of the 153 water wells within the AoR, 151 are inferred to have primarily been drilled into the shallow glacial deposits and Salina Group Silurian bedrock (Figure 21). Due to the complexity of glacial geology, the groundwater resources of the Defiance Moraine within the AoR are poorly constrained at the Maple Project site. To reduce the uncertainty of the depth to the base of the glacial deposits, the Salina Group, and the Lockport Dolomite, as well as their relative thicknesses within the AoR, the lithology will be logged and depth to water noted during the drilling of the MPL USDW1, MPL ACZ1, MPL INJ1 and MPL OBS1 wells.

Figure 52: Map of the Lake Erie watershed with individual drainage basins within the watershed.

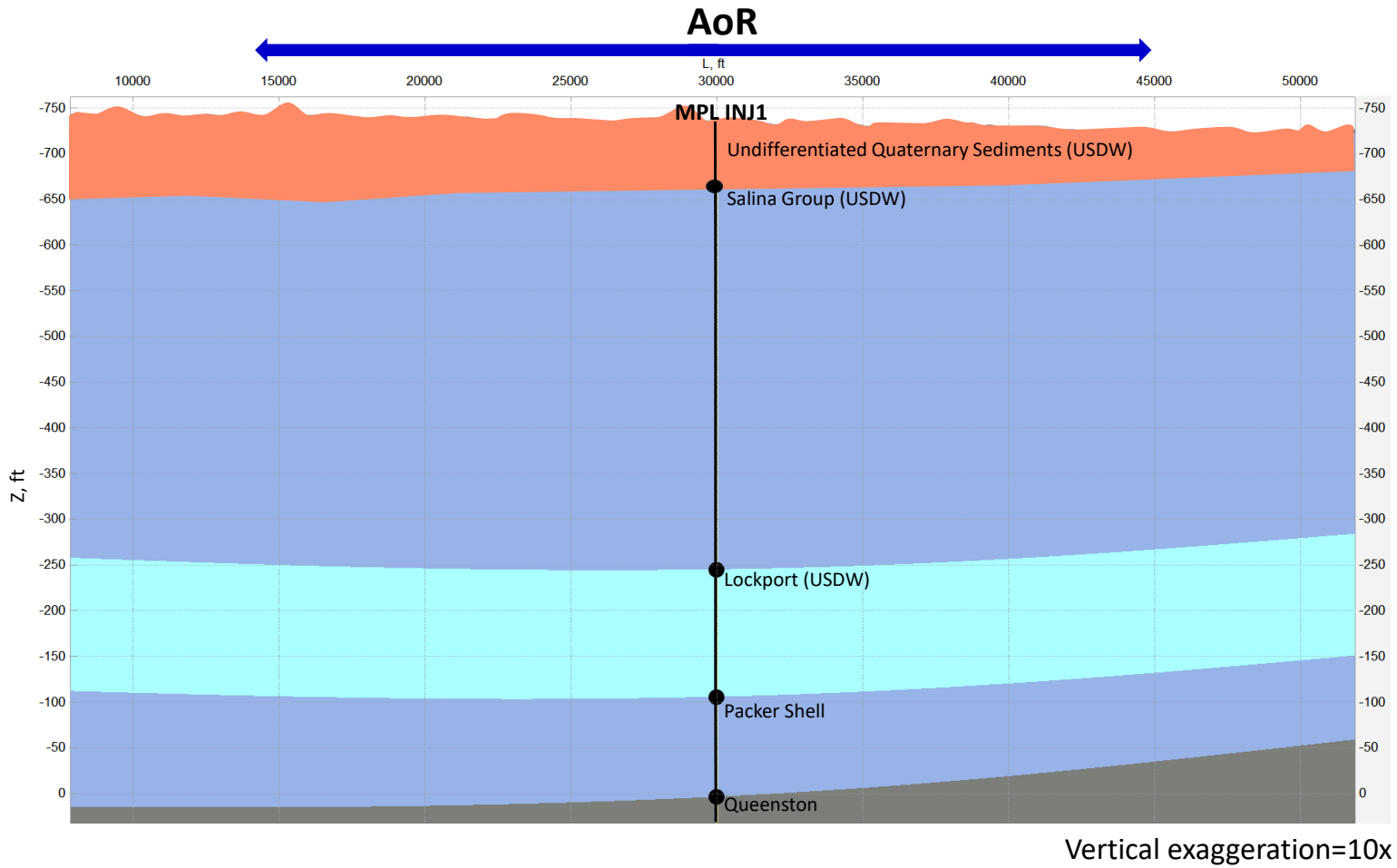

Figure 53: West to east cross section of the shallow hydrostratigraphy in the AoR. See Figure 7 for location. Depth is in fbsl and vertical exaggeration= 10x.

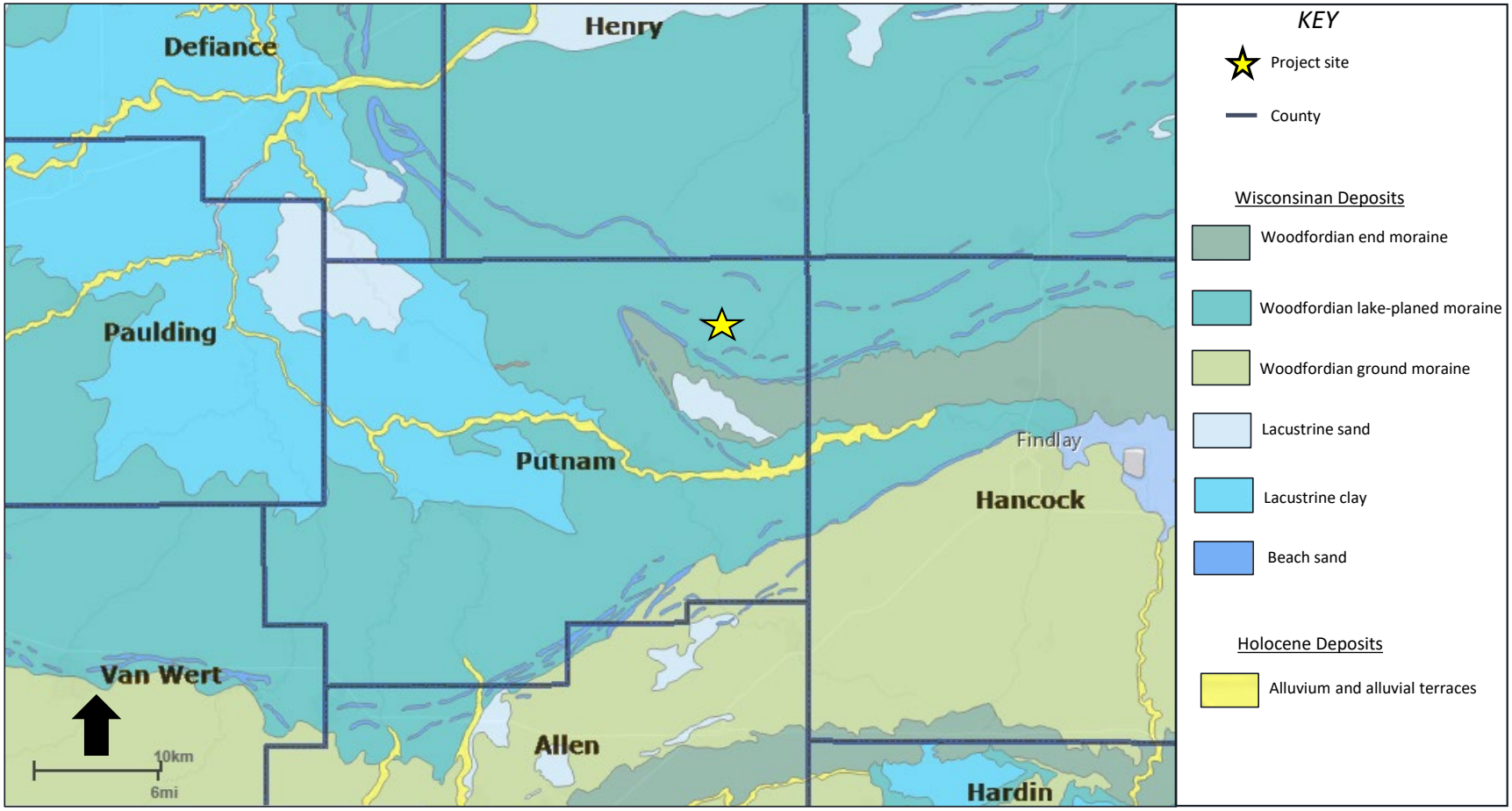

Figure 54: Map of Ohio glacial deposits shows that the Maple Project site is located on glacial deposits composed of till, sand, and gravel. Modified from ODNR Ohio Geology Interactive Map (ohiodnr.gov).

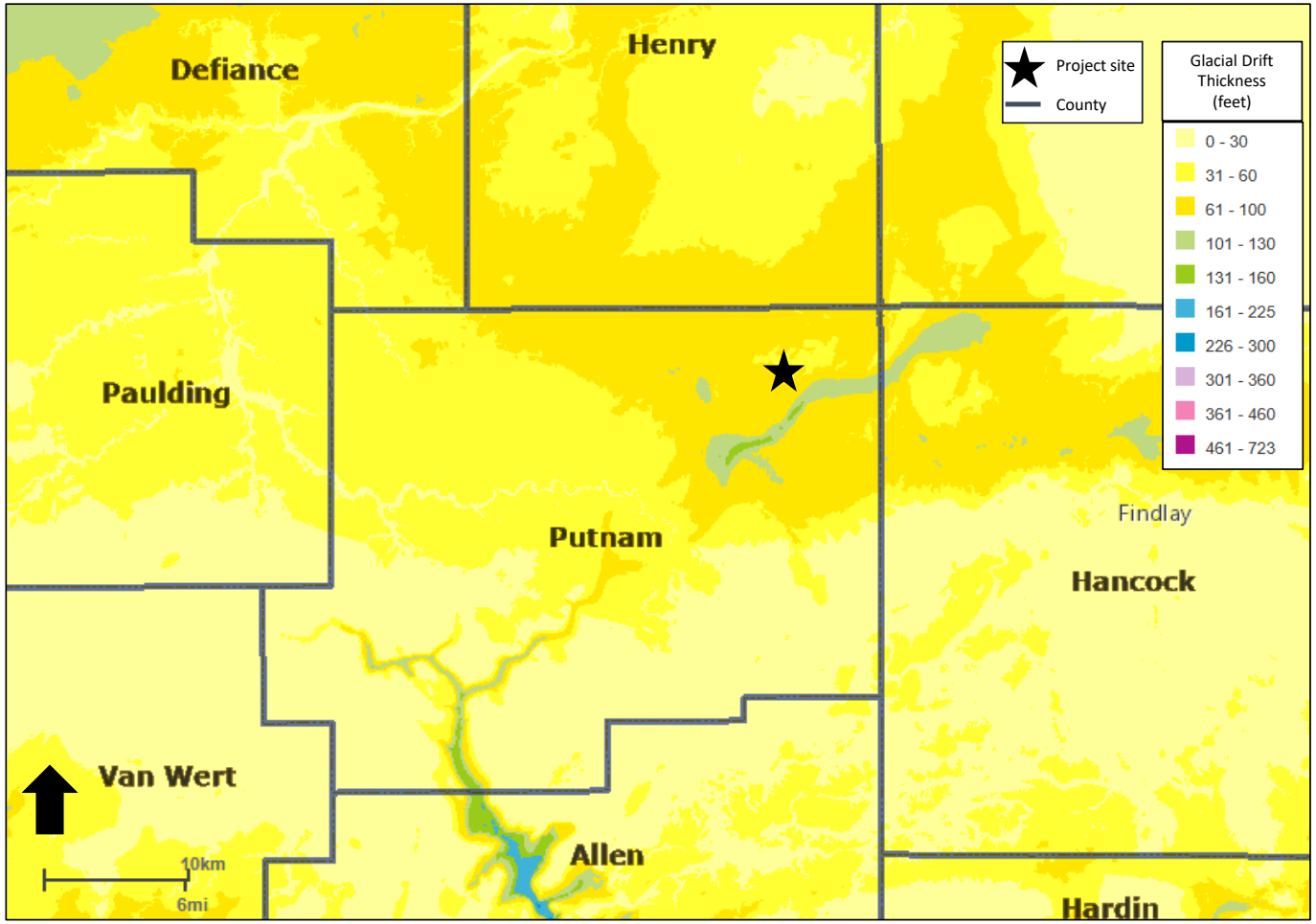

Figure 55: Map of glacial drift thickness in feet. At the project site, less than 100 feet of glacial drift are expected. Modified from ODNR Ohio Geology Interactive Map (ohiodnr.gov).

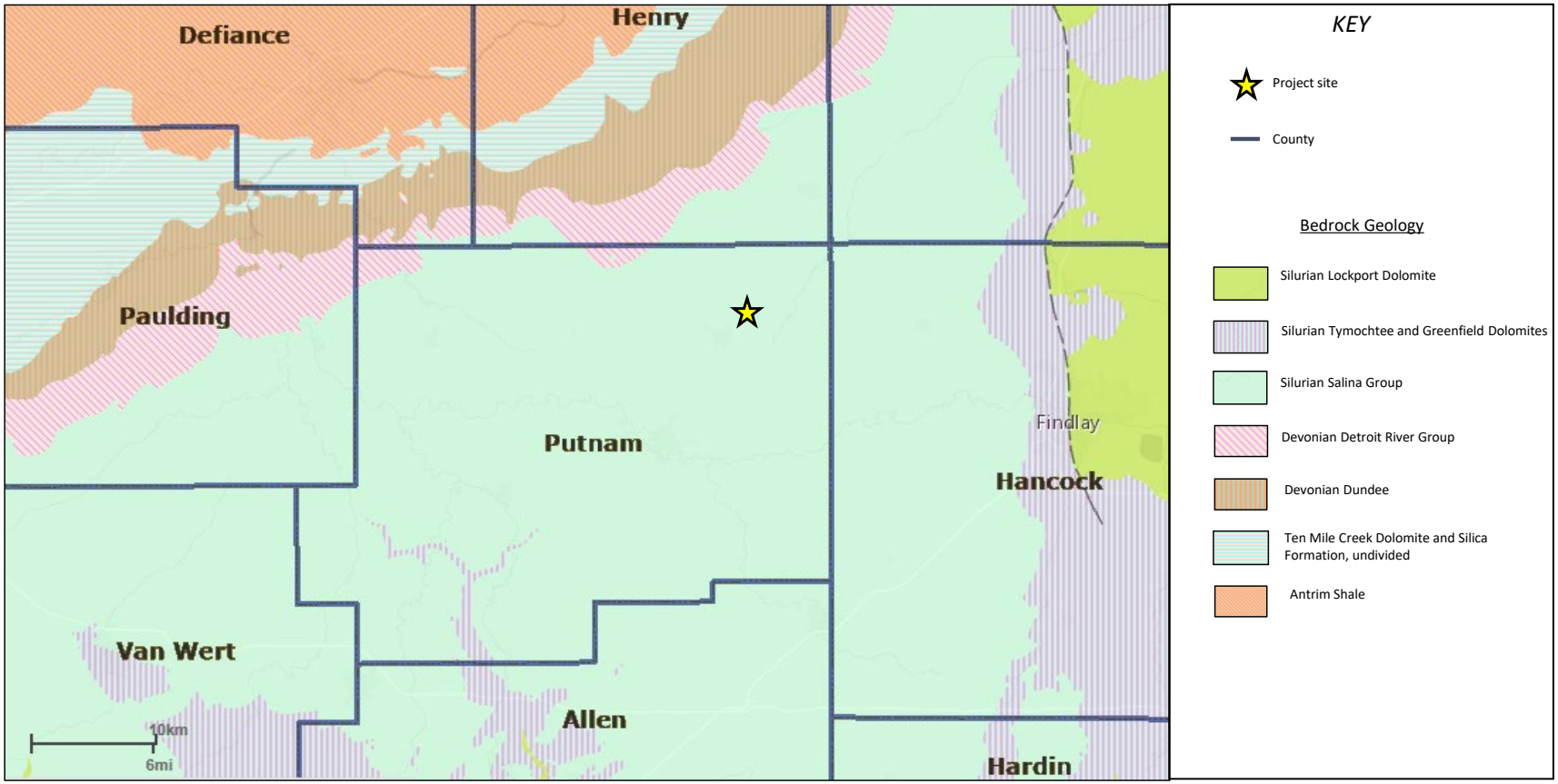

Figure 56: Bedrock geology underlying unconsolidated glacial deposits. The Project site, indicated by the yellow star, is located above the Silurian Salina Group bedrock. Modified from ODNR Ohio Geology Interactive Map (ohiodnr.gov).

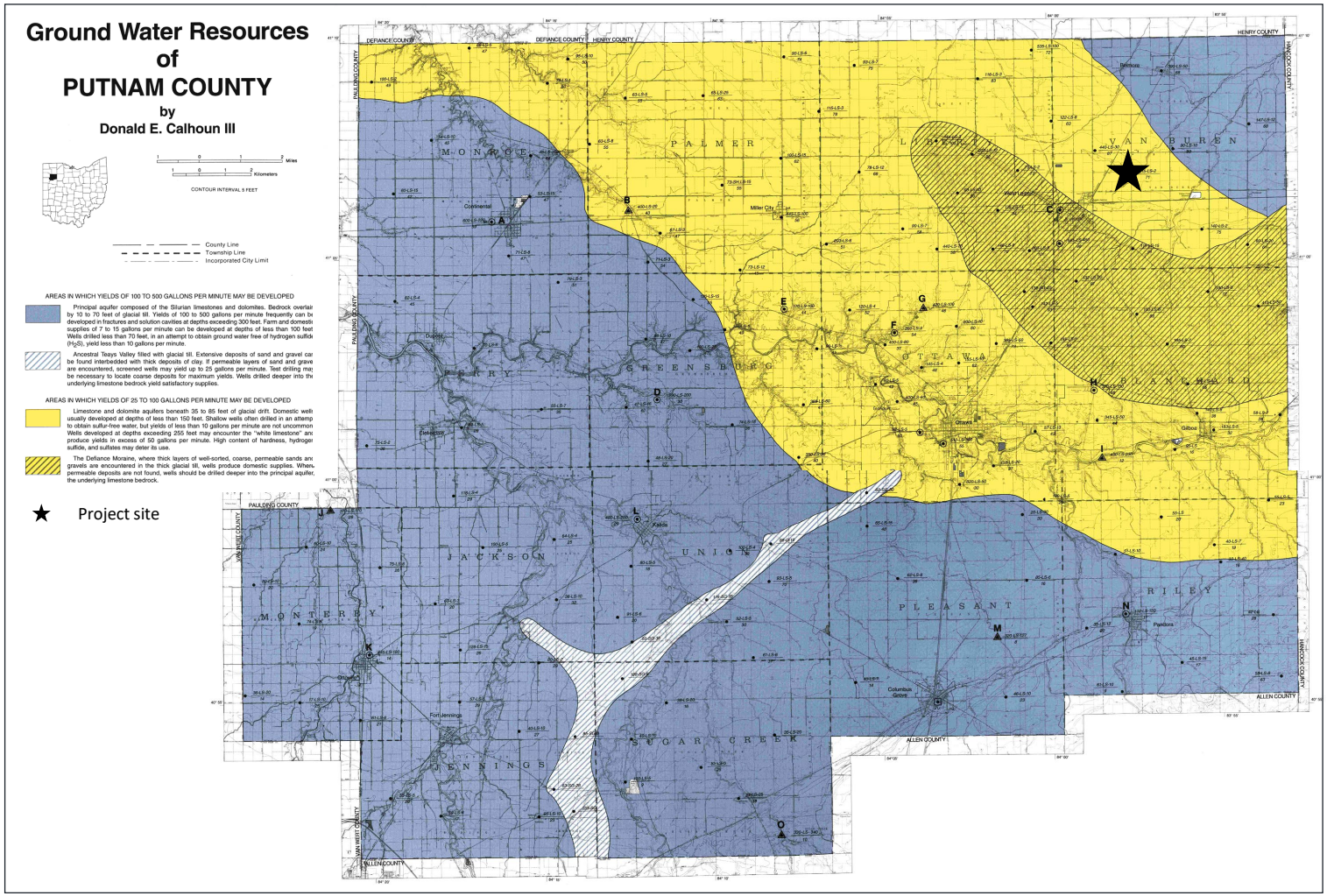

Figure 57: Aquifer map of Putnam County, Ohio. Modified from (Calhoun and Orr, 1992).

2.9.4. Determination of Lowermost USDW

At the Maple Project site, the Silurian Lockport Dolomite is the lowermost USDW as identified by the Ohio Department of Natural Resources (Figure 58, Riley et al., 2012). At the Maple Project site, the depths to the top and bottom of the Lockport Dolomite are prognosed to be 493 fbgl and 632 fbgl, respectively, and the dolomite is expected to be approximately 139 feet thick (Figure 7 and Figure 47). The top of the primary confining zone is separated from the lowermost USDW by 1,916 vertical feet.

There are 97 water wells within the AoR with total depths greater than 100 feet, two of which have total depths greater than 500 fbgl and are inferred to be within the Lockport Dolomite. Water samples from the bedrock aquifers in Putnam County up to 600 feet deep have TDS values ranging from 532 to 1,113 mg/L with most producing from the Salina Group and Lockport Dolomite (Calhoun and Orr, 1992). The Ohio EPA Division of Drinking and Groundwater maintains the Ambient Ground Water Monitoring Network as part of an effort to characterize general water quality conditions across Ohio (Ohio EPA). There is one well in the Lockport Dolomite approximately 4 miles south of the AoR with a total depth of 510 feet deep and average TDS concentrations of 581 mg/L. Approximately 11 miles to the northeast of the AoR is a second groundwater monitoring well within the Lockport Dolomite with a total depth of 65 feet and average TDS concentrations of 1,063 mg/L (Ohio EPA). Wells drilled into the Silurian aquifers typically have high content of hardness, sulfides, and sulfates, which typically deters use (Calhoun,1992). Regional data indicates that the sub-Lockport strata are saline and not suitable for sources of drinking water (Sanders, 1991).

Regional groundwater flow direction in the Lockport Dolomite is generally to the north-northeast (Eberts, S.M. and George, L.L., 2000), and localized flow is developed in fractures and solution cavities in the carbonate bedrock (Calhoun and Orr, 1992).

2.9.5. Addressing Uncertainty

Uncertainty regarding the depth and thickness of the Lockport Dolomite within the AoR will be reduced through cuttings examination and geophysical logging during the drilling of the project wells.

The project will attempt to collect groundwater samples from the Salina Group and the Lockport Dolomite, the known USDWs within the AoR. The identification of the lowermost USDW will be confirmed by evaluating salinity in strata below the Lockport Dolomite through collection of water samples or resistivity logs during the drilling of project wells.

2.9.6. Non-USDWs

Based on regional data and mapping, the Mt. Simon Sandstone injection zone formation water TDS is expected to be about 125,000 mg/L at the Maple Project site (Figure 59). Isotopic data also suggest that the Mt. Simon Sandstone brine originated as connate seawater that mixed with meteoric water and was also influenced by evaporite dissolution (Labotka et al., 2015). Therefore, the Mt. Simon Sandstone is not a USDW.

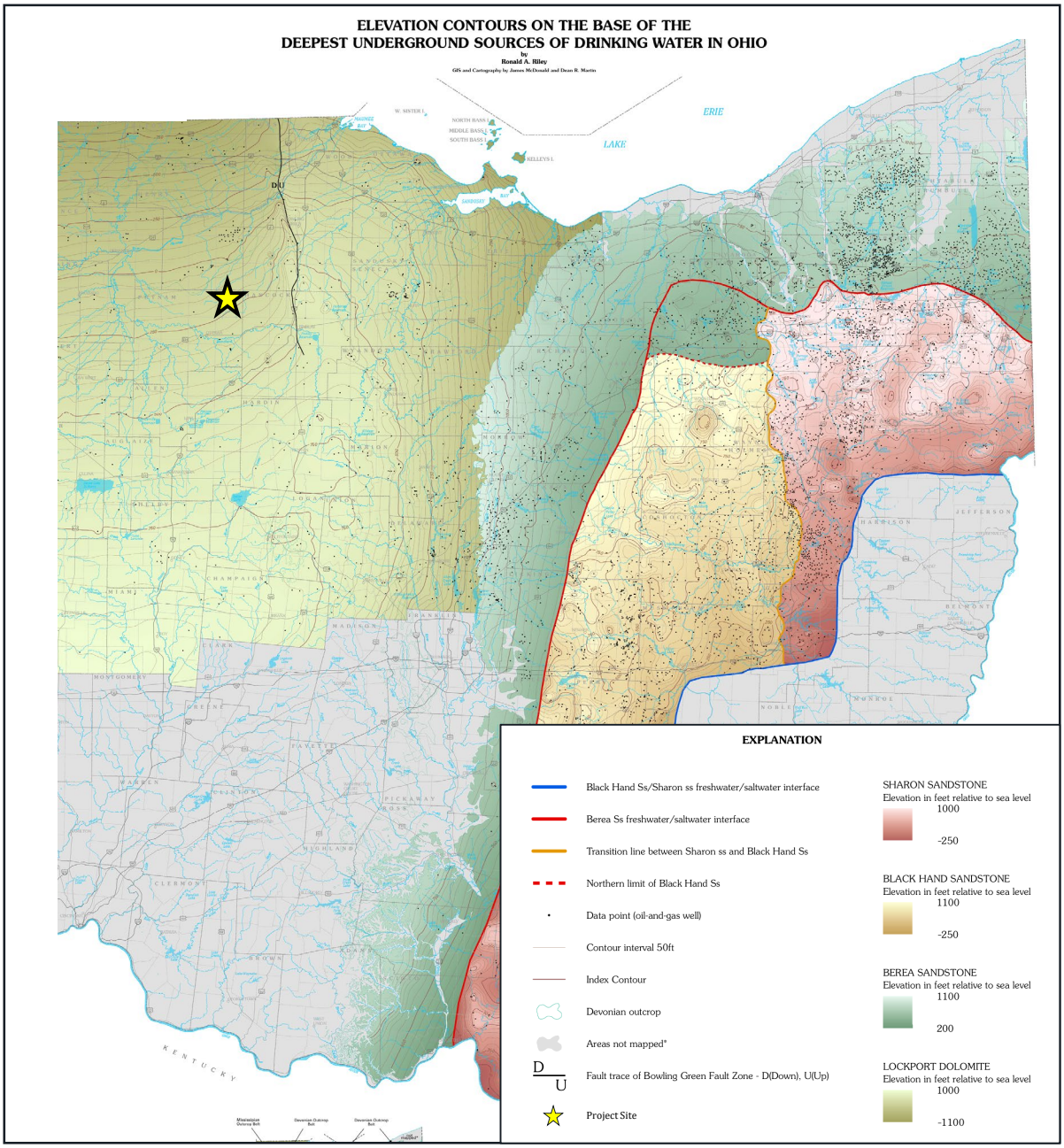

Figure 58: Map of the base of the lowermost USDW in Ohio. The Silurian Lockport Dolomite is the lowermost USDW at the Maple project site. Modified from (Riley et al., 2012).


Claimed as PBI

2.9.7. Topographic Description

Claimed as PBI

The site has an elevation of approximately [redacted] feet above sea level. It is part of the Huron-Erie Lake Plains Physiographic Province of Ohio. This region is characterized by generally flat or gently sloping topography with glacial deposits overlying bedrock.

The land within the project AoR is considered an area of minimal flood hazard as established by FEMA. The proposed project site is located within a FEMA Zone A flood hazard risk, 1% chance of annual flooding along Brush Creek (Figure 60, FEMA).


Claimed as PBI

2.10. Geochemistry [40 CFR §146.82(a)(6)]

2.10.1. Baseline Geochemical Characterization

Geochemical modeling was performed to assess the maximum reactivity of CO_2 interactions within the injection zone and at the injection-confining zone interface. Modeling inputs included mineralogy of the injection and confining zones, injection gas composition, and aqueous chemistry. Baseline geochemical data will be collected during the Pre-operational Testing Program to confirm or update the results of the geochemical modeling(Attachment 05: Pre-operational Testing Program, 2025).

Geological characterization and mineralogy of the injection and the confining systems are discussed in detail in Sections 2.6. *Injection and Confining Zone Details* and 2.7.2. *Petrophysics*. A mineralogical dataset including XRD and petrographic thin-section point counting data was compiled from samples spanning the entirety of the Mt. Simon Sandstone and Rome Formation from three wells associated with the Vickery Environmental, Inc. Class I UIC permit in Sandusky County, OH (Vickery Environmental, Inc., 1989; Vickery Environmental Inc., 2020) which are considered strong analogs for the Maple Project site. Only XRD data were used for model inputs.

2.10.2. Mineralogical Model Input

The Mt. Simon Sandstone in west-central Ohio consists primarily of arkose and subarkose sandstones comprised of mostly quartz and feldspar minerals (entirely K-feldspar based on XRD analyses) with some carbonate cement and grains (dolomite and calcite) and a small clay mineral component (primarily chlorite) (Table 15; Vickery Environmental, Inc., 1989). Mt. Simon Sandstone samples have highly variable quartz-feldspar ratios. In order to capture this variability, the Mt. Simon mineralogy samples were separated into two groups within the geochemical modelling: an arkose-dominated lithology that has greater than or equal to 40% total feldspar, and a quartz-dominated lithology that has less than 40% total feldspar.

The lower portion of the primary confining zone at the Maple Project site is the low porosity dolomitic strata of the Rome Formation above the Rome Silt. Two samples collected above the Rome Silt are representative of the tight dolomite component of the Rome Formation; they contain high dolomite contents (93 and 94 wt.%) and low total porosities (0.8 and 1.2%) measured by XRD and point counting, respectively (Vickery Environmental, Inc., 1989). The tight dolostones could potentially interact with CO_2-influenced liquids. The two Rome XRD samples collected from the Vickery UIC investigation were averaged to generate a single representative model input to define the primary confining zone model cases.

Three mineralogical inputs were used in model runs: primary confining zone, injection zone arkose lithology, and injection zone quartz lithology. Mineralogical inputs for each of the three groups were generated by calculating the mean abundances of each mineral from the XRD datasets. XRD samples were analyzed for clay mineralogy, so individual clay mineral abundances were directly averaged in instances where results were provided as weight fractions of the total sample, and individual clay mineral proportions were applied to a total clay component in instances where results were provided as weight fractions of the clay-sized component (Table 15).

Table 15: Mineralogical inputs for geochemical modeling of the confining zone and the quartz-dominated and arkose-dominated lithologies of the injection zone. g/mol = grams per mole, mol/L= moles per liter of specified mineral

Mineral	Idealized Mineral Formula	Molar Mass (g/mol)	Primary Confining Zone		Target Injection Zone - Arkose Lithology		Target Injection Zone - Quartz Lithology	
			Mineral Abundance (%)	Model Input (mol/L)	Mineral Abundance (%)	Model Input (mol/L)	Mineral Abundance (%)	Model Input (mol/L)
Quartz	SiO_2	60.08	2.00	0.869	43.5	17.2	65.3	25.8
K-Feldspar	$KAlSi_3O_8$	278.3	3.00	0.281	47.9	4.08	24.2	2.06
Calcite	$CaCO_3$	100.1	0.000	0.000	2.20	0.522	1.27	0.300
Dolomite	$CaMg(CO_3)_2$	184.4	94.4	13.2	2.60	0.335	6.35	0.816
Smectite (High-Fe,Mg)	$Ca_{0.02}Na_{0.15}K_{0.2}Fe{++}_{0.29}Fe{+++}_{0.16}Mg_{0.9}Al_{1.25}Si_{3.75}H_2O$	549.1	0.000	0.000	0.100	0.00400	0.00	0.000
Illite	$K_{0.6}Mg_{0.25}Al_{1.8}Al_{0.5}Si_{3.5}O_{10}(OH)_2$	389.3	0.000	0.000	0.750	0.0460	0.600	0.0400
Kaolinite	$Al_2Si_2O_5(OH)_4$	258.2	0.550	0.0550	0.000	0.000	0.0300	0.00200
Chlorite (Chamosite-7A)	$(Fe{++},Mg,Fe{+++})_5Al(Al,Si)_4O_{10}(OH)_8$	664.2	0.0500	0.00200	2.91	0.104	2.18	0.0780
Mineral formulas displayed are idealized formulas and represent the stoichiometry used in model calculations.								

2.10.3. Aqueous Model Input

Mt. Simon Sandstone formation water data is available from the Vickery UIC permit applications for Disposal Well No 1 and Disposal Well No. 4 (Vickery Environmental, Inc., 1989; Vickery Environmental Inc., 2020). The Mt. Simon Sandstone formation water samples contained measured TDS concentrations ranging from 120,000 to 132,000 mg/L, with an average of 126,000 mg/L. A TDS concentration of 125,000 mg/L is expected at the Maple Project site, so these water samples are considered representative. Formation water pH values are relatively consistent across the samples with values ranging from 6.0 to 6.9 standard units (SU). These measurements indicate that injection zone formation water chemistry is neutral to slightly acidic.

Three samples of the formation water were averaged to generate a representative Mt. Simon Sandstone formation water composition (Table 16). This representative sample contained a calculated charge imbalance error of 0.45%. A charge imbalance error of +/- 5% is conventionally considered high quality data for brine solutions.

Formation water data is not available from the primary confining zone due to the low porosity and permeability within the Rome Formation. The aqueous input for the Rome Formation was generated by equilibrating the representative Mt. Simon Sandstone composition with the mineralogical input of the Rome Formation. This technique has been applied to estimate porewater chemistry of low permeability rocks in multiple studies (Gaus et al., 2005). Results of this calculation were used as the aqueous geochemical input for the primary confining zone model runs and are provided in Table 16.

Table 16: Concentrations of elements used in aqueous inputs for geochemical modeling of the Rome Formation confining interval and the Mt. Simon Sandstone injection interval.

Parameter	Unit	Mt. Simon Sandstone	Rome Formation
Calcium	mg/L	10,483	10,845
Magnesium	mg/L	1,933	2,000
Sodium	mg/L	33,500	34,646
Potassium [1]	mg/L	717	462
Iron [1]	mg/L	42.0	240.8
Chloride	mg/L	75,250	77,819
Sulfate	mg/L	1,092.0	1,129.7
Aluminum[2]	mg/L	0.00203	0.00136
Manganese [1]	mg/L	4.300	4.400
Silica [1]	mg/L	9.0	3.9
Strontium [1]	mg/L	165	171
Total Alkalinity	mg/L	42	15
Total Dissolved Solids	mg/L	124,105	
Temperature	°C	67.5	33.9
pH	standard units	6.43	6.41
Specific Gravity	grams per cubic centimeter	1.0900	1.1100
Cation/Anion Charge Balance Error	%	0.45	0.48

Cation/Anion charge balance for the model input was calculated in Geochemists Workbench ™

[1] Potassium, iron, manganese, silica, and strontium were not analyzed in formation water samples used to generate the representative sample. Concentrations used as inputs are from (Zhao et al., 2015).

[2] Aluminum was not reported in Zhao et al., 2015). Concentration was calculated from equilibrium model.

2.10.4. Injection Gas Input

The composition of the gas stream for injection is expected to consist of >98% CO_2, with minor impurities including oxygen, hydrogen sulfide, and hydrogen (Table 33). Additional impurities (carbon monoxide, glycol, non-condensable gases) are anticipated to be present at minor quantities, which are not expected to chemically interact with injection or confining zone minerals significantly; therefore, they were not included in model inputs. To examine the impact of impurities within the CO_2 stream on mineral reactivity, a high impurity and low impurity case were evaluated in the modeling effort (Table 17). For nearly all model cases, the lower impurity gas composition (i.e., higher CO_2 component) was observed to be more reactive (greater geochemical change), and thus only the results from the low impurity compositions have been presented here to provide the most conservative estimates of the extent of mineral reactions.

Table 17: Injection gas composition estimates used in sensitivity modeling of the impact of gas impurities on geochemical reactions. (H_2=hydrogen, O_2=oxygen, H_2S=hydrogen sulfide)

Model Input Case		High Impurity Estimate (Low CO_2)	Low Impurity Estimate (High CO_2)
Chemical Component	**Unit**		
CO_2	%	98.9	99.9
H_2	%	1.00	0.10
O_2	ppm	800	100
H_2S	ppm	100	10

2.10.5. Geochemical Modeling

Geochemical modeling was performed to evaluate the reactivity of the solid-liquid-gas system during and following CO_2 injection. Two modeling approaches were used for this evaluation:

1) equilibrium modeling (thermodynamic considerations only), and
2) reaction pathway modeling (thermodynamic and kinetic considerations).

Multiple model cases were generated to assess the maximum reactivity of geochemical interactions within the injection zone and at the injection-confining zone interface. Model case inputs differed to address mineralogical heterogeneity in the injection zone and variability in injection gas impurities. Model runs were conducted at a pressure of 1,607 psi and a temperature of 93.4°F that are the expected maximum pressure and temperature values at the end of the gas injection period at the interface between the injection zone and the primary confining zone.

In all models, the formation-injectate-fluid system was modeled as porous material fully saturated with one liter of fluid in the defined effective pore space. Computational modeling predicts a maximum CO_2 saturation of 0.78 at the interface between the injection zone and the primary confining zone. This conservative gas saturation value is assumed for all model runs. The saturation value was incorporated into calculations using the ideal gas law to calculate the number of moles of CO_2 and impurity gases H_2, O_2, and H_2S that are introduced into the modeled systems. These values were supplied as model inputs, and CO_2 solubility within formation water was calculated in the modeling software based on temperature, pressure, and compositional inputs using a Henry's Law approach (Bethke, 1998; Gundogan et al., 2011; Parkhurst and Appelo, 2013).

Following methods proposed in Trémosa et al (2014) for modeling geochemical compatibility of geologic carbon sequestration, geochemical modeling efforts employed a batch reactor modeling approach where the formation-injectate-fluid system was assumed to be a perfectly mixed reactor with homogenous distribution of every chemical compound and reactant.

Equilibrium modeling was conducted using the USGS software package PHREEQC (Parkhurst and Appelo, 2013). Equilibrium modeling was completed for each mineral model case by fixing individual mineral saturation indices to a value of zero in the presence of the formation water and injectate gas, thereby quantifying mineral and aqueous changes associated with equilibrium with injectate gas. Reaction pathway modeling was conducted using the React module in Geochemist's Workbench (Bethke, 1998). Reaction pathway modeling was completed for all model cases. Each model was set to run for an initial injection period of 12 years and a subsequent period of 50 years post-injection for a total model runtime of 62 years.

2.10.6. Equilibrium Modeling

For the Rome Formation, the mineral reactions predicted to occur include the complete dissolution of chlorite and kaolinite and the partial dissolution of K-feldspar. Dolomite exhibited minor dissolution, which indicated relative geochemical stability. Quartz and dawsonite were predicted to precipitate. Porewater pH decreased by approximately 1.22 SU at equilibrium, which was mainly due to the dissolution of CO_2 into formation water (Table 18). Quartz precipitation is the primary driver of net mineral mass increases. However, its slow reaction kinetics suggests limited impact within operational timescales.

In the injection zone where arkose lithologies dominated, the mineral reactions predicted by equilibrium geochemical modeling included the complete dissolution of clay minerals (chlorite, illite, smectite) and partial dissolution of calcite and K-feldspar. The calcite dissolution is attributed to its role in buffering pH decreases induced by CO_2 dissolution (Table 18). The formation water pH decreased slightly more than 1 SU at equilibrium. Dawsonite, dolomite, quartz, and siderite formed as a result of increased alkalinity and dissolved ions from clays and feldspars. These reactions effectively trap CO_2 in mineral form. Dissolution of CO_2 significantly increased aqueous alkalinity, which drives carbonate mineral precipitation. Dissolution and precipitation reactions partially offset each other and limited overall mass changes. Quartz and dawsonite precipitation were identified as the primary contributors to net mineral mass increases.

In the injection zone where quartz lithologies dominated, the reactions in the quartz dominated lithology largely mirrored those of the arkose lithology. These included complete dissolution of chlorite, illite, and kaolinite, along with partial dissolution of calcite and K-feldspar. Dawsonite, dolomite, quartz, and siderite precipitation were predicted. The formation water pH decreased by 1.15–1.16 SU at equilibrium, which was a slightly greater pH decrease than in the arkose lithology and was attributed to the comparatively lower initial calcite content that resulted in reduced buffering capacity (Table 18). Quartz precipitation dominated net mass increases as was observed in the arkose lithology. However, its slow kinetics suggest minimal short-term changes during CO_2 injection operations.

The extent of the mineral mass increase as determined through equilibrium geochemical modeling is variable and depends most strongly on mineralogy inputs and the modeling indicates that variability in gas impurities would have negligible impact on the overall direction or magnitude of mineral reactions (Table 18). The primary confining zone (Rome Formation above the Rome Silt) is predicted to experience the greatest degree of mineral precipitation with the models predicting between 5.53 and 5.54% of net mineral mass increase. The influence of the gas impurity range was found to be minimal in primary confining zone model scenarios. Net mineral precipitation is predicted for both of the Mt. Simon Sandstone lithologies as well, although to a lesser extent when compared to the Rome Formation. The arkose lithology was predicted to experience between 3.50 and 3.62% net mineral mass increase, and the quartz lithology was predicted to experience between 3.19 and 3.28% increase. The quartz lithology was predicted to be less reactive than the arkose lithology due in large part to the lower degree of reactivity of quartz compared to feldspar minerals.

Table 18: Summary of equilibrium modeling indicating changes in pH, and mineral mass in the confining zone and the quartz-dominated and arkose-dominated lithologies of the injection zone. (kg=kilograms)

		Primary Confining Zone		Injection Zone - Arkose		Injection Zone - Quartz	
Parameter	**Units**	**High Impurity Estimate**	**Low Impurity Estimate**	**High Impurity Estimate**	**Low Impurity Estimate**	**High Impurity Estimate**	**Low Impurity Estimate**
Final pH	Standard units	5.19	5.19	5.37	5.35	5.28	5.27
Delta pH	Standard units	-1.22	-1.22	-1.07	-1.08	-1.15	-1.16
Delta formation water mass	kg	-0.114	-0.114	-0.093	-0.093	-0.092	-0.095
Delta mineral mass	% of total moles	5.53	5.54	3.50	3.62	3.19	3.28

- Final pH indicates the model output pH value.
- Delta indicates the change in final parameter between the initial model input and the calculated model output.

2.10.7. Reactive Pathway Modeling

At the Mt. Simon Sandstone – Rome Formation interface, the kinetic modeling results predict that porewater pH will decline to 4.93 SU over 62 years (Figure 61). An initial sharp pH decrease occurs during CO_2 injection that is followed by gradual stabilization after injection ceases. Clay minerals and feldspar were predicted to dissolve early, and dolomite remains generally stable throughout (Figure 62). Dawsonite forms during injection and remains stable post-injection, contributing to CO_2 trapping. Quartz precipitation is also predicted to begin during injection and proceed slowly.

A minor net mineral mass decrease (-0.008%) is accompanied by a slight porosity increase (+0.016%). Over time, this trend is expected to reverse due to persistent quartz precipitation, which aligns with equilibrium modeling projections that predicted an increase in mineral mass (Figure 62). As with equilibrium modeling, gas composition variations had negligible effects on reaction directions or magnitudes in any of the modeled cases.


Claimed as PBI


Claimed as PBI

In the arkose-dominated part of the injection zone lithology, pH decreased to 4.95–4.96 SU during the 62-year period. The pH decline is steady except for a brief, slightly elevated period during injection and stabilization occurs post-injection. Nearly complete dissolution of clay minerals and partial dissolution of K-feldspar occur (Figure 63). Hematite forms rapidly during early injection and temporarily offsets mass loss from dissolution. Dawsonite and dolomite precipitate during injection and contribute to CO_2 trapping. Quartz precipitation continues slowly post-injection.

Overall, a minor net mineral mass decrease (-0.025%) corresponds to a small porosity increase (0.012 to 0.013%). As quartz precipitation persists, porosity is expected to decline over geologic timescales.


Claimed as PBI

In the quartz -dominated injection zone lithology, geochemical trends are similar to the arkose lithology. Formation water pH decreases to 4.92–4.93 SU and stabilizes post-injection. This pH range is consistent with other lithologies but reflects the quartz lithology's lower initial calcite content and reduced buffering capacity. Clay minerals nearly dissolve completely, and feldspar dissolves partially (Figure 64). The small amounts of calcite in the initial system dissolve immediately during injection and act as a pH buffer. Hematite and dawsonite form briefly during injection and contribute to mass stability. Dolomite and quartz precipitation continue post-injection with quartz dominating long-term mass increases. A small net mineral mass decrease (-0.030%) is predicted that corresponds to a porosity increase of 0.019 to 0.020%. Over time, quartz precipitation is expected to reverse these trends


Claimed as PBI

2.10.8. Geochemical Impacts on Storage and Containment

Equilibrium and kinetic modeling each indicate that geochemical reactions are mainly driven by CO_2 dissolution into formation water. The process generates carbonic acid, which dissociates into bicarbonate and carbonate and lowers the pH while increasing alkalinity. These changes alter mineral solubilities and prompt the dissolution of certain minerals (e.g., calcite, chlorite, feldspar, and clays) and precipitation of others (e.g., dawsonite, dolomite, siderite, and quartz). These carbonate reactions are part of mineral trapping mechanisms that stabilize CO_2 in solid phases. Quartz precipitation accounts for the largest net mineral mass increase but proceeds at slow kinetic rates, minimizing its immediate impact on porosity.

The Rome Formation (above the Rome Silt) demonstrated geochemical stability and compatibility with CO_2 storage. These results align with studies that conclude dolomite formations are compatible with CO_2 injection and storage (Mohamed et al., 2012).
Both feldspar-dominant and quartz-dominant lithologies of the injection zone displayed comparable geochemical responses to CO_2 injection regardless of the dominant mineral type. Minor decreases in porosity associated with mineral precipitation are predicted in both injection zone lithologies at equilibrium conditions.

The geochemical modeling for the Maple Project site indicates that CO_2 injection induces a predictable sequence of geochemical reactions with minimal impact on reservoir quality or containment over operational timescales. Carbonate mineral formation is a primary driver of long-term mineral trapping, while pH buffering and mineral dissolution reactions influence short-term geochemical behavior. The summary of kinetic reaction pathway modeling is shown in Table 19.

2.10.9. Potential Geochemical Impacts to USDWs

The lowermost USDW within the AoR is the Silurian Lockport Dolomite, which is overlain by the Salina Group USDW. The Salina Group also primarily consists of microcrystalline dolomite. Upward migration of CO_2 into these USDWs is unlikely, as described in Section 2.6. *Injection and Confining Zone Details*. In the event of a leak allowing CO_2 to migrate vertically into the lowermost USDW, the geochemical impacts of the gas-USDW aquifer interactions are not expected to be significant. Should CO_2 dissolution into the lowermost USDW groundwater occur, pH would decrease slightly, and the concentration of bicarbonate ions would increase due to carbonic acid dissociation reactions. There would be a negligible impact on total alkalinity of the shallow groundwater by adding dissolved CO_2. The slight decrease in pH resulting from carbonic acid formation could result in some dissolution of the dolomitic matrix; however, this carbonate dissolution produces bicarbonate ions that react with the carbonic acid to buffer any pH decrease. A study that modeled the results of CO_2 release into an aquifer (Berger and Roy, 2011) demonstrated that dissolution of dolomite buffered the pH and the main resulting changes to the groundwater chemistry were increases in magnesium, calcium, and bicarbonate ions. Since pH is buffered by carbonate mineral dissolution, the likelihood of increased acidity mobilizing metals is negligible (Berger and Roy, 2011). Groundwater quality monitoring in the lowermost

USDW wells will include monitoring of pH, magnesium, and calcium, allowing for the detection of any inadvertent releases of CO_2 into the USDWs.

In addition to the Lockport Dolomite USDW and Salina Group USDW, in some areas near the project site there are shallow aquifers in sands and gravels in glacial till such as in the Defiance Moraine aquifer (Section 2.9.2. *Near Surface Aquifers*; Calhoun and Orr, 1992). The glacial tills and moraines contain a high proportion of fragments of the underlying limestone bedrock and thus have a variable content of carbonate minerals (Aden et al., 2012). Migration of CO_2 into these shallow aquifers is highly unlikely; however, if such a release occurred, decreases to groundwater pH within the sand and gravel aquifer would also be buffered in part by dissolution of carbonate minerals present in the till. In addition, there may be additional capacity for pH buffering from protonation and metal complexation reactions within clay minerals present in till aquifers. The potential to mobilize additional constituents into the groundwater, including metals, is influenced by the mineralogy of the aquifer, although increased groundwater concentrations of any mobilized metals would be negligible (Berger and Roy, 2011) and likely mitigated by sorption to aquifer sediments. A review of field studies of the impact of CO_2 releases on groundwater quality concluded that trace metal releases are generally small and do not pose a significant risk to groundwater quality (Qafoku et al., 2015).

The lithology of USDWs will be logged during the drilling of project wells.

Table 19: Summary of kinetic reaction pathway modeling results for the confining zone, and the arkose and quartz dominated lithologies of the injection zone. SU=standard units, mol=moles of mineral(s)

		Confining Zone		Injection Zone - Arkose		Injection Zone - Quartz	
Parameter (after 62-year run)	**Units**	**High Impurity Estimate**	**Low Impurity Estimate**	**High Impurity Estimate**	**Low Impurity Estimate**	**High Impurity Estimate**	**Low Impurity Estimate**
pH	SU	4.93	4.93	4.96	4.95	4.93	4.92
Delta porosity	%	0.00016	0.00016	0.00013	0.00012	0.00019	0.00020
Delta mineral mass	%	-0.008	-0.008	-0.025	-0.023	-0.030	-0.030
Delta total carbonate	mol	0.186	0.187	0.372	0.379	0.351	0.355
Delta total clay	mol	-0.061	-0.061	-0.111	-0.111	-0.083	-0.083
Delta total feldspar	mol	-0.188	-0.188	-0.140	-0.144	-0.168	-0.173
Delta total quartz	mol	0.003	0.003	0.053	0.053	0.079	0.079

- Results displayed in the table represent the indicated values following completion of the 62 year modeling duration which consists of a 12 year gas injection period and a 50 year post-injection period.
- Delta values indicate the difference between initial input conditions and model outputs.
- Cells highlighted in red indicate a decrease compared to initial model inputs, and cells in green indicate an increase compared to initial model inputs.

The CO_2 trapping mechanisms that include dissolution and mineral trapping were also evaluated with the computational modeling presented in Attachment 02: AoR and Corrective Action Plan, (2025). Table 20 indicates the trapping mechanisms and percentage of CO_2 trapped 50-year post-injection at the Maple Project site as predicted by the computational modeling that considers the spatial and 3D extent of the storage site. The geochemical and computational modeling results are largely consistent as the computational modeling predicts that about 85% of the CO_2 at the end of PISC will be structurally and residually trapped and most of the remainder will be trapped by dissolution (Figure 65). Whereas the computational modeling predicts a slight decrease in mineral mass and geochemical modeling indicates a slight increase, all methods indicate mineralization will play a very small role during the operational period of the project.


Claimed as PBI

Claimed as PBI

2.11 Other Information (Including Surface Air and/or Soil Gas Data, if Applicable)

Attachment 05: Pre-operational Testing Program, (2025) presents the data that will be collected to determine and verify the depth, thickness, mineralogy, lithology, porosity, permeability, and geomechanical information of the injection zone, confining zone, and other relevant geologic formations via petrophysical logging and analysis, and core acquisition and testing. In addition, baseline 3D surface seismic data will be acquired during the pre-injection phase of the project to assist in characterizing injection zone and confining zone rock properties away from the project wells.

The project does not plan to acquire baseline atmospheric or soil gas data nor are there plans to pursue atmospheric or soil gas monitoring during the injection phase of the project.

2.12. Site Suitability [40 CFR §146.83]

2.12.1. Summary

The Mt. Simon Sandstone and Rome Silt at the Maple Project site meets all requirements necessary to serve as a competent injection zone and can sequester an estimated 4.3 Mt of CO_2 over 12 years as evidenced through geologic evaluation, static modeling, and computational modeling results, and AoR delineation reported in Attachment 02: AoR and Corrective Action Plan, (2025). The Rome Formation and Conasauga Formation will be an effective primary confining zone based on their thickness, continuity, and low permeability at the project site.

Table 21 summarizes the properties of the Mt. Simon Sandstone that contribute to its suitability as an injection zone.

The Rome Silt is expected to be Claimed feet thick at the Maple Project site. Although it is considered part of the injection zone, its contribution to storage will be minimal. CO_2 plume development will likely be controlled by heterogeneities within the Mt. Simon Sandstone, and these heterogeneities will be characterized using a combination of well log, core, and 3D surface seismic data (Attachment 05: Pre-operational Testing Program, 2025).

There are no wells within the AoR that penetrate the primary confining zone. The closest well penetration of the primary confining zone is the Barlage Louis well, which is located approximately 7 miles southwest of the injection well (ODNR; S&P Global).

FEMA classifies the project site to have a very low risk of experiencing damaging earthquake effects, the project site is located in seismic category A with no potential shaking effects (Figure 50), and there is minimal flood hazard risk with only a 1% chance of experiencing annual flooding (Figure 60, FEMA).

2.12.2. Primary Confining Zone

The Rome Formation and Conasauga Formation together will be a competent primary confining zone. They are estimated to be 262 feet thick at the project site and are laterally continuous across the surrounding area. Based on the petrophysical analysis of wells in the region, the Rome Formation is expected to have porosity and permeability values of around 7% and 0.22 mD, and the Conasauga Formation is expected to have values of 4% and 0.09 mD (Attachment 02: AoR and Corrective Action Plan, 2025). Data gathered during the pre-operational phase of the project will be used to verify that the Rome and Conasauga Formations form a highly competent confining zone (Attachment 05: Pre-operational Testing Program, 2025).

2.12.3. Lowermost USDW

The Silurian Lockport Dolomite is the lowermost USDW at the project site with a depth to the base of the formation of Claimed as fbgl. The base of the Lockport Dolomite is expected to be more than Claimed as PBI feet above the top of the primary confining zone.

2.12.4. Additional Confinement Strata

The Glenwood Shale, the Utica Shale, and the Queenston Formation/Maquoketa Group are all additional confining beds between the primary confining zone and the lowermost USDW (Lockport Dolomite) and will prevent injection zone fluids from reaching the lowermost USDW, should they migrate past the primary confining zone.

2.12.5. Structural Integrity

The 2D surface seismic data acquired for the project indicates there are no faults or fractures, or other natural conduits, which can be identified that would allow injection zone fluid migration beyond the primary confining zone. All faults in the project area identified through the 2D surface seismic surveys are within the upper Precambrian Basement and none extend into the overlying Phanerozoic strata. Fault slip analyses of these faults conclude that there is a very low probability of fault slippage within the Precambrian Basement in the AoR due to the planned injection operations. A future baseline 3D surface seismic survey at the Maple Project site will further reduce uncertainty associated with formation thickness/depth and potential structural features.

2.12.6. Capacity and Storage

The AoR and Corrective Action Plan show that the Mt. Simon Sandstone at the Maple Project Site storage location has the capacity and hydrogeologic characteristics necessary to store an estimated 4.3 Mt over the life of the project (Attachment 02: AoR and Corrective Action Plan, 2025).

Computational modeling was used to simulate multiphase (brine and CO_2) flow in the subsurface and considered the injection zone and primary confining zone geologic and hydrogeologic characteristics. The computational modeling included one injection well within the sequestration site and resulting AoR. CO_2 trapping mechanisms modeled include structural/stratigraphic trapping, residual phase trapping, solubility trapping, and mineral trapping. The computational model demonstrates that the pressure front will dissipate rapidly in the PISC phase of the project, and the CO_2 plume movement stabilizes and will be confined to the injection zone (Attachment 02: AoR and Corrective Action Plan, 2025; Attachment 08: Post-injection Site Care and Site Closure, 2025).

2.12.7. Injection Zone and Compatibility with the Injectate

The well casing, tubing, and cement used through the primary confining zone and injection zone will be CO_2 resistant (Attachment 04: Injection Well Construction Plan, 2025).

2.12.8. Addressing Uncertainty

Vault GSL CCS LP has proposed a comprehensive core and logging program at the Maple Project site in Attachment 05: Pre-operational Testing Program, (2025) as well as a 3D surface seismic survey to address uncertainties prior to injection operations. The purpose of acquiring this data is to validate current understanding of subsurface conditions and site suitability while providing details for modeling and confinement. Should data collected be contrary to current understanding, Vault GSL CCS LP will update appropriate models and material, and a Pre-operational Narrative will be submitted to the EPA that will provide the new data and updated static and computational models prior to the start of injection.

3. AoR and Corrective Action

The AoR for the Maple Project is shown in Figure 1.

Attachment 02: AoR and Corrective Action Plan, (2025) provides a detailed summary of the computational modeling and AoR delineation. After a thorough review of all identified wells in the region, it has been determined that there are no wells within the AoR that penetrate the primary confining zone, and there are no requirements for corrective action.

AoR and Corrective Action Geologic Sequestration Data Tool (GSDT) Submissions
GSDT Module: AoR and Corrective Action ***Tab(s):*** All applicable tabs Please use the checkbox(es) to verify the following information was submitted to the GSDT: ☒ Tabulation of all wells within AoR that penetrate confining zone ***[40 CFR §146.82(a)(4)]*** ☒ AoR and Corrective Action Plan *[40 CFR §146.82(a)(13) and 146.84(b)]* ☒ Computational modeling details ***[40 CFR §146.84(c)]***

4. Financial Responsibility

The financial assurance estimation for the project was divided into four components:

1) Corrective Action,
2) Injection Well Plugging and Abandonment,
3) Post Injection Site Care and Closure, and
4) the Emergency and Remedial Response Plan (ERRP).

Claimed as PBI [redacted]

Internal estimates and external vendor quotes were used to assemble the estimates for the first three components. All appropriate quotes from vendors have been provided with the submittal documentation. The cost estimate for the ERRP was developed in tandem with Industrial Economics, Inc. Their full report is provided with the submittal documentation.

Further detail is provided in the Financial Assurance section of this permit application (Attachment 03: Financial Assurance Plan, 2025).

Financial Responsibility GSDT Submissions
GSDT Module: Financial Responsibility Demonstration ***Tab(s):*** Cost Estimate tab and all applicable financial instrument tabs Please use the checkbox(es) to verify the following information was submitted to the GSDT: ☒ Demonstration of financial responsibility ***[40 CFR §146.82(a)(14) and 146.85]***

5. Injection Well Construction

A stratigraphic well (Maple / INJ1, API #: 34-137-2-0064-00-00) will be drilled under an ODNR Division of Oil and Gas Resources Management Permit to Drill a Stratigraphic Well. This stratigraphic well is intended to be used as the injection well (MPL INJ1) upon the final Class VI authorization to inject.

Vault GSL CCS LP will drill the injection well into the Precambrian rocks beneath the Mt. Simon Sandstone to characterize the entire depth of the injection interval and confirm the lithology of the Precambrian at this location as being either crystalline or metasediments of the Middle Run Formation (Figure 15). No injection will take place in the Precambrian Basement. MPL INJ1 will be used to collect most of the pre-operational testing data for the project (Attachment 05: Pre-operational Testing Program, 2025).

Vault GSL CCS LP intends to use materials for the construction of the project wells (casing, cement, etc.) that are verified by independent third-party sources as suitable for the worst-case corrosive and operational loading expected to occur during the life of the project (Tuboscope - NOV Wellbore Technologies, 2017; Baker Hughes, 2021; Schlumberger, 2021; AMPP, 2023; "API 5CT," 2023. Documentation verifying the suitability of the selected materials are provided in Appendix 1D – *Suitability of Selected Materials*. This suitability is discussed further in Section 5.5. *Additional Design Parameters*.

All work will be performed in accordance with guidance documents, approved work plans, and reporting timelines as approved by the EPA. MPL INJ1 will be constructed with multiple casing strings. Each string will be smaller in diameter than the previous string and cemented to surface to provide multiple layers of protection for USDWs.

The wellhead will use appropriately sized components and materials of construction based on the build of the wellbore. The wellhead design will vary depending on whether the intermediate

casing contingency section is needed or not. Once the open hole data has been collected in the long string segment of the well, casing will be run with sufficient rat hole and cemented in place. The casing and cement will be installed and, if necessary, the well plugged back in manner that will ensure CO_2 is injected directly solely into the Mt. Simon Sandstone. Following installation of the long string casing and cement, perforations will be made into the casing to access the Mt. Simon Sandstone for injection.

This section of the document summarizes the methods and materials to be used for the construction of the injection well. Schematics of the well that illustrate its construction and wellhead are provided in Attachment 04: Injection Well Construction Plan, (2025). Well schematics are subject to change pending finalization of completion design.

5.1. Proposed Stimulation Program [40 CFR §146.82(a)(9)]

Well stimulation is not expected to be required after initial completion other than to clean out the perforations made in the long string casing.

Intermediate stimulations during the life of the project may be required based on well conditions and performance. For instance, near-wellbore salt precipitation may cause a reduction in well performance that may be remediated using a hot water flush to dissolve and remove the precipitated salt.

The requirements and methods of stimulation will be identified through the evaluation of well performance over time. The EPA will be notified prior to any field mobilization and will include details on the proposed procedure, equipment, and chemicals to be used.

A list of common remediation techniques that may be deployed is listed below. This list is not exhaustive and additional technologies or treatments may be used.

- Matrix acid stimulation,
- Coil tubing chemical stimulation,
- Coil tubing mechanical stimulation,
- Coil tubing stimulation with a saltwater flush,
- Perforations.

All treatments will be performed at or below 90% of the fracture pressure of the Mt. Simon Sandstone to prevent the development of fractures and to ensure that containment is maintained. Calculations to determine safe working pressures during stimulation operations will be determined prior to any work and be strictly enforced while stimulation operations are carried out.

Potential additives to stimulations may include but are not limited to hydrochloric (HCl) acid, dilute mud acid (HCl and hydrofluoric acids), citric acid, scale reducer, defoamers, or saline solution (potassium chloride or other non-reactive mineral solution). Prior to the use of any acids, additives, or other stimulation fluid, analysis of the drill cuttings and/or core will be performed to ensure compatibility between any solutions and the injection zone.

5.2. Construction Procedures [40 CFR §146.82(a)(12)]

Multiple strings of casing consisting of carbon steel, 13-Chrome (13Cr) and 25-Chrome (25Cr) will be installed and cemented in place across the entire length of the well to protect the USDWs and other strata overlying the injection zone. 25Cr casing will be installed across the entire injection zone and confining zone to maximize protection from the injected fluids. 13Cr will be run from above the confining zone to surface above the 25Cr in the long string section. These fluids will be injected into the Mt. Simon Sandstone using internally coated carbon steel tubing landed in a nickel or chrome-coated packer. The Mt. Simon Sandstone will be accessed through Claimed as PBI .

The injection well has been designed such that monitoring equipment will be accessible and retrievable should failure occur. Downhole gauges are planned to be landed in a mandrel above the packer. The lines from these gauges will be run back up the casing-tubing annulus through a port in the wellhead. This mandrel and port will be properly rated for the anticipated pressure loading to be experienced downhole and at the wellhead.

Table 22 provides a summary of the open hole sections of the injection well construction. Vault GSL CCS LP may elect to utilize an intermediate hole section and intermediate casing to mitigate the potential for lost circulation pending operational results from drilling activities

Should a lost circulation zone be encountered while drilling, all attempts will be made to cure the lost circulation. Should these efforts be unsuccessful, an intermediate casing string will be installed. These efforts would take place within Step 6. Further details on the casing and cementing for this string are provided in Section 5.3. *Casing and Cementing*. Schematics for the design are provided in Attachment 04: Injection Well Construction Plan, (2025).

A high-level procedure for the well installation is provided below. A more detailed schedule and procedure will be provided to the EPA prior to spudding the well.

1. Conductor casing will be driven into place.
2. Surface hole section will be drilled to a sufficient depth below the base of the Lockport Dolomite such that the entirety of the Lockport Dolomite can be logged during open and cased hole logs.
3. Open hole logs will be run.
4. Casing will then be run and cemented in place.
5. After allowing sufficient time for the cement to harden, cased hole logs will be run, and the casing will be pressure tested.
6. Long string hole section will be drilled into basement. Should a substantial lost circulation zone be encountered while drilling this section:
    a. Well control and loss prevention measures will be implemented until the well is stable.
    b. Should these measures be effective, continue drilling the long string hole.
    c. Should these measures be ineffective:
        i. The hole will be reamed up to the required size and open hole logs will be run.
        ii. Casing will then be run and cemented in place.
        iii. After allowing sufficient time for the cement to harden, cased hole logs will be run, and the casing will be pressure tested.
        iv. The long string hole section will be drilled.
7. Open hole logs will be run.
8. Casing will then be run and cemented in place.
9. After allowing sufficient time for the cement to harden, cased hole logs will be run, and the casing will be pressure tested.
10. Perforations will be made in the long string casing into the Mt. Simon Sandstone.
11. The tubing, packer, and wellhead will then be installed. The annulus will be filled with a non-corrosive fluid with additives, approximately 8.34 lb/gallon in weight.
    a. The components to be used, but not limited to, are:
        i. freshwater
        ii. biocide
        iii. corrosion inhibitor
        iv. oxygen scavenger

Specifications on the tools, equipment, casing, cement, and other equipment or materials required to install the well are provided in more detail in the following sections. All materials of construction are designed to API standards and are intentionally chosen to maximize protection from corrosive, operational, and installation loading. Each item is suitably rated for the loading it will experience.

5.3. Casing and Cementing

5.3.1. Casing

Table 23 and Table 24 display the design safety factors and safety factor loads based on the proposed well design. The safety factor is determined by dividing the pipe rating by the calculated load. It is noted that a standard 80% derating factor for new pipe is applied prior to any analyses. Additionally, material and specification derating based on tensile loading has also been considered for the collapse analysis. For purposes of this application, three scenarios were considered for the casing and tubing analysis: burst analysis scenario, collapse analysis scenario, and tensile analysis scenario. Note that within this section, tensile analysis refers to the axial loading analysis performed on the casing.

The casing burst analysis scenario considers the impact of the plug bump at the predetermined holding pressure following the full pumping of cement. Note that the holding pressure is typically 500 psi over the hydrostatic pressure required to pump the cement or 80% of the burst rating of the pipe, whichever is less.

The tubing burst analysis consisted of analyzing the burst loading during injection operations at the surface where the tubing-annulus differential is at its greatest. The point used for the analysis was the maximum allowable injection pressure (MAIP) at surface (Section 7.1.1. *Determination of Maximum Injection Pressure*).

The casing collapse analysis scenario considers the impact of a full column of cement in the annulus following the bleed-off of the pressure utilized to hold the plug in place at the conclusion of the cement job. Note that this analysis includes the derating of the collapse rating of the pipe when in tension.

The tubing collapse analysis considers the collapse loading during a modeled annulus pressure test (APT) that will be run with 1,500 psi of pressure on the annulus. In this scenario, the maximum collapse load will be experienced at the packer.

The tensile analysis scenario evaluates the impact of a 100,000-pound overpull on the casing string. Overpull is defined as the pulling weight less the weight of the pipe. The tubing tensile analysis was performed in an equivalent manner as the casing, with the exception of the tensile loading used an 85,000 pound overpull. Note that this scenario will typically occur prior to any cement being pumped, and hydrostatic differences in fluid have not been considered.

The resulting safety factors from these analyses are presented in Table 24. In addition, operational, cyclic, and temperature loading analyses were performed that are discussed in greater detail in Section 5.5. *Additional Design Parameters*. Further discussion on the suitability of the corrosion resistant cement system to be used in the well is provided in Section 5.5.7.3. *Suitability of EverCRETE*.

Table 25 displays the setting depths and specifications of the casing to be used for the well. All of the casing conforms with API specifications as detailed in API 5CT, (2023). Table 26 shows the design parameters of the casing and tubing to be used for the well.

Details on the cement program are provided in Section 5.3.2. *Cementing*. All cement used will conform with API standards. Corrosion resistant cement will be used from the bottom of the long string casing in the Mt. Simon Sandstone to above the top of the Conasauga Formation.

Mechanical integrity will be demonstrated as part of the initial completion and as needed during injection operations as discussed in Attachment 05: Pre-operational Testing Program (2025) and Attachment 06: Testing and Monitoring (2025).

All materials for the construction will be suitable for the anticipated loading and are not anticipated to decrease in suitability over time.


Claimed as PBI


Claimed as PBI


Claimed as PBI

5.3.2. Cementing

Table 27 provides a summary of the cement systems that will be used during the construction of the injection well; this includes the systems for the contingency intermediate string. All cement systems used will conform with API standards where applicable.

Cement will be pumped with the following excess:

- Surface: 100% open-hole excess
- Intermediate (contingency): 50% open-hole excess
- Long string: 30% open-hole excess

Note that the excess cement pumped will be subject to change pending field results.

The Maple Project plans to use CO_2-resistant cement (e.g., EverCRETE from SLB, or an equivalent alternative system) for the lower portion of the long string section. These cement systems are stable in extreme acidic conditions, are highly resistant to the CO_2 stream (both wetted and supercritical), and formation fluids in the Mt. Simon Sandstone, and are of sufficient quality to maintain integrity over the design life of the injection well. Further details on the suitability of use for the proposed CO_2-resistant cement are provided in Section 5.5.7.3. *Suitability of EverCRETE*.

No cement will be used for the installation of the conductor casing.

The surface casing cement system will provide the isolation for the Lockport Dolomite, the lowermost USDW, from the drilling process for the remainder of the well installation. The surface cement will serve as an additional layer of protection from potential upward migration of deeper fluids. The surface casing cement will utilize a single-stage program comprising of Class A Portland Cement with additives (Table 27).

The intermediate casing cement system, if required, will provide isolation from any potential lost circulation zone, and serve as an additional layer of protection from potential upward migration of injection zone fluids. It is anticipated that if a lost circulation zone is impacted, it would likely be at the contact of the Gull River and Trempealeau Formations. As such, the intermediate section is planned to be drilled a maximum of 100 feet into the Trempealeau Formation. The intermediate casing cement system will utilize a single stage program comprising of Class H Portland Cement with additives (Table 27).

The long string cement system will provide the primary isolation of USDWs from potential migration of injection zone fluids above the injection zone. The system will use one stage with two types of cement, separated into a lead and tail. The lead cement will contain Class H Portland Cement with additives (Table 27). The tail cement will utilize EverCRETE, a CO_2 resistant cement blend (or equivalent CO_2 resistant cement) (Table 27). Note that this cement system will also be used for MPL OBS1.

Single stage cementing will achieve the required zonal isolation as part of the program that ensures quality cement placement. Further details on how these practices will be implemented and how they assist with quality cement placement and zonal isolation is provided in Section 5.3.2.1. *Ensuring Quality Cement Placement*.

The quality of the bond between the cement, casing, and borehole for all hole sections, will be verified by the cased hole logs that will be run after each string of casing is cemented in place (Attachment 05: Pre-operational Testing Program, 2025).

5.3.2.1. Ensuring Quality Cement Placement

The proposed cementing program will use single-stage cementing for each casing to attain the required zonal isolation. This method will achieve the required zone isolation through deploying, at minimum, the following techniques:

- Running centralizers,
- Using concentric and properly rated casing,
- Reciprocating the pipe,
- Rotating the pipe,
- Pumping spacers and hole cleaning material, and,
- Rigorous testing and inspection of casing prior to installation.

Centralizers will be run as follows in each of the casing sections:

- Surface: one bow string (BS) centralizer every third joint
- Intermediate: one BS centralizer every 100 feet
- Long String:

  13Cr80 Section (surface to 2,529 feet): one BS centralizer every other joint
  25Cr125 Section (2,529 feet to 3,084 feet): one BS centralizer per joint

API Specification 10D ("API 10D - Specification for Centralizer Placement and Stop-collar Testing," 2004) provides an equation to determine optimal centralizer separation for a two-dimension (2D) wellbore. Although the wellbore is planned to be vertical (zero inclination), the well is anticipated in reality to have some minor inclination. The plan to measure well inclination is provided in the Pre-operational Testing Program (Attachment 05: Pre-operational Testing Program, 2025). An average inclination of the wellbore of 1.5 degrees has been conservatively assumed for the calculations presented below.

As an example, the long-string casing was evaluated using Equation 1 below at the bottom of the 13Cr section, which terminates above the top of the confining zone (Table 25).

$$l_c = \sqrt[4]{\frac{d_{max} \times 384 \times E \times I}{W_b \times \sin\theta}} \quad (1)$$

Where,

lc is the optimum centralizer spacing, in inches
d_{max} is the maximum deflection of the casing between centralizers, in inches
E is casing modulus of elasticity in psi (defined as 2.92 E06 psi for 13Cr steel alloy)
I is the casing moment of inertia, in inches^4
W_b is the buoyant weight of the casing, in pounds per inch
θ is the inclination of the well, in degrees

To determine d_{max}, the following equation was used:

$$d_{max} = e_c - e_s \quad (2)$$

Where,

e_c is defined as the standoff at the centralizer, in inches
e_s is defined as the standoff at the sag point, in inches

e_s was determined by multiplying the standoff ratio (standard 66.7% was utilized, per API recommendations) by the maximum annual clearance for perfectly centered pipe.

Utilizing long-string parameters in Equation 2, the d_{max} was determined to be 0.25 inches.

The moment of inertia was determined using Equation 3 to be 37.24 inches^4.

$$I = \frac{\pi \times (OD^4 - ID^4)}{64} \quad (3)$$

The buoyant weight of the casing was determined by multiplying the buoyancy factor by the weight of the casing in air. The buoyancy factor (f_b) was evaluated at two different scenarios. The first is when the entire casing string is full of cement. In this scenario, the casing will fall to the bottom of the hole, and the deflection will be assessed at the bottom of the hole. In the second scenario, the annulus is full of cement and the casing string is full of the displacement fluid. In this scenario, the casing floats to the top of the hole and the deflection is assessed at the top of the hole. Note that within this scenario, the buoyant weight of the pipe is negative, consistent with the pipe floating. The absolute value of the weight of the pipe was utilized to determine the centralizer separation.

Using Equation 4, a cement weight of 15.6 pounds per gallon (ppg), a displacement fluid weight of 8.5 ppg, and the casing weight and cross-sectional area for the 13Cr portion of the long string section, the buoyancy factors for both scenarios were calculated.

$$f_b = \frac{\left(1 - \frac{\rho_e}{\rho_s}\right) - \left(\frac{ID}{OD}\right)^2 \times \left(1 - \frac{\rho_i}{\rho_s}\right)}{1 - \left(\frac{ID}{OD}\right)^2} \quad (4)$$

Where,

ρ_e is the density of the external fluid, in ppg
ρ_s is the density of the casing, in ppg
ρ_i is the density of the internal fluid, in ppg

The weight of the casing was determined to be 4.80 pounds per inch (pounds/in) and 3.74 pounds/in for scenarios one and two, respectively.

Using the determined inputs in Equation 1, optimal centralizer separation for scenarios one and two were determined to be 80 feet and 85 feet, respectively. The minimum value was taken to determine the optimal spacing.

Based on this analysis an 80-foot centralizer separation (nominally every other joint) will be utilized in the 13Cr section, while one centralizer per joint (~40 foot separation) will be used conservatively in the 25Cr section of the hole. This approach in the 25Cr section of the hole, which covers the injection and confining zones, is consistent with published guidance and publicly available sources ("API Specification 10D - Specification for Centralizer Placement and Stop-collar Testing," 2004).

This same approach was utilized to evaluate the other casing strings and resulted in an optimum centralizer separation of approximately 130 feet and approximately 100 feet in the surface and intermediate sections, respectively.

The centralizer program will be run as detailed in Table 28 for the injection well.

This analysis was also performed for each of the monitoring wells. The results of the analysis for those wells is provided in Attachment 06: Testing and Monitoring (2025).

In addition to an effective centralizer program, the pipe will be reciprocated (moved up and down) and rotated while cement is being pumped. Note that once the cement has reached the backside of the casing reciprocation will cease, but rotation will continue. These actions will help to agitate any remaining mud cake or debris in the backside of the casing following the spacer and hole cleaning buffer fluids, improving the overall quality of cement. These actions will be employed for each cementing system for each well.

5.4. Tubing and Packer

The tubing will be internally coated 2.875-inch L-80 pipe designed for CO_2 service. An example of a CO_2 service coating is National Oilwell Varco (NOV) Tuboscope™, TK-15XT, which is used in CO_2 floods for enhanced oil recovery. Material specifications and suitability for use were determined from material provided by NOV (*Tuboscope Coatings Spec Sheet*, 2022).

The injection packer will use CO_2 resistant materials for the CO_2-wet surfaces. An example of this type of packer is the Baker Hughes' Signature F ™ Injection packer system. The packer can be used with either a retrievable or permanent configuration and will be made of 25-Chrome (25Cr) or a nickel alloy to resist corrosion effects of the CO_2 stream (Baker Hughes, 2021). Tubing and packer setting depths and materials of construction are detailed in Table 29.

5.5. Additional Design Parameters

This section discusses the application of the design ratings to ensure the suitability of the construction materials for this project in addition to the analysis performed in Section *5.3. Casing and Cementing.*

Consistent with Section 5.3. *Casing and Cementing*, all tubulars have been derated to 80% of their initial ratings. All comparative evaluations detailed in this section are in reference to these derated values.

The injection packer will have a differential rating of 10,000 psi and a max load rating of 80,000 pound-force.

5.5.1. Temperature

5.5.2. Injection Pressure

Claimed as PBI

5.5.3. Annulus Pressure

Claimed as PBI

Claimed as PBI

5.5.4. Formation Pressure

Claimed as PBI

Claimed as PBI

5.5.5. Tensile Loading

Claimed as PBI

5.5.6. Cyclic Loading

Claimed as PBI

Claimed as PBI

5.5.7. Corrosion Loading

Claimed as PBI

5.5.7.1. Casing

Claimed as PBI

Claimed as PBI

5.5.7.2. Tubing and Packer

Claimed as PBI

Claimed as PBI

5.5.7.3. Suitability of EverCRETE

Claimed as PBI

5.5.8. Operational Considerations

Emergency shut-down equipment will be used for this project. Details on the equipment are provided in Section 7 *Well Operation* and Attachment 06: Testing and Monitoring (2025).

Surface monitoring equipment as detailed in (Attachment 06: Testing and Monitoring, 2025) will be connected to the surface supervisory control and data acquisition (SCADA) system.

Permanent downhole gauges will be used to monitor pressure and temperature at the packer. These gauges will be located in a gauge nipple above the packer and will transmit data through a wire that is run up the annulus to the SCADA system.

Tubulars have been designed such that logging tools and other equipment that are needed for routine annual monitoring will be able to pass through with no restrictions.

6. Pre-operational Logging and Testing

Details on the pre-operation testing plan are provided in the relevant section of this permit application (Attachment 05: Pre-operational Testing Program, 2025).

Pre-Operational Logging and Testing GSDT Submissions
GSDT Module: Pre-Operational Testing ***Tab(s):*** Welcome tab Please use the checkbox(es) to verify the following information was submitted to the GSDT: ☒ Proposed pre-operational testing program ***[40 CFR §146.82(a)(8) and 40 CFR §146.87]***

7. Well Operation

This section provides a brief overview of the well operation conditions. The operational parameters for MPL INJ1 provided in Table 30 will be monitored continuously.

7.1. Operational Procedures [40 CFR §146.82(a)(10)]

Table 31 displays the parameters that will be used during injection operations. Details on the methods of calculations and inputs for these values are provided in Section 7.1.1. *Determination of Maximum Injection Pressure*. Injection pressures will remain below 90% of the fracture pressure and manage the pressure loading experienced during operations in order to protect equipment. It is not anticipated that significant deviation from these values will occur during the life of the project.

7.1.1. Determination of Maximum Injection Pressure

Claimed as PBI

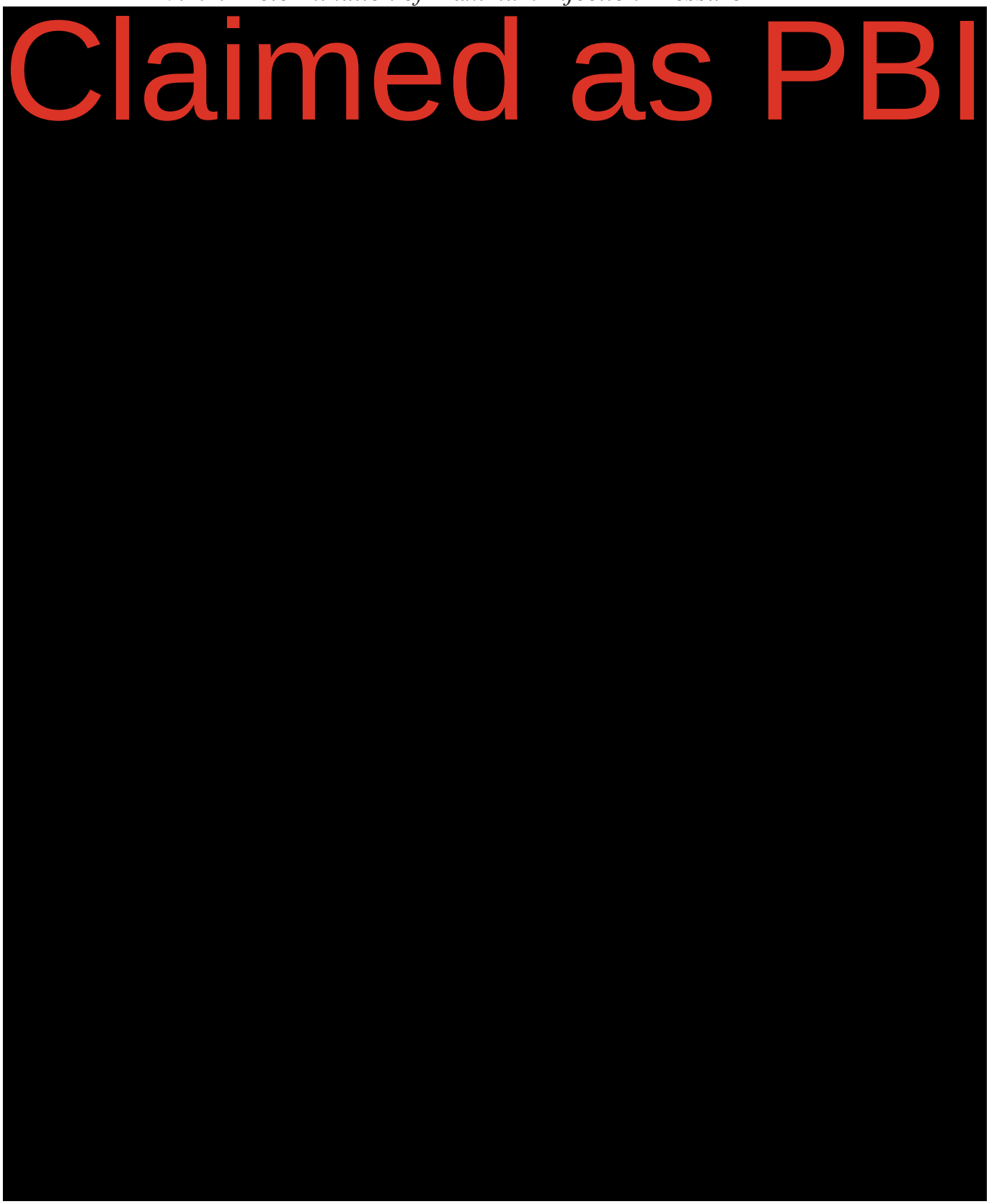

Claimed as PBI

7.1.2. Determination of Operational Annulus Pressure

Claimed as PBI

Claimed as PBI

Claimed as PBI

The annular pressure operations will be performed as follows:

1. The fluids in the annulus will be managed to mitigate the effects of thermal expansion or contraction during start-up and shut down conditions. Annulus fluids will be required to be bled off during any injection start-ups following the initial completion or subsequent workovers. Nitrogen will be added to the annulus in order to maintain minimum pressure during shutdowns or when the injection rate is reduced.
2. Pressure alarm set points will be at:
    a. 1,250 psi for the high alarm
    b. 1,500 psi for the high-high automatic shut down
    c. 300 psi for the low alarm
    d. 100 psi for the low-low automatic shut down
    e. 100 psi differential for the automatic shut down
3. Should a high or low alarm occur, the occurrence will be noted in daily logs.
4. Should a shut-down event occur, the well will be shut-in, and the mechanical integrity event will be investigated via an annulus pressure test.

Any time the annulus is blown down and fluid is removed, the volume of fluid removed from the annulus will be measured.

7.1.3. Potential Future Variation in Operational Parameters

The Maple Project does not anticipate any variations from the current operational parameters outlined in Section 7.1. *Operational Procedures*. Should variations occur which would necessitate any changes to those parameters, EPA Region 5 would be consulted prior to making any such changes.

7.2. Proposed CO_2 Stream [40 CFR §146.82(a)(7)(iii) and (iv)]

The CO_2 injection stream will be sourced from an ethanol production facility located in Putnam County, Ohio and is anticipated to have the fluid composition as shown in Table 33.

Vault GSL CCS LP will analyze the CO_2 stream during the injection phase of the project to provide data representative of its chemical characteristics and to meet the requirements of 40 CFR §146.90 (a). Quarterly sampling and analysis of the CO_2 injection stream will be performed to track the composition of the stream (Attachment 06: Testing and Monitoring, 2025). Additional details on technical standards, QA/QC policy, sample collection and storage policies, and analytical methods are provided in Attachment 10: Quality Assurance and Surveillance Plan, (2025).

The CO_2 stream produced from an ethanol production facility will be of high purity based on the nature of the ethanol fermentation process. The CO_2 stream from ethanol fermentation typically exceeds 99 % CO_2 (mole basis), with minor impurities including common atmospheric gases (e.g., O_2, N_2) and H_2O. The stream will be dehydrated to a low water content prior to entering the pipeline to the injection well.

7.3. Planned Shutdowns and Well Interventions

Through the injection phase of the project, Vault GSL CCS LP anticipates that the project wells will need to be shut down for maintenance or have intermediate stimulations performed on them. These scenarios were considered when evaluating the materials, the design of the wells, and through the development of the operational procedures in order to minimize and mitigate risk of damage to well materials.

7.4. Well Maintenance

Through the life of the project, it is anticipated that the project wells may require well maintenance or a workover to modify the injection interval. Should there be a need to pull tubing, several steps will be taken to minimize potential contact of the casing with CO_2 or brine from the injection zone.

1. Prior to removing the tubing or packer, the well will be killed using a brine of sufficient weight to displace CO_2 in the well and near wellbore CO_2. A minimum of two casing volumes (cased hole interval plus the tubing string) will be pumped to kill the well at a rate sufficient to achieve plug flow.
2. During a workover, the rig crew will have CO_2 detectors to monitor for CO_2 influx or migration from the injection zone and re-kill the well if necessary.
3. Blow-out preventors will be installed during all workover to act as a second barrier to flow.
4. If the well if left without tubing and packers for an extended period of time, a retrievable bridge plug will be run in the well and set above the perforations. This plug will be made of sufficient materials to resist corrosion. The wellbore above the bridge plug will be filled with corrosion inhibited fluid.

At the end of the operational life of the project, the wells will be worked over to fully replace the tubing string and downhole gauges to minimize the likelihood of the need to workover the wells within the PISC period.

8. Testing and Monitoring

Testing and Monitoring GSDT Submissions
GSDT Module: Project Plan Submissions **Tab(s):** Testing and Monitoring tab Please use the checkbox(es) to verify the following information was submitted to the GSDT: ☒ Testing and Monitoring Plan [40 CFR §146.82(a)(15) and 146.90]

This section is meant to provide a brief overview of the Testing and Monitoring Plan. Further details on the well operation program are provided in Attachment 06: Testing and Monitoring (2025).

The Maple Project uses a risk-based Testing and Monitoring Plan that includes operational, verification, and environmental assurance components that meet the regulatory requirements of 40 CFR §146.90. This Testing and Monitoring Plan is based on experience gained from other approved Class VI projects, as well as extensive geologic evaluation and computational modeling.

Goals of the monitoring strategy include, but are not limited to:

- Fulfillment of the regulatory requirements of 40 CFR §146.90,
- Protection of USDWs,
- Risk mitigation over the life of the project,
- Confirmation that MPL INJ1 is operating as planned while maintaining mechanical integrity,
- Acquisition of data to validate and calibrate the models used to predict the distribution of CO_2 and pressure changes within the injection zone, and
- Support AoR re-evaluations over the course of the project.

The Testing and Monitoring Plan will be adaptive over time, and is subject to alteration should one of the following potential scenarios occur:

- Project risks evolve over the course of the project outside of those envisioned at the beginning of the project,
- Significant differences between the monitoring data and predicted computational modeling results are identified,
- Key monitoring techniques indicate anomalous results related to well integrity or the loss of containment.

The monitoring activities fall within three categories based on project objectives: operational, verification, and assurance monitoring.

- ***Operational monitoring*** focuses on day-to-day injection operations such as system performance.

- ***Verification monitoring*** confirms that the injected CO_2 remains contained within the injection zone. The CO_2 plume and pressure front development are tracked over time to provide data for model calibration. Integration of verification monitoring data into project models allows the project to demonstrate conformance between the computational modeling and the testing and monitoring data collected during the operations and post injection phases of the project's lifecycle.

- ***Assurance monitoring*** is performed at surface and near-surface (i.e., soil, shallow groundwater, USDWs, etc.) to monitor for any changes from baseline sample data that might indicate CO_2 or injection zone fluid migration towards surface.

The three monitoring categories encompass:

- Well operations,
- Containment,
- Non-endangerment of USDWs,
- Capacity,
- Injectivity,

- Injection pressure, and
- Conformance.

Table 34 provides a summary of the general monitoring strategy with subcategories.

9. Injection Well Plugging

During the PISC period the injection well will be permanently plugged and abandoned (Attachment 08: Post-injection Site Care and Site Closure, 2025). Details on the methods of these operations are provided in Attachment 07: Injection Well Plugging Plan, (2025). The methods and procedures presented in the attachment are consistent with industry standards and the requirements detailed in 40 CFR §146.92. All materials to be used for the plugging and abandonment are suitable for the anticipated corrosive loading below the top of the Conasauga Formation. Above the top of the Conasauga Formation, Portland cement will be used that conforms to the API specifications ("API RP 65-3," 2021).

Injection Well Plugging GSDT Submissions
GSDT Module: Project Plan Submissions ***Tab(s):*** Injection Well Plugging tab Please use the checkbox(es) to verify the following information was submitted to the GSDT: ☒ Injection Well Plugging Plan [40 CFR §146.82(a)(16) and 146.92(b)]

10. Post-injection Site Care and Closure

The requested documents listed below have been included in the file submission (Attachment 08: Post-injection Site Care and Site Closure, 2025). These documents address the rule requirements for the EPA citations. The Maple Project is not requesting an alternative PISC timeframe.

PISC and Site Closure GSDT Submissions
GSDT Module: Project Plan Submissions ***Tab(s):*** PISC and Site Closure tab Please use the checkbox(es) to verify the following information was submitted to the GSDT: ☒ PISC and Site Closure Plan [40 CFR §146.82(a)(17) and 146.93(a)]
GSDT Module: Alternative PISC Timeframe Demonstration ***Tab(s):*** All tabs (only if an alternative PISC timeframe is requested) Please use the checkbox(es) to verify the following information was submitted to the GSDT: ☐ Alternative PISC timeframe demonstration ***[40 CFR §146.82(a)(18) and 146.93(c)]***

11. Emergency and Remedial Response

The requested documents listed below have been included in the file submission (Attachment 09: Emergency and Remedial Response Plan, 2025). These documents address the rule requirements for the above EPA citations.

Emergency and Remedial Response GSDT Submissions
GSDT Module: Project Plan Submissions ***Tab(s):*** Emergency and Remedial Response tab Please use the checkbox(es) to verify the following information was submitted to the GSDT: ☒ Emergency and Remedial Response Plan *[40 CFR §146.82(a)(19) and 146.94(a)]*

12. Injection Depth Waiver and Aquifer Exemption Expansion

Vault GSL CCS LP does not intend to apply for a Depth Waiver or Aquifer Exemption. As such, no supplemental documents have been filed.

Injection Depth Waiver and Aquifer Exemption Expansion GSDT Submissions
GSDT Module: Injection Depth Waivers and Aquifer Exemption Expansions ***Tab(s):*** All applicable tabs Please use the checkbox(es) to verify the following information was submitted to the GSDT: ☐ Injection Depth Waiver supplemental report ***[40 CFR §146.82(d) and 146.95(a)]*** ☐ Aquifer exemption expansion request and data ***[40 CFR §146.4(d) and 144.7(d)]***

13. Optional Additional Project Information

The National Wild and Scenic River System database indicates that no designated wild and scenic rivers exist in Putnam or Henry County, Ohio. Within the state of Ohio, there are three rivers designated as national wild and scenic river, all of which are located well away from the project area. Big & Little Darby Creeks are located in the central portion of the state west of Columbus, Little Beaver Creek is in the eastern portion of the state near Calcutta, and the Little Miami River is located in the southwest corner of the state traversing from Cincinnati to Fairborn. (National Information Services Center and National Park Service, 2023; National Wild and Scenic Rivers System).

Blanchard River, a Nationwide Rivers Inventory (NRI) river located in Putnam County, runs from Ottawa to Findlay (National Park Service). Although located in Putnam County, Blanchard River is located over 6 miles from the project AoR and over 8 miles from MPL INJ1. There are no NRI rivers located in Henry County. A review of NRI river segments was undertaken because

NRI river segments are potential candidates for inclusion in the National Wild and Scenic River System.

The Maple Project is located on agricultural land in inland Ohio, far from coastal zones, therefore project activities will not affect any coastal zones.

The Maple Project well site will be located on private land. The Ohio State Historic Preservation Office conducted a cultural resources desktop review in the area surrounding the AoR to determine known archaeological, historic, and cultural properties that could potentially be affected by the Maple Project. The desktop review identified two previously surveyed areas, eight previous archaeological sites, two historic structures, and two cemeteries located within the AoR (Table 35). No National Register Historic Districts or National Register Historic Sites were identified within the Maple Project AoR. (Tetra Tech, 2024; National Park Service). None of the identified archaeological or historic inventory sites or cemeteries are expected to be disturbed, as they are located outside of the proposed wellsite and pipeline disturbance areas.

Table 35: Cultural Resources identified by Ohio State Historic Preservation Office (SHPO) during desktop review (Tetra Tech, 2024)

SHPO ID	Description
PU17212	An Intensive Phase I Archaeological Survey of a Proposed 127-Acre Industrial Park Site Near Leipsic in Van Buren Township, Putnam County, Ohio
PU14689	Phase I Cultural Resource Management Survey of the Proposed American Tower Cell Tower (Verizon: Leipsic Site #50780) in Van Buren Township, Putnam County, Ohio
PU0049	Historic archaeological site
PU0085	Prehistoric archaeological site
PU0173	Historic archaeological site
PU0174	Historic archaeological site
PU0191	Prehistoric archaeological site
PU0195	Prehistoric archaeological site
PU0196	Prehistoric archaeological site
PU0235	Unknown archaeological site, pending review
PUT0030204	Wilhelm Tile Mill
PUT0048904	Tooman Farmstead
OGS ID	**Description**
10167	West Belmore Cemetery
10166	East Belmore Cemetery

On August 8, 2025 a review of the US Fish and Wildlife Service (USFWS) Information for Planning and Consultation system identified threatened, endangered, candidate, or proposed species that may potentially be affected by the Maple Project (Table 36).

Table 36: Federal threatened or endangered, candidate, or proposed species potentially affected by the Maple Project (USFWS, 2025).

Name	Federal Status	Critical Habitat
Indiana Bat	Endangered	Project location does not overlap critical habitat
Whooping Crane	Experimental non-essential	No critical habitat designated
Monarch Butterfly	Proposed Threatened	Project location does not overlap proposed critical habitat

IPaC indicates bald eagles are likely present in the Maple Project area. Bald eagles are protected under the Bald and Golden Eagle Protection Act and the Migratory Bird Treaty Act. Migratory birds of particular concern that may be present in the AoR include the USFWS Birds of Conservation Concern listed in Table 37.

Table 37: Migratory birds of conservation concern potentially affected by the Maple Project (USFWS, 2025). BCC=Birds of Conservation Concern, BCR=Bird Conservation Regions.

Name	Level of Concern	Breeding Season
American Golden-plover	BCC Rangewide [1]	Breeds elsewhere
Bald Eagle	Non-BCC Vulnerable [2]	Dec 1 to Aug 31
Bobolink	BCC Rangewide	May 20 to Jul 31
Chimney Swift	BCC Rangewide	Mar 15 to Aug 25
Grasshopper Sparrow	BCC Bird Conservation Regions (BCR)[3]	Jun 1 to Aug 20
Lesser Yellowlegs	BCC Rangewide	Breeds elsewhere
Long-eared Owl	BCC Rangewide	Mar 1 to Jul 15
Pectoral Sandpiper	BCC Rangewide	Breeds elsewhere
Red-headed Woodpecker	BCC Rangewide	May 10 to Sep 10
Semipalmated Sandpiper	BCC - BCR	Breeds elsewhere
Short-billed Dowitcher	BCC Rangewide	Breeds elsewhere
Wood Thrush	BCC Rangewide	May 10 to Aug 31

[1] BCC Rangewide birds are of concern throughout their range anywhere within the USA.

[2] Non-BCC Vulnerable birds are not BCC species in the project area but are listed because of Eagle Act requirements.

[3] BCC-BCR birds are of concern only in particular BCRs in the continental USA.

There is potential to encounter threatened or endangered (T&E) flora or fauna within the project AoR. The Ohio State Listed Species includes 10 T&E animal species in Putnam County, and 15 T&E animal species and 32 T&E plant species within Henry County (Table 38, Table 39, Ohio Natural Heritage Database, 2023c, 2023a, 2023b) No T&E plant species have been recorded in Putnam County since 1980.

Table 38: Threatened and endangered fauna of Putnam and Henry County, Ohio (Ohio Natural Heritage Database, 2023c, 2023a).

Species Name	**Common Name**	**State Status**	**County**
Ixobrychus exilis	Least Bittern	Threatened[1]	Putnam
Porzana carolina	Sora Rail	Species of Concern[2]	Putnam
Rallus limicola	Virginia Rail	Species of Concern	Putnam
Etheostoma microperca	Least Darter	Species of Concern	Putnam
Moxostoma valenciennesi	Greater Redhorse	Threatened	Putnam & Henry
Alasmidonta marginata	Elktoe	Species of Concern	Putnam
Cyclonaias tuberculata	Purple Wartyback	Species of Concern	Putnam
Lasmigona compressa	Creek Heelsplitter	Species of Concern	Putnam & Henry
Pleurobema sintoxia	Round Pigtoe	Species of Concern	Putnam
Truncilla truncata	Deertoe	Species of Concern	Putnam & Henry
Hemidactylium scutatum	Four-toed Salamander	Species of Concern	Henry
Bartramia longicauda	Upland Sandpiper	Endangered[3]	Henry
Geothlypis philadelphia	Mourning Warbler	Special Interest[4]	Henry
Faxonius propinquus	Northern Clearwater Crayfish	Species of Concern	Henry
Gomphus externus	Plains Clubtail	Threatened	Henry
Phanogomphus spicatus	Dusky Clubtail	Species of Concern	Henry
Taxidea taxus	American Badger	Species of Concern	Henry
Obliquaria reflexa	Threehorn Wartyback	Species of Concern	Henry
Clemmys guttata	Spotted Turtle	Threatened	Henry
Clonophis kirtlandii	Kirtland's Snake	Threatened	Henry
Emydoidea blandingii	Blanding's Turtle	Threatened	Henry
Terrapene carolina carolina	Woodland Box Turtle	Species of Concern	Henry

[1] A threatened species is not in immediate jeopardy, but a threat exists. Continued or increased stress may result in the species becoming endangered.

[2] A species of concern may become threatened under continued or increased stress.

[3] An endangered species is threatened with extirpation from the state resulting from one or more causes.

[4] Special interest species are capable of breeding in Ohio but are at the edge of their range.

Table 39: Threatened and endangered flora of Henry County, Ohio (Ohio Natural Heritage Database, 2023b). U=Undetermined, P=Potentially Threatened, T=Threatened, E=Endangered.

Common Name	*Scientific Name*	Last Observed	State Status
Unicorn Root	*Aletris farinosa*	2000	U
Prairie Brome	*Bromus kalmii*	2000	P
Golden-fruited Sedge	*Carex aurea*	1995	P
Field Sedge	*Carex conoidea*	1993	T
Little Yellow Sedge	*Carex cryptolepis*	2007	T
Slender Sedge	*Carex lasiocarpa*	2011	P
Sweet-fern	*Comptonia peregrina*	1987	T
Plains Frostweed	*Crocanthemum bicknellii*	2021	T
Long-bracted Orchid	*Dactylorhiza viridis*	2021	E
Tansy Mustard	*Descurainia pinnata*	2000	P
Carolina Flat-topped Goldenrod	*Euthamia caroliniana*	2007	T
Fringed Gentian	*Gentianopsis crinita*	2000	P
Small Fringed Gentian	*Gentianopsis procera*	1990	T
Rough Pennyroyal	*Hedeoma hispida*	2016	P
Kalm's St. John's-wort	*Hypericum kalmianum*	2007	E
Thyme-leaved Pinweed	*Lechea minor*	2000	E
Hairy Pinweed	*Lechea mucronata*	2000	P
Wood Lily	*Lilium philadelphicum*	1982	E
Drummond's Dwarf Bulrush	*Lipocarpha drummondii*	2013	E
Dwarf Bulrush	*Lipocarpha micrantha*	1990	T
Wild Lupine	*Lupinus perennis*	2000	P
Prairie Rattlesnake-root	*Nabalus racemosus*	2000	P
Common Prickly Pear	*Opuntia cespitosa*	2011	P
Sand Cherry	*Prunus pumila* var. *cuneata*	1987	E
Long-beaked Willow	*Salix bebbiana*	1989	U
Blue-leaved Willow	*Salix myricoides*	1995	P
Slender Willow	*Salix petiolaris*	2008	T
Leathery Grape Fern	*Sceptridium multifidum*	2021	E
Slender Showy Goldenrod	*Solidago rigidiuscula*	2000	E
Shining Ladies'-tresses	*Spiranthes lucida*	2017	P
Bushy Aster	*Symphyotrichum dumosum*	1993	T
Lance-leaved Violet	*Viola lanceolata*	1993	P

14. References

Aden, D., R. Pavey, D. Jones, M. Angle, D. Martin, and J. Wells, 2012, Surficial geology of the Defiance 30 X 60-minute quadrangel in Ohio: Ohio Department of Natural Resources, Division of Geological Survey Map SG-2 DEF.

AMPP, 2023, Guideline for Materials Selection and Corrosion Control for CO2 Transport and Injection, AMPP Guide 21532–2023.

American Petroleum Institute 5CT, 11th Edition, Casing and Tubing, 2023: American Petroleum Institute.

API RP 65-3 : Wellbore Plugging and Abandonment, 2021: American Petroleum Institute (API), 53 p.

API Specification 10D - Specification for Centralizer Placement and Stop-collar Testing, 2004: American Petroleum Institute.

Attachment 02: AoR and Corrective Action Plan, 2025, Underground Injection Control Class VI Permit Application: Maple.

Attachment 03: Financial Assurance Plan, 2025, Underground Injection Control Class VI Permit Application: Maple.

Attachment 04: Injection Well Construction Plan, 2025, Underground Injection Control Class VI Permit Application: Maple.

Attachment 05: Pre-operational Testing Program, 2025, Underground Injection Control Class VI Permit Application: Maple.

Attachment 06: Testing and Monitoring, 2025, Underground Injection Control Class VI Permit Application: Maple.

Attachment 07: Injection Well Plugging Plan, 2025, Underground Injection Control Class VI Permit Application: Maple.

Attachment 08: Post-injection Site Care and Site Closure, 2025, Underground Injection Control Class VI Permit Application: Maple.

Attachment 09: Emergency and Remedial Response Plan, 2025, Underground Injection Control Class VI Permit Application: Maple.

Attachment 10: Quality Assurance and Surveillance Plan, 2025, Underground Injection Control Class VI Permit Application: Maple.

Baker Hughes, 2021, Signature Series F Retainer Production Packer Brochure: Baker Hughes Company.

Banjade, B., 2011, Subsurface Facies Analysis of the Cambrian Conasauga Formation and Kerbel Formation in East - Central Ohio: Geology.

Baranoski, M. T., 2002, Structure contour map on the Precambrian unconformity surface in Ohio and related basement features: Ohio Division of Geological Survey, and 18-page text.

Baranoski, M. T., 2013, Structure Contour Map on the Precambrian Unconformity Surface in Ohio and Related Basement Features, Version 2.0: Columbus, OH, Department of Natural Resources, Division of Geological Survey, Digital Map Series PG-23, 17 p. text.

Baranoski, M. T., S. L. Dean, J. L. Wicks, and V. M. Brown, 2009, Unconformity-bounded seismic reflection sequences define Grenville-age rift system and foreland basins beneath the Phanerozoic in Ohio: Geosphere, v. 5, no. 2, p. 140–151, doi:10.1130/GES00202.1.

Barlet-Gouedard, V., G. Rimmele, B. Goffe, and O. Porcherie, 2007, Well Tecnologies for CO2 Geoligical Storage: CO2-Resistant Cement: Oil and Gas Science and Technology, v. 62, no. No. 3, p. 325–334, doi:10.2516.

Barree, R. D., and M. W. Conway, 2009, Stress and Rock Property Profiling for Unconventional Reservoir Stimulation: SPE, v. Paper 11873.

Berger, P. M., and W. R. Roy, 2011, Potential for iron oxides to control metal releases in CO2 sequestration scenarios: Energy Procedia, v. 4, p. 3195–3201, doi:10.1016/j.egypro.2011.02.235.

Bergstrom, S., and C. Mitchell, 1992, The Ordovician Utica Shale in the eastern midcontinent region: Age, lithofacies, and regional relationships: Oklahoma Geological Survey Bulletin, v. 14, p. 67–89.

Bethke, C. M., 1998, The Geochemist’s Workbench Users Guide: University of Illinois.

Bickford, M. E., W. R. Van, and I. Zietz, 1986, Proterozoic history of the midcontinent region of North America: Geology, v. 14, no. 6, p. 492–496, doi:10.1130/0091-7613(1986)14%3C492:PHOTMR%3E2.0.CO;2.

Bloxson, J., and A. Valdez, 2024, Far–field tectonic controls on deposition in the Appalachian Basin – A case study of Late Cambrian–Late Ordovician strata in Morrow County, Ohio: Results in Earth Sciences, v. 2, doi:https://doi.org/10.1016/j.rines.2024.100035.

Bowen, B. B., R. I. Ochoa, N. D. Wilkens, J. Brophy, T. R. Lovell, N. Fischietto, C. R. Medina, and J. A. Rupp, 2011, Depositional and diagenetic variability within the Cambrian Mount Simon Sandstone: Implications for carbon dioxide sequestration: Environmental Geosciences, v. 18, no. 2, p. 69–89, doi:10.1306/eg.07271010012.

Bugliosi, E.F., 1990, Plan of study for the Ohio-Indiana carbonate-bedrock and glacial-aquifer system, No. 90-151: US Geological Survey.

Byerlee, J. D., 1978, Friction of Rock: Pure and Applied Geophysics, v. 116, p. 615–626.

Calhoun, D. E., and D. S. Orr, 1992, Ground Water Resources of Putnam County: Columbus, OH, Ohio Department of Natural Resources, Division of Water.

Calvert, W., 1962, Sub-Trenton rocks from Lee County, Virginia to Fayette County, Ohio: Ohio Division of Geological Survey.

Casey, G.D., 1994, Hydrogeology of the Silurian and Devonian carbonate-rock aquifer system in the Midwestern Basins and Arches Region of Indiana, Ohio, Michigan, and Illinois, No. 93-663: US Geological Survey.

Conner, A., E. Howat, I. Fukai, and S. Mishra, 2016, Analysis and Integration of Advanced Logs and Core Data: Characterization of the Copper Ridge Dolomite in Morrow County, Ohio, *in* Lexington, KY: AAPG.

Dart, R. L., and M. C. Hansen, 2008, Earthquakes in Ohio and Vicinity 1776-2007: U.S. Geological Survey, Open-File Report 2008-1221.

Denison, R. E., E. G. Lidiak, M. E. Bickford, and E. G. Kisvarsanyi, 1984, Geology and geochronology of Precambrian rocks in the Central Interior Region of the United States: U.S: Geological Survey Professional Paper, v. 1241– C, p. 20.

Dickas, A. B., M. G. Mudrey Jr., R. W. Ojakangas, and D. L. Shrake, 1992, A possible southeastern extension of the Midcontinent Rift System located in Ohio: Tectonics, v. 11, no. 6, p. 1406–1414, doi:10.1029/91TC02903.

Drahovzal, J. A., D. C. Harris, L. H. Wickstrom, D. Walker, M. T. Baranoski, B. Keith, and L. C. Furer, 1992, The East Continent Rift Basin: A New Discovery, Special Publication 18: Kentucky Geological Survey, Series XI.

Droste, J. B., and J. B. Patton, 1985, Lithostratigraphy of the Sauk Sequence: Bloomington: Indiana Geological Survey, Occasional Paper, v. 47, p. 24.

Eberts, S.M. and George, L.L., 2000, Regional groundwater flow and geochemistry in the Midwestern basins and arches aquifer system in parts of Indiana, Ohio, Michigan, and Illinois, No. 1423-C: US Geological Survey.

Fakhari, M., 2016, Revisiting the Structural Geology of Northwestern Ohio, *in* Champaign, IL: doi:10.1130/abs/2016NC-275634.

FEMA, National Flood Hazard Layer: <https://www.fema.gov/flood-maps/national-flood-hazard-layer> (accessed April 27, 2023, a).

FEMA, National Risk Index Map: Federal Emergency Management Agency.

Fisher, D., and S. Nightengale, 2006, The rise and fall of the Taconic Mountains: A geological history of eastern New York: Nensonville, New York, Black Dome Press, 184 p.

Freeman, L., 1953, Regional subsurface stratigraphy of the Cambrian and Ordovician in Kentucky and vicinity: Kentucky Geological Survey, 12,352 p.

Freiburg, J. T., R. W. Ritzi, and K. S. Kehoe, 2016, Depositional and diagenetic controls on anomalously high porosity within a deeply buried CO2 storage reservoir—The Cambrian Mt. Simon Sandstone, Illinois Basin, USA: International Journal of Greenhouse Gas Control, v. 55, p. 42–54, doi:10.1016/j.ijggc.2016.11.005.

Gaus, I., M. Azaroual, and I. Czernichowski-Lauriol, 2005, Reactive transport modelling of the impact of CO2 injection on the clayey cap rock at Sleipner (North Sea): Chemical Geology, v. 217, no. 3, p. 319–337, doi:10.1016/j.chemgeo.2004.12.016.

Gollakota, S., and S. McDonald, 2014, Commercial-scale CCS Project in Decatur, Illinois - Construction Status and Operational Plans for Demonstration: Energy Procedia, p. 5986–5993.

Green, M. R., 2018, Geophysical Exploration of the Upper Crust Underlying North-Central Indiana: New Insight into the Eastern Granite-Rhyolite Province: Wright State University.

Greenberg, S. E., 2021, Illinois Basin-Decatur Project Final Report: An Assessment of Geologic Carbon Sequestration Options in the Illinois Basin: Phase III: United States Department of Energy.

Gundogan, O., E. Mackay, and A. Todd, 2011, Comparison of numerical codes for geochemical modelling of CO2 storage in target sandstone reservoirs: Chemical Engineering Research and Design, v. 89, no. 9, p. 1805–1816, doi:10.1016/j.cherd.2010.09.008.

Gupta, N. et al., 2017, Integrated Sub-Basin Scale Exploration for Carbon Storage Targets: Advanced Characterization of Geologic Reservoirs and Caprocks in the Upper Ohio River Valley: Energy Procedia, v. 14, p. 2781–2791.

Haneberg-Diggs, D. M., 2015, The “Clinton” Oil-And-Gas Play in Ohio, GeoFacts 30: Ohio Department of Natural Resources, Division of Geological Survey.

Hansen, M.C., 1998, GEOLOGY OF OHIO—THE SILURIAN.

Hansen, Michael C., 1998, The Geology of Ohio—The Cambrian, GeoFacts No. 20: Ohio Department of Natural Resources, Division of Geological Survey.

Harris, D. C., and M. T. Baranoski, 1997, CAMBRIAN PRE-KNOX GROUP PLAY: State of Ohio Information Circular, v. 60, p. 31.

Heidbach, O., M. Rajabi, K. Reiter, M. Ziegler, and WSM Team, 2016, World Stress Map Database Release 2016: GFZ Data Servies.

Hickman, J., C. Eble, and D. Harris, 2015, A geologic play book for Utica Shale Appalachian basin exploration, Final report of the Utica Shale Appalachian basin exploration consortium, *in* Patchen, D.G. and Carter, K.M.: Lithostratigraphy, p. 19–21.

Hurd, O., and M. D. Zoback, 2012, Regional Stress Orientations and Slip Compatibility of Earthquake Focal Planes in the New Madrid Seismic Zone: Seismological Research Letters, v. 83, no. 4, p. 672–679, doi:10.1785/0220110122.

INEOS Nitriles, 2016, Underground Injection Control Permit to Operate Class I Hazardous Well; Ohio Permit UIC 03-02-005-PTO-I, Ohio Permit UIC 03-02-005-PTO-I: Ohio Environmental Protection Agency Division of Drinking and Ground Waters.

Jaeger, J. C., and N. G. W. Cook, 1971, Fundamentals of Rock Mechanics: London, Chapman and Hall.

Janssens, A., 1973, Stratigraphy of the Cambrian and lower Ordovician in Ohio,1973 Ohio Div: Geol. Survey Bull, v. 64.

Janssens, A, 1977, Silurian rocks in the subsurface of northwestern Ohio. Ohio. Division of Geological Survey.

Knight, W. V., 1969, Historical and Economic Geology of Lower Silurian Clinton Sandstone of Northeastern Ohio1: AAPG Bulletin, v. 53, no. 7, p. 1421–1452, doi:10.1306/5D25C85D-16C1-11D7-8645000102C1865D.

Kolata, D. R., and W. J. Nelson, 1990, Tectonic History of the Illinois Basin, *in* Interior Cratonic Basins: American Association of Petroleum Geologists, doi:10.1306/M51530C19.

Kolata, D. R., and C. K. Nimz (eds.), 2010, Geology of Illinois: Illinois State Geological Survey.

Komara, K., 2017, Lithologic and Well Log Analysis of a Four Well Case Study, in Morrow County, Ohio: Senior Independent Study Theses, v. 7653.

Korose, C., 2022, Wabash CarbonSAFE, Final Report, Final Report, DE-FE0031626-FINAL, 1874030: DE-FE0031626-FINAL, 1874030 p., doi:10.2172/1874030.

Labotka, D. M., S. V. Panno, R. A. Locke, and J. T. Freiburg, 2015, Isotopic and geochemical characterization of fossil brines of the Cambrian Mt. Simon Sandstone and Ironton–Galesville Formation from the Illinois Basin, USA: Geochimica et Cosmochimica Acta, v. 165, p. 342–360, doi:10.1016/j.gca.2015.06.013.

Lacy, L. L., 1997, Dynamic Rock Mechanics Testing for Optimized Fracture Design: 38716.

Leetaru, H., C. Blakley, C. Carman, D. Garner, and C. Korose, 2019, Carbon Storage Assurance Facility Enterprise (CarbonSAFE): Integrated CCS Pre-Feasibility CarbonSAFE Illinois East Sub-Basin Final Report, Final Report, DOE-FE0029445, 1576199: Prairie Research Institute, DOE-FE0029445, 1576199 p., doi:10.2172/1576199.

Leetaru, H. E., and J. H. McBride, 2009, Reservoir uncertainty, Precambrian topography, and carbon sequestration in the Mt. Simon Sandstone, Illinois Basin: Environmental Geosciences, v. 16, no. 4, p. 235–243, doi:10.1306/eg.04210909006.

Medina, C. R., and J. A. Rupp, 2012, Reservoir characterization and lithostratigraphic division of the Mount Simon Sandstone (Cambrian): Implications for estimations of geologic sequestration storage capacity: Environmental Geosciences, v. 19, no. No. 1, p. 1–15, doi:10.1306/eg.07011111005.

Mehnert, E., and P. Weberling, 2014, Groundwater Salinity Within the Mt. Simon Sandstone in Illinois and Indiana, 582: Illinois State Geological Survey, Prairie Research Institute, University of Illinois, Circular, 31 p.

Meyer, James P., 2007, Summary of Carbon Dioxide Enhanced Oil Recovery Injection Well Technology: American Petroleum Institute.

Mohamed, I. M., J. He, and H. A. Nasr-El-Din, 2012, Carbon Dioxide Sequestration in Dolomite Rock: European Association of Geoscientists & Engineers, p. cp, doi:10.3997/2214-4609-pdb.280.iptc14924_noPW.

National Information Services Center, and National Park Service, 2023, National Wild and Scenic Rivers System Map: Harpers Ferry Center, National Wild and Scenic Rivers System, originally published in September 2018.

National Park Service, National Register of Historic Places Database and Research: <https://www.nps.gov/subjects/nationalregister/database-research.htm>.

National Park Service, Nationwide Rivers Inventory: <https://www.nps.gov/maps/full.html?mapId=8adbe798-0d7e-40fb-bd48-225513d64977>.

National Wild and Scenic Rivers System, Find a River: <https://www.rivers.gov/find-a-river>.

Norris, S.E. and Fidler, R.E., 1971, Carbonate equilibria distribution and its relation to an area of high ground-water yield in northwest Ohio.: Geological Survey Professional Paper, 750, 202.

NORSOK/EG D, 2024, Well integrity in drilling and well operations, NORSOK Standard NORSOK D-010:2021+AC2:2024: Standards Norway.

ODNR, ODNR Oil & Gas Well Viewer: Ohio Department of Natural Resources, Division of Oil & Gas.

Ohio Department of Natural Resources, 2006, Bedrock geologic map of Ohio: Ohio Department of Natural Resources, Division of Geological Survey, Map BG-1.

Ohio Division of Geologic Survey, 2004, Oil and Gas Fields Map of Ohio: Ohio Department of Natural Resources, Division of Geological Survey Map PG-1,.

Ohio Division of Geologic Survey, 2017, Shaded drift-thickness map of Ohio: Ohio Department of Natural Resources, Division of Geological Survey, Ohio Department of Natural Resources, Division of Geological Survey Map.

Ohio Division of Geological Survey, 2014, A Brief Summary of the Geologic History of Ohio.

Ohio EPA, Ambient Ground Water Monitoring Network: Ohio Environmental Protection Agency, Division of Drinking and Ground Waters.

Ohio Natural Heritage Database, 2023a, Henry County State Listed Animal Species: Division of Natural Heritage, Ohio Department of Natural Resources.

Ohio Natural Heritage Database, 2023b, Henry County State Listed Plant Species: Division of Natural Heritage, Ohio Department of Natural Resources.

Ohio Natural Heritage Database, 2023c, Putnam County State Listed Animal Species: Division of Natural Heritage, Ohio Department of Natural Resources.

The Ohio Seismic Network (OhioSeis) Earthquake Database, 2025: Ohio Department of Natural Resources, Division of Geological Survey.

Onasch, C., 2007, Structural evolution of the bowling green fault.

Panno, S. V., K. C. Hackley, R. A. Locke, I. G. Krapac, B. Wimmer, A. Iranmanesh, and W. R. Kelly, 2013, Formation waters from Cambrian-age strata, Illinois Basin, USA: Constraints on their origin and evolution: Geochimica et Cosmochimica Acta, v. 122, p. 184–197, doi:10.1016/j.gca.2013.08.021.

Parkhurst, D. L., and C. A. J. Appelo, 2013, USGS - Description of Input and Examples for PHREEQC Version 3—A Computer Program for Speciation, Batch-Reaction, One-Dimensional Transport, and Inverse Geochemical Calculations, *in* U.S. Geological Survey Techniques and Methods: Book 6 Chapter A43, p. 497.

Qafoku, N., L. Zheng, D. H. Bacon, A. R. Lawter, and C. F. Brown, 2015, A Critical Review of the Impacts of Leaking CO_2 Gas and Brine on Groundwater Quality, PNNL--24897, 1347881: PNNL--24897, 1347881 p., doi:10.2172/1347881.

Riley, R. A., J. McDonald, and D. R. Martin, 2012, Elevation contours on the base of the deepest underground sources of drinking water in Ohio: Columbus, OH, Department of Natural Resources, Division of Geological Survey, Map EG_6.

Riley, R. A., J. Wicks, and J. Thomas, 2002, Cambrian-Ordovician Knox Production in Ohio: Three Case Studies of Structural-Stratigraphic Traps: AAPG Bulletin, v. 86, no. 4, p. 539–555, doi:10.1306/61EEDB3E-173E-11D7-8645000102C1865D.

Ruff, L., R. LaForge, R. Thorson, T. Wagner, and F. Goudaen, 1994, Geophysical Investigations of the Western Ohio-Indiana Region: Final Report for the U.S. Nuclear Regulatory

Commission, October 1986-September 1992, NUREG/CR-3145, Vol. 10: The University of Michigan Department of Geological Sciences.

Saeed, A., and J. E. Evans, 2012, Subsurface Facies Analysis of the Late Cambrian Mt. Simon Sandstone in Western Ohio (Midcontinent North America), 2: Open Journal of Geology, v. 2, no. 2, p. 35–47, doi:10.4236/ojg.2012.22004.

Sanders, L. L., 1991, Geochemistry of Formation Waters from the Lower Silurian Clinton Formation (Albion Sandstone), Eastern Ohio1: AAPG Bulletin, v. 75, no. 10, p. 1593–1608, doi:10.1306/0C9B29A7-1710-11D7-8645000102C1865D.

Schlumberger, 2021, EverCRETE CO2 Resistant cement system: Schlumberger.

Sminchak, J., 2012, SIMULATION FRAMEWORK FOR REGIONAL GEOLOGIC CO2 STORAGE ALONG ARCHES PROVINCE OF MIDWESTERN UNITED STATES: United States, Battelle Memorial Institute, Columbus, OH (United States), doi:10.2172/1110321.

Smith, Dr. L, 2012, Establishing and Maintaining the Integrity of Wells used for Sequestration of CO2.: NACE.

S&P Global, S&P Global Energy Portal: <https://my.ihs.com/Energy/Products> (accessed May 5, 2023).

Sutton, E., 1965, Trempealeau Reservoir Performance, Morrow County Field, Ohio: Journal of Petroleum Technology, v. 17, no. 12, p. 1391–1395, doi:10.2118/1208-PA.

Syed, T., R. Sweatman, and G. Benge, 2018, Well Engineering and Injection Regularity in CO_2 Storage Wells, Technical Report 2018–08: IEAGHG, IEA Greenhouse Gas R&D Programme, 415 p.

Tetra Tech, 2024, Critical Issues Analysis - Carbon Sequestration Project in Putnam, Hancock, and Henry Counties, Ohio.

Trémosa, J., C. Castillo, C. Q. Vong, C. Kervévan, A. Lassin, and P. Audigane, 2014, Long-term assessment of geochemical reactivity of CO2 storage in highly saline aquifers: Application to Ketzin, In Salah and Snøhvit storage sites: International Journal of Greenhouse Gas Control, v. 20, p. 2–26, doi:10.1016/j.ijggc.2013.10.022.

Tuboscope - NOV Wellbore Technologies, 2017, TK-15XT Specifications: National Oilwell Varco.

Tuboscope Coatings Spec Sheet, 2022: National Oilwell Varco.

USFWS, 2025, IPaC: Information for Planning and Consultation Resource List, Maple Project.

USGS, 2025, USGS Earthquake Catalog Search: <https://earthquake.usgs.gov/earthquakes/search/> (accessed July 3, 2025).

USGS, 2024, USGS Earthquake Catalog Search: <https://earthquake.usgs.gov/earthquakes/search/> (accessed September 24, 2024).

Vickery Environmental, Inc., 1989, Petrography report.

Vickery Environmental Inc., 2020, Vault 4401 - Renewal Application for UIC Permits 3-5-2020.pdf - All Documents.

Walsh, F. R. I., M. D. Zoback, S. P. Lele, D. Pais, M. Weingarten, and T. Tyrell, 2018, FSP 2.0: A program for probabilistic estimation of fault slip potential resulting from fluid injection: University of Texas.

Whittaker, S., 2022, Illinois Storage Corridor, *in* NETL, ed.: NETL Annual Review Meeting 2022.

Whittaker, S., and C. Carman, 2022, CarbonSAFE Illinois - Macon County Final Report.

Wickstrom, L. H. et al., 2005, Characterization of Geologic Sequestration Opportunities in the MRCSP Region Phase I, Open-File Report 2005–1: Midwest Regional Carbon Sequestration Partnership (MRCSP).

Wickstrom, L., J. Gray, and R. Stieglitz, 1992, Stratigraphy, structure, and production history of the Trenton Limestone (Ordovician) and adjacent strata in northwestern Ohio, Report of Investigations No. 143: Columbus, Ohio, Department of Natural Resources, Division of Geological Survey.

Zhao, H., R. Dilmore, D. E. Allen, S. W. Hedges, Y. Soong, and S. N. Lvov, 2015, Measurement and Modeling of CO2 Solubility in Natural and Synthetic Formation Brines for CO2 Sequestration: Environmental Science & Technology, v. 49, no. 3, p. 1972–1980, doi:10.1021/es505550a.

Zoback, M. D., 2010, Reservoir Geomechanics: Cambridge University Press, 505 p.

15. PBI Appendix 1A – List of Landowners Within the AoR

Claimed as PBI

Claimed as PBI

Claimed as PBI

Claimed as PBI

Claimed as PBI

Claimed as PBI

Claimed as PBI

Claimed as PBI

Claimed as PBI

Claimed as PBI

Claimed as PBI

Claimed as PBI

Claimed as PBI

Claimed as PBI

Claimed as PBI

Claimed as PBI

Claimed as PBI

Claimed as PBI

Claimed as PBI

Claimed as PBI

Claimed as PBI

16. Appendix 1B – Wells used for Geologic Evaluation

UWI	Permit License Number	Well Name	Latitude	Longitude	Kelly Bushing Elevation (feet above sea level)	Ground Surface Elevation (feet above sea level)	Max TD	Current Status	Spud Date	Permit License Date	Completion Date	Abandonment Date	Current Operator	Formation at TD	Hole Direction	Current Class	Plot Symbol Description
34175201730000	173	Isodore Frey	40.81847792	-83.4131473		862.9	2875	Dry & abandoned	1964-01-02	1963-12-23	1964-02-01		Comanche Oil Co	Trempealeau Sd	Vertical	New field wildcat-dry (including temporarily abandoned well)	Dry and abandoned
34101201670000	167	Herr John F	40.64464134	-83.34170837	905	892.4	2934	Dry & abandoned	1984-04-25	1984-04-15	1984-05-05		Delray Oil Inc	Granite	Vertical	New field wildcat-dry (including temporarily abandoned well)	Dry and abandoned
34175606100000		P M Parsell	40.74373181	-83.42154493		908.8	5632	Dry & abandoned	1947-01-01	1946-12-22	1947-03-07		Dibble & Miller	Unknown	Vertical	Development well-dry (including temporarily abandoned well)	Dry and abandoned
34175202580000	258	Brocklesby C	40.82693053	-83.18628958	890	879.3	3169	Dry & abandoned	1981-05-21	1981-05-11	1982-01-21		Berea Oil & Gas Corp	Granite	Vertical	New field wildcat-dry (including temporarily abandoned well)	Dry and abandoned
34117240120000	4012	Morris L & R	40.56856947	-82.69714184	1331	1315.6	3936	Oil producer	1991-02-27	1991-02-17	1991-04-12		Maram Energy	Trempealeau	Vertical	Development well-oil	Oil
34161200440000		A A & M J Miller	40.75737063	-84.3995901	820	807.1	3242	Dry & abandoned	1972-04-17	1972-04-07	1972-10-17		West Ohio Gas Co	Basement	Vertical	Development well-dry (including temporarily abandoned well)	Dry and abandoned
34083214130000	1413	E E Cunningham	40.51990865	-82.38730715	1253	1253.3	5747	Dry & abandoned -oil & gas shows	1961-07-10	1961-06-30	1961-08-07		Cantway David L	Granite	Vertical	New field wildcat-dry (including temporarily abandoned well)	Dry and abandoned
34083214680001	1468	G D Larimore	40.32566591	-82.56444416		1194.2	5376	Dry & abandoned-old well worked over	1963-01-01	1962-12-22	1963-02-04		Ohio Fuel Gas	Basal/Sd/	Vertical	New field wildcat-dry (including temporarily abandoned well)	Dry and abandoned
34159200740000	74	Low	40.22484494	-83.27590023	975	964.6	3438	Dry & abandoned	1984-12-27	1984-12-17	1985-01-05		Funk Exploration Inc	Trempealeau	Vertical	New field wildcat-dry (including temporarily abandoned well)	Dry and abandoned
34041201260000	126	D Rouse	40.3802606	-82.99203216	974	964.6	3750	Dry & abandoned	1964-07-28	1964-07-18	1964-11-14		Atha Howard D	Mount Simon /Sd/	Vertical	New field wildcat-dry (including temporarily abandoned well)	Dry and abandoned
34041203220000	322	Jolliff	40.35130675	-83.22606401	933	921.9	3382	Dry & abandoned	1985-01-09	1984-12-30	1985-01-19		Funk Exploration Inc	Granite	Vertical	New field wildcat-dry (including temporarily abandoned well)	Dry and abandoned
34063203600000	20360	Knox High	41.1676796	-83.8051319	729	715.2	2992	Dry & abandoned	2018-03-30	2018-02-02	2019-11-06		Hilcorp Energy Co	Black River /Lm/	Vertical	Development well-dry (including temporarily abandoned well)	Dry and abandoned
34041203540000	354	Cockrell-Godshall Unit	40.26175736	-82.7701322	1118	1112.2	4873	Temporarily abandoned	1991-01-10	1990-11-09	1995-04-26		Poling Richard C	Precambrian	Vertical	Deeper pool wildcat-dry	Dry and abandoned
34069200360000		K A Hall	41.35808495	-84.02292702	683	679.1	3480	Dry & abandoned	1973-08-22	1973-08-12	1973-10-10		Callander & Kimbrel Inc	Cambrian	Vertical	Deeper pool wildcat-dry	Dry and abandoned
34159200840000	84	Hutchins	40.34147335	-83.50792861	1079	1069.6	2765	Dry & abandoned -gas shows	1992-05-09	1992-04-29	1992-05-17		Majestic Oil & Gas Inc	Rome	Vertical	New field wildcat-dry (including temporarily abandoned well)	Dry and abandoned
34117219350000	1935	E-V Bush	40.51739646	-82.9575862	999	987.5	3867	Dry & abandoned -oil shows	1964-08-06	1964-07-27	1964-08-22		Comanche Oil Co	Granite	Vertical	New field wildcat-dry (including temporarily abandoned well)	Dry and abandoned
34091200860000	86	Comer Lena	40.34398425	-83.63478883	1439	1437	3402	Dry & abandoned	1976-04-28	1976-04-18	1976-05-12		Worthington Oil	Mount Simon /Sd/	Vertical	New field wildcat-dry (including temporarily abandoned well)	Dry and abandoned
34101200610000	61	M G Kennedy	40.68039117	-83.09012523		961.3	2565	Dry & abandoned	1964-07-16	1964-07-06	1964-09-01		Mitchell & Donelson	Trempealeau	Vertical	New field wildcat-dry (including temporarily abandoned well)	Dry and abandoned
34101200710000	0071	Ferguson B S	40.64566098	-83.30571913		889.1	1933	Dry & abandoned	1964-09-23	1964-08-21	1964-11-05	1964-11-18	Petroleum Services Inc	Unknown	Vertical	New field wildcat-dry (including temporarily abandoned well)	Dry and abandoned
34083240170000	4017	Ernest Unit	40.29583907	-82.47210186	1003	994.1	5238	Oil producer	1993-04-12	1993-04-02	1993-06-14		Knox Energy Inc	Mount Simon /Sd/	Vertical	Development well-oil	Oil
34149201030000	103	Borland	40.27127945	-84.06003451	1074	1063	3227	Dry & abandoned	1985-01-24	1985-01-14	1985-03-24		Funk Exploration Inc	Mount Simon /Sd/	Vertical	New field wildcat-dry (including temporarily abandoned well)	Dry and abandoned
34117200120000	12	O & E Myers	40.57025103	-82.91191827		1007.2	4100	Abandoned oil producer	1961-07-06	1961-06-26	1961-07-28	1967-09-05	Ashland Oil Inc	Unknown	Vertical	Development well-oil	Abandoned oil
34101201440001	144	Kyle J & J	40.51883353	-83.11908525	997	987.5	3485	Dry & abandoned old well worked over	1982-11-18	1982-11-08	1982-11-22		Ohio Natural Fuel	Mount Simon /Sd/	Vertical	Deeper pool wildcat-dry	Dry and abandoned
34159200250000	25	George A Beeson	40.29015736	-83.38482978	1027	1017.1	3187	Dry & abandoned	1964-07-30	1964-07-20	1964-08-16		Branoco of Ohio	Mount Simon /Sd/	Vertical	New field wildcat-dry (including temporarily abandoned well)	Dry and abandoned
34147202110000	211	Shults Howard R	41.19003651	-83.18644199	723	708.7	2847	Temporarily abandoned - oil	1979-01-23	1979-01-13	1979-01-31		A & S Energy LLC	Basement	Vertical	Development well-oil	Suspended undesignated
34063201390000	0139	Frazier C & M	40.93696352	-83.76859186		826.8	3017	Dry & abandoned	1964-04-27	1964-04-24	1964-06-02	1964-06-04	Dever Frank M	Middle Run	Vertical	New field wildcat-dry (including temporarily abandoned well)	Dry and abandoned
34083239440000	3944	White Donald	40.29255868	-82.66925989	1212	1200.8	5024	Temporarily abandoned - gas	1991-06-24	1991-06-14	1991-06-30		Petro Evaluation Services	Granite	Vertical	New field wildcat-discovery	Suspended gas
34159200690000	69	Yoder	40.2276614	-83.26536818	971	958	3505	Dry & abandoned	1984-08-09	1984-07-30	1984-08-17		Funk Exploration Inc	Granite	Vertical	New field wildcat-dry (including temporarily abandoned well)	Dry and abandoned
34143202350000	0235	Ohio Liquid Disposal Inc	41.37150031	-82.98234783	616	610.2	2980	Water injection	1979-09-10	1979-09-05	1979-09-27		Ohio Liquid Disposal	Precambrian	Vertical	Injection	Water injector
34143201470000	147	Paul L Kerbel	41.43771454	-83.31621467	647	636.5	2785	Dry & abandoned	1965-11-24	1965-11-14	1965-11-30		Maguire Russell	Granite	Vertical	New field wildcat-dry (including temporarily abandoned well)	Dry and abandoned
34175202110000	211	George Eyestone	40.89556902	-83.12098496		935	3260	Dry & abandoned	1965-10-04	1965-09-24	1965-10-11		Minnesota Ohio Oil	Precambrian	Vertical	New field wildcat-dry (including temporarily abandoned well)	Dry and abandoned
34091200960000	96	Prinkey R Unit	40.41359015	-83.61646949	1125	1122	3260	Dry & abandoned-oil & gas shows	1991-10-29	1991-10-19	1991-11-06		Ashtola Exploration Co Inc	Granite	Vertical	New field wildcat-dry (including temporarily abandoned well)	Dry and abandoned
34091200180000		Virgil Johns Etal	40.45617755	-83.77165686		1161.4	3361	Dry & abandoned	1947-05-21	1947-05-11	1947-07-09		Marathon Oil Co	Unknown	Vertical	Development well-dry (including temporarily abandoned well)	Dry and abandoned
34033200500000	50	Leonhardt V E	40.90998866	-82.88340863	1008	997.4	3775	Dry & abandoned	1965-09-30	1965-09-20	1965-10-12		Fishburn Producing	Trempealeau	Vertical	New field wildcat-dry (including temporarily abandoned well)	Dry and abandoned
34147608400000	0840	M & B Asphalt Co	41.22645369	-83.19882961		695.5	2870	Observation well-no shows	1984-12-17	1984-12-07	1985-01-01		DNR Geological Survey	Precambrian	Vertical	Unclassified	Service
34101201650000	165	McNamara John & Sarah	40.51383565	-83.04980377	965	958	3657	Dry & abandoned	1984-08-07	1984-07-28	1987-12-22		Double D Well Service	Mount Simon /Sd/	Vertical	New field wildcat-dry (including temporarily abandoned well)	Dry and abandoned
34089220570000	2057	H-M Roberts	40.23327679	-82.71556453	1178	1168	4952	Dry & abandoned	1964-01-29	1964-01-19	1964-02-29		Atha Howard D	Precambrian	Vertical	New field wildcat-dry (including temporarily abandoned well)	Dry and abandoned
34039200280000		Pearl A Haver	41.32444436	-84.59391315		715.2	3609	Dry & abandoned	1962-10-22	1962-10-12	1963-01-04		Brown S E Trustee	Granite	Vertical	New field wildcat-dry (including temporarily abandoned well)	Dry and abandoned
34101201680000	168	Gracely Farms	40.58637168	-83.25419599	924	915.4	3074	Dry & abandoned	1984-06-12	1984-06-02	1984-06-20		Anschutz Corp	Granite	Vertical	New field wildcat-dry (including temporarily abandoned well)	Dry and abandoned
34041200500000	50	J B Rupple	40.2799222	-83.07338094	915	889.1	3487	Dry & abandoned	1964-05-12	1964-05-02	1964-06-07		Texas Coastal Oil Co	Mount Simon /Sd/	Vertical	New field wildcat-dry (including temporarily abandoned well)	Dry and abandoned
34101200080000	8	H T & M E Mitchell	40.58127331	-83.00288186	1001	987.5	3672	Dry & abandoned	1962-02-23	1962-02-13	1962-03-14		United Producing Co Inc	Precambrian	Vertical	Development well-dry (including temporarily abandoned well)	Dry and abandoned
34117240430000	4043	Hickok E & F	40.60524844	-82.72318221	1398	1394.4	4707	Dry & abandoned -oil & gas shows	1991-08-28	1991-08-18	1991-10-23		EEI Inc	Granite	Vertical	Deeper pool wildcat-dry	Dry and abandoned
34101201740000	174	Gracely Farms	40.58709224	-83.22773955	916	908.8	3198	Dry & abandoned	1984-11-02	1984-10-23	1984-11-08		Texas Gas Exploration Corp	Granite	Vertical	New field wildcat-dry (including temporarily abandoned well)	Dry and abandoned
34083240000000	4000	Mccoy	40.27147491	-82.46025013	987	977.7	5216	Oil producer	2007-05-21	1992-09-10	2007-07-18		Knox Energy Inc	Precambrian	Vertical	New field wildcat-discovery	Oil
34065201330000	133	Fewell	40.75174127	-83.54153049	934	925.2	2928	Dry & abandoned-oil shows	1997-03-14	1997-03-04	1997-03-21	1999-11-17	Knox Energy Inc	Precambrian	Vertical	Deeper pool wildcat-dry	Dry and abandoned
34117200330000	33	J W Henry	40.43668817	-82.92450909	995	981	4048	Dry & abandoned	1961-12-17	1961-12-07	1962-01-08		Wehmeyer Karl	Precambrian	Vertical	Development well-dry (including temporarily abandoned well)	Dry and abandoned
34033200440000	44	Spitler-Brown Unit	40.91796291	-83.06329802	977	967.8	3415	Dry & abandoned	1965-05-15	1965-05-05	1965-05-30		Piggott G M Jr	Precambrian	Vertical	New field wildcat-dry (including temporarily abandoned well)	Dry and abandoned
34143202260000	226	Ohio Liquid Disposal Inc	41.36877764	-82.97693858	618	607	2910	Saltwater disposal oil & gas operator	1976-07-15	1976-01-26	1976-11-25		Ohio Liquid Disposal	Basement	Vertical	Injection	Disposal
34093207940000	794	Born A & A	41.28946753	-82.32049123		846.5	4590	Dry & abandoned -oil shows	1960-07-15	1960-07-05	1960-11-14		East Ohio Gas Co The	Precambrian	Vertical	Development well-dry (including temporarily abandoned well)	Dry and abandoned
34083238650000	3865	Daniels-Weller Unit	40.51147365	-82.61925248	1179	1168	4400	Dry & abandoned	1989-07-28	1989-07-18	1990-08-06		Smail James R	Kerbel	Vertical	New field wildcat-dry (including temporarily abandoned well)	Dry and abandoned
34147202120000	212	Watson John W	41.15819652	-83.18418528	741	731.6	2859	Dry & abandoned	1979-02-11	1979-02-01	1979-02-24		A & S Energy LLC	Precambrian	Vertical	Deeper pool wildcat-dry	Dry and abandoned
34041203290000	329	Case	40.34318583	-83.06005586	919	908.8	3569	Dry & abandoned	1985-02-09	1985-01-30	1985-02-20		Funk Exploration Inc	Granite	Vertical	New field wildcat-dry (including temporarily abandoned well)	Dry and abandoned
34091201010000	101	Wish Trust	40.40455777	-83.74875609	1275	1269.7	3258	Dry & abandoned -gas shows	2002-05-16	2001-04-02	2002-05-22		Bakerwell Inc	Mount Simon /Sd/	Vertical	New field wildcat-dry (including temporarily abandoned well)	Dry and abandoned
34117238500000	3850	Hershner	40.58811759	-82.82700124	1166	1158.1	4300	Dry & abandoned	1988-06-21	1988-06-11	1988-06-29		United Operating Co	Mount Simon /Sd/	Vertical	Deeper pool wildcat-dry	Dry and abandoned
34143202250000	225	Ohio Liquid Disposal Inc	41.36840065	-82.98052869	618	610.2	2960	Saltwater disposal oil & gas operator	1976-07-01	1976-01-26	1976-11-22		Ohio Liquid Disposal	Basement	Vertical	Injection	Disposal
34063202330000	233	Rader M & P	41.09287747	-83.43331037		823.5	2410	Dry & abandoned	1981-08-21	1981-08-11	1982-11-08		Belden & Blake & Co	Mount Simon	Vertical	New field wildcat-dry (including temporarily abandoned well)	Dry and abandoned
34043200110000	11	Krysik-Wakefield	41.30364497	-82.35066254	828	823.5	4463	Oil producer	1966-05-11	1966-05-01	1966-06-24		Franklin Gas & Oil Co LLC	Precambrian	Vertical	New field wildcat-discovery	Oil

UWI	Permit License Number	Well Name	Latitude	Longitude	Kelly Bushing Elevation (feet above sea level)	Ground Surface Elevation (feet above sea level)	Max TD	Current Status	Spud Date	Permit License Date	Completion Date	Abandonment Date	Current Operator	Formation at TD	Hole Direction	Current Class	Plot Symbol Description
34139204480000	448	Empre Reves Stl Div	40.77894092	-82.51920944	1176	1168	5085	Dry & abandoned	1967-07-27	1967-07-17	1967-08-18		Empire Reeves Steel Div	Precambrian	Vertical	Development well-dry (including temporarily abandoned well)	Dry and abandoned
34159200710000	71	Black	40.2763072	-83.27685665	987	971.1	3396	Dry & abandoned	1984-08-25	1984-08-15	1984-09-01		Funk Exploration Inc	Mount Simon /Sd/	Vertical	New field wildcat-dry (including temporarily abandoned well)	Dry and abandoned
34117213880000	1388	J-B Mcbee	40.35618304	-82.82281233	1140	1135.2	4450	Dry & abandoned	1964-03-19	1964-03-09	1964-04-20		Wray Robert	Precambrian	Vertical	New field wildcat-dry (including temporarily abandoned well)	Dry and abandoned
34101200490000	49	F L Gruber	40.56644591	-83.05089063	981	974.4	3459	Dry & abandoned	1964-05-02	1964-04-22	1964-06-16		Midland Drilling	Precambrian	Vertical	New field wildcat-dry (including temporarily abandoned well)	Dry and abandoned
34065200740000	74	D & D Jones	40.75055488	-83.52812954	941	928.5	2834	Dry & abandoned -gas shows	1962-04-02	1962-03-23	1962-04-10		Edmund Norman W	Precambrian	Vertical	Development well-dry (including temporarily abandoned well)	Dry and abandoned
34101201730000	173	Oehler	40.59930143	-83.37424468	976	964.6	2989	Dry & abandoned	1984-11-18	1984-11-08	1984-11-26		Texas Gas Exploration Corp	Rome	Vertical	New field wildcat-dry (including temporarily abandoned well)	Dry and abandoned
34101200030000	0003	Baker Stanley W	40.62747173	-83.0294239		987.5	2711	Dry & abandoned	1954-04-28	1954-04-18	1954-06-02	1954-06-05	White	Unknown	Vertical	Development well-dry (including temporarily abandoned well)	Dry and abandoned
34101600200000	0020	Strickler & Hanson	40.59819935	-83.13356713		961.3	1790	Dry & abandoned	1899-12-17 00:00:00.000	1899-12-07 00:00:00.000	1900-01-01		Unknown	Trenton /Lm/	Vertical	Development well-dry (including temporarily abandoned well)	Dry and abandoned
34101202070000	207	Forry Evelyn Etal	40.69198789	-83.19985938	913	895.7	3142	Dry & abandoned	1997-12-31	1997-12-21	1998-01-06		Equitable Resources Exploration Inc	Mount Simon /Sd/	Vertical	New field wildcat-dry (including temporarily abandoned well)	Dry and abandoned
34041200220000	22	F Jones	40.36997411	-83.15568419	945	931.8	3426	Dry & abandoned	1963-12-30	1963-12-20	1964-01-16		Southern Triangle Oil Co	Precambrian	Vertical	New field wildcat-dry (including temporarily abandoned well)	Dry and abandoned
34143202100000	210	Ohio Liquid Disposal	41.37121861	-82.98127073	620	613.5	2933	Dry & abandoned	1972-03-02	1972-02-21	1972-03-17		Ohio Liquid Disposal	Precambrian	Vertical	Stratigraphic/structure test hole	Dry and abandoned
34041203580000	358	Longshore R Etal Unit	40.24383143	-82.80364219	1071	1059.7	4272	Abandoned oil producer	1993-02-16	1993-02-06	1993-02-25	2001-12-07	CGas Exploration	Granite	Vertical	New field wildcat-discovery	Abandoned oil
34117225500000	2550	J&J Irey	40.58824621	-82.9506825	1004	990.8	3876	Dry & abandoned	1965-05-29	1965-05-19	1965-06-11		Otter Creek Exploration	Unknown	Vertical	Deeper pool wildcat-dry	Dry and abandoned
34147202440000	20244	Watson John W Swdw 1	41.15295441	-83.18405761	751	741.5	2830	Saltwater disposal	1980-06-09	1980-06-06	1980-07-15		A-S Energy Inc	Granite Wash	Vertical	Injection	Disposal
34143203120000	312	Weickert B T Unit	41.42136757	-83.10393962	591	584	2773	Gas producer	2009-06-25	2009-06-15	2009-09-01		Fo Energy LLC	Mount Simon	Vertical	Development well-gas	Gas
34003200670000	67	Standard Oil Company	40.71620359	-84.12777517	872	866.1	3133	Saltwater disposal	1968-01-20	1968-01-10	1968-01-27		Vistron Corp	Mount Simon	Vertical	Injection-water	Disposal
34083239760000	3976	Parkinson Harold & Wanda	40.25288119	-82.47373051	1028	1017.1	4898	Oil producer	1992-10-01	1992-03-24	1994-01-21		Maram Energy	Rome	Vertical	Development well-oil	Oil
34043201540000	154	Baum Elton	41.36265145	-82.76106451	735	721.8	3394	Dry & abandoned	1991-07-05	1991-06-25	1991-07-14		Peninsula Group	Mount Simon /Sd/	Vertical	New field wildcat-dry (including temporarily abandoned well)	Dry and abandoned
34091200870000	87	Earnest Hemleben	40.38586316	-83.67391425	1364	1364.8	3276	Suspended well	1976-05-16	1976-05-06			Worthington Oil	Mount Simon /Sd/	Vertical	Suspended well	Suspended undesignated
34041200980000	98	Russell Cryder	40.28676756	-83.11703697		941.6	3507	Dry & abandoned	1964-06-22	1964-06-12	1964-07-06		Eastern Drilling	Cambrian Lower /Series/	Vertical	New field wildcat-dry (including temporarily abandoned well)	Dry and abandoned
34041203560000	356	Sheets Lula Mae	40.32785698	-82.91547737	987	964.6	4013	Dry & abandoned	1993-03-30	1993-03-20	1993-04-05		NGO Development Corp	Granite	Vertical	New field wildcat-dry (including temporarily abandoned well)	Dry and abandoned
34147201280000	128	Wella R Stigamire	41.18177402	-83.05665525		787.4	3175	Dry & abandoned	1965-01-04	1964-12-25	1965-01-26		Ashland Oil Inc	Precambrian	Vertical	New field wildcat-dry (including temporarily abandoned well)	Dry and abandoned
34139206780000	678	Copperweld Shelby Division	40.87425192	-82.67288728	1100	1099.1	4113	Abandoned gas producer	1993-09-21	1993-09-11	1993-10-01	1995-05-08	Copperweld Energy	Kerbel	Vertical	New field wildcat-discovery	Abandoned gas
34091200930000	93	State Of Ohio	40.30392402	-83.56186066	1103	1092.5	3140	Dry & abandoned	1985-01-02	1984-12-23	1985-01-11		Texas Gas Exploration Corp	Mount Simon /Sd/	Vertical	New field wildcat-dry (including temporarily abandoned well)	Dry and abandoned
34139204310000	431	Scott C D & K	40.68808564	-82.48050758	1448	1430.4	5503	Dry & abandoned	1966-08-19	1966-08-09	1966-09-05		Tri-State Production	Precambrian	Vertical	Development well-dry (including temporarily abandoned well)	Dry and abandoned
34101600220000	0022	Coulter Chas	40.66965359	-82.97824468		997.4		Dry & abandoned					Unknown	Trenton /Lm/	Vertical	Development well-dry (including temporarily abandoned well)	Dry and abandoned
34117241900000	4190	Lee Family Trust	40.56522096	-82.89836066	1028	1020.3	4200	Dry & abandoned	2007-02-03	2007-01-30	2007-02-18		Knox Energy Inc	Precambrian	Vertical	Development well-dry (including temporarily abandoned well)	Dry and abandoned
34089254890000	5489	Uhde Richard & Sally	40.23426799	-82.26306482	1100	1184.4	4937	Abandoned oil producer	1993-01-04	1992-12-23	1993-07-02	2011-10-26	Wray James Inc	Rome	Vertical	Development well-oil	Abandoned oil
34083239150000	3915	Donaldson J	40.31010952	-82.5360991	1086	1079.4	5366	Dry & abandoned	1990-12-02	1990-11-22	1990-12-18		EDCO Drilling & Production	Precambrian	Vertical	New field wildcat-dry (including temporarily abandoned well)	Dry and abandoned
34143202240000	224	Ohio Liquid Disposal Inc	41.37119661	-82.9833068	618	607	2961	Saltwater disposal oil & gas operator	1976-06-17	1976-01-26	1976-11-24		Ohio Liquid Disposal	Basement	Vertical	Injection	Disposal
34083240640000	4064	Ernest E	40.29717101	-82.47524529	1010	997.4	5234	Oil producer	1994-11-02	1994-10-23	1995-02-15		Knox Energy Inc	Precambrian	Vertical	Development well-oil	Oil
34147202140000	214	Hoover Stanley	41.16544936	-83.24938601	764	754.6	2600	Temporarily abandoned - gas	1979-08-18	1979-08-08	1980-01-25		A & S Energy LLC	Basement	Vertical	Development well-gas	Suspended gas
34101200140000	0014	Key Harry D	40.63232745	-83.00269226		997.4	2882	Dry & abandoned	1962-10-23	1962-10-13	1963-11-21		Adams John W	Maynardville	Vertical	Development well-dry (including temporarily abandoned well)	Dry and abandoned
34175203360000	0336	Hensel	40.73976027	-83.46122096		912.1	2855	Oil producer	2001-02-08	2001-02-05	2001-03-04		Mar Oil Co	Mount Simon	Vertical	Development well-oil	Oil
34173203670000	367	Breneman Donelda	41.21779562	-83.51171088		718.5	2200	Dry & abandoned	1980-03-15	1980-03-05	1980-04-26		Allerton Resources	Conasauga	Vertical	Deeper pool wildcat-dry	Dry and abandoned
34173202390000	0239	Asmusclarence Etal	41.46107719	-83.71118621	670	659.4	2825	Dry & abandoned	1965-05-10	1965-04-30	1965-05-25	1965-05-26	J R S Co	Precambrian	Vertical	New field wildcat-dry (including temporarily abandoned well)	Dry and abandoned
34175606260000	0626	Sears D	40.71885953	-83.24874319		876		Dry & abandoned	1903-12-17	1903-12-07	1904-01-01		Unknown	Trenton /Lm/	Vertical	Development well-dry (including temporarily abandoned well)	Dry and abandoned
34065200790000	0079	Wolf G W	40.6412534	-83.48410208	971	961.3	3002	Dry & abandoned	1963-12-27	1963-12-17	1964-01-07	1964-01-07	McMahon-Bullington Drilling Co	Precambrian	Vertical	New field wildcat-dry (including temporarily abandoned well)	Dry and abandoned
34083214680000	1468	Gerald D Larimore	40.32566591	-82.56444416		1194.2	5376	Dry & abandoned -gas shows	1962-12-01	1962-11-21	1963-01-09		Ohio Fuel Gas	Basal/Sd/	Vertical	Development well-dry (including temporarily abandoned well)	Dry and abandoned
34159200670000	67	Graver J & B	40.24941201	-83.27600657	966	954.7	3446	Dry & abandoned	1984-07-29	1984-07-19	1984-08-08		Funk Exploration Inc	Granite	Vertical	New field wildcat-dry (including temporarily abandoned well)	Dry and abandoned
34173204230000	423	Kramer	41.34258438	-83.68171785		685.7	2880	Dry & abandoned -oil shows	1984-05-13	1984-05-03	1984-07-20		Anschutz Corp	Precambrian	Vertical	New field wildcat-dry (including temporarily abandoned well)	Dry and abandoned
34101201750000	175	Wenig George D Et Ux	40.63832701	-83.34180852	909	899	2935	Dry & abandoned	1985-01-14	1985-01-04	1986-08-15		Delray Oil Inc	Mount Simon /Sd/	Vertical	New field wildcat-dry (including temporarily abandoned well)	Dry and abandoned
34143201460000	146	E Ray Aleshire	41.37253451	-83.34218521	705	695.5	2762	Dry & abandoned -oil shows	1965-09-30	1965-09-20	1965-10-04		Maguire Russell	Precambrian	Vertical	Deeper pool wildcat-dry	Dry and abandoned
34117216810000	1681	Shaver-Neff Unit	40.39419404	-82.87002725	1007	994.1	4215	Oil producer	1964-06-10	1964-05-31	1964-07-16		Kin-Ark Oil Co	Granite	Vertical	Development well-oil	Oil
34101201760000	176	Gracely Farms	40.58814986	-83.25511634	926	915.4	3078	Dry & abandoned	1984-11-10	1984-10-31	1984-11-18		Texas Gas Exploration Corp	Granite	Vertical	New field wildcat-dry (including temporarily abandoned well)	Dry and abandoned
34117242540000	24254	Bush	40.57315863	-82.90380069	1030	1013.8	2952	Oil producer	2012-12-14	2012-12-04	2013-02-04		Salamanca Energy LLC	Trempealeau	Vertical	Development well-oil	Oil
34043200190000	20019	Herman A Et Al Unit	41.31105634	-82.3517368	830	820.2	4466	Saltwater disposal	1966-09-09	1966-08-30	1967-05-01		Sun Oil Co	Precambrian	Vertical	Injection-water	Disposal
34077201030000	103	Wolf Unit	41.2736652	-82.34363668	856	846.5	4574	Dry & abandoned	1981-09-26	1981-09-16	1982-10-22		Appalachian Exploration LLC	Precambrian	Vertical	New field wildcat-dry (including temporarily abandoned well)	Dry and abandoned
34083239770000	3977	Miller	40.44060707	-82.61240668	1128	1115.5	4506	Abandoned gas producer	1992-05-27	1992-05-17	1992-06-06	1993-04-29	Dalton & Hanna Co	Rome	Vertical	New field wildcat-discovery	Abandoned gas
34143202370000	0237	Ohio Liquid Disposal Inc	41.37158245	-82.99088522	618	610.2	2943	Water injection	1980-11-01	1980-06-11	1980-11-16		Ohio Liquid Disposal	Precambrian	Vertical	Injection	Water injector
34083239310000	3931	Carter James D	40.29043388	-82.48533101	1032	1020.3	5111	Dry & abandoned -gas shows	1991-04-17	1991-04-07	1991-04-26		B & J Drilling Co	Mount Simon /Sd/	Vertical	Deeper pool wildcat-dry	Dry and abandoned
34159200130000	13	Ralph & Alta Lane	40.46547624	-83.40323904	1003	994.1	2989	Dry & abandoned	1964-07-11	1964-07-01	1964-07-28		T & W Oil Co	Precambrian	Vertical	New field wildcat-dry (including temporarily abandoned well)	Dry and abandoned
34091200910000	91	Robson Kerman Et Ux	40.38192747	-83.58643569		1095.8	3013	Dry & abandoned -gas shows	1980-01-05	1979-12-26	1980-03-10		Allerton Resources	Mount Simon /Sd/	Vertical	New field wildcat-dry (including temporarily abandoned well)	Dry and abandoned
34159200700000	70	Kindig G M	40.30088284	-83.27570853	962	951.4	3353	Dry & abandoned	1984-08-17	1984-08-07	1984-08-26		Funk Exploration Inc	Mount Simon /Sd/	Vertical	New field wildcat-dry (including temporarily abandoned well)	Dry and abandoned
34033200040000	0004	White G	40.70408084	-83.10627145		951.4	2532	Dry & abandoned	1961-10-12	1961-10-02	1961-11-07	1961-11-13	Reliance Oil Corp	Trempealeau	Vertical	New field wildcat-dry (including temporarily abandoned well)	Dry and abandoned
34107201410000		M & M Yewey	40.63166304	-84.51611867		830.1	3200	Suspended well					Harner Union Oil	Unknown	Vertical	Suspended well	Suspended undesignated
34175600010000	0001	Martin G W & M	40.70378885	-83.13432336		951.4	2471	Dry & abandoned	1919-02-21	1919-02-11	1919-04-10		Logan Natural Gas&Fuel	Trenton /Lm/	Vertical	Development well-dry (including temporarily abandoned well)	Dry and abandoned
34041202420000	242	H & H Smith	40.35203048	-82.98715236	992	974.4	4035	Dry & abandoned	1965-02-24	1965-02-14	1965-03-07		McClure Oil Co	Precambrian	Vertical	New field wildcat-dry (including temporarily abandoned well)	Dry and abandoned
34063202320000	232	Holman W & S	41.09984216	-83.4772431		810.4	2525	Dry & abandoned	1981-09-03	1981-08-24	1982-11-19		Belden & Blake & Co	Mount Simon	Vertical	New field wildcat-dry (including temporarily abandoned well)	Dry and abandoned

UWI	Permit License Number	Well Name	Latitude	Longitude	Kelly Bushing Elevation (feet above sea level)	Ground Surface Elevation (feet above sea level)	Max TD	Current Status	Spud Date	Permit License Date	Completion Date	Abandonment Date	Current Operator	Formation at TD	Hole Direction	Current Class	Plot Symbol Description
34083239550000	3955	Parkinson	40.24999986	-82.47369653	1060	1049.9	4933	Oil producer	1991-09-26	1991-09-16	1991-12-17		Maram Energy	Rome	Vertical	Development well-oil	Oil
34005239380000	3938	Fingulin	41.01300001	-82.39230319	1083	1072.8	5163	1 oil & 1 gas well	1991-12-18	1991-12-08	1993-09-01	2007-11-15	Bass Energy Inc	Granite	Vertical	Deeper pool wildcat-discovery	Oil and gas
34063201520000		Jesse Drummelsmith	40.98554179	-83.63926177	809	800.5	2807	Dry & abandoned -oil & gas shows	1966-07-03	1966-06-23	1966-07-13		Kin-Ark Oil Co	Granite	Vertical	Deeper pool wildcat-dry	Dry and abandoned
34089258170000	5817	Dager J	40.23194816	-82.45901941	958	948.2	4972	Gas producer	2006-05-24	2006-05-18	2006-06-20		Knox Energy Inc	Precambrian	Vertical	Development well-gas	Gas
34117237330000	3733	Fry-Morris Unit	40.56440958	-82.68984083	1318	1299.2	4700	Oil producer	1986-12-28	1986-12-18	1987-03-08		Maram Energy	Rome	Vertical	Development well-oil	Oil
34173202360000	236	Smith V Ruth	41.42860146	-83.66121412	677	672.6	2786	Dry & abandoned -oil shows	1964-12-23	1964-12-13	1965-02-10	1965-02-10	Kin-Ark Oil Co	Granite	Vertical	New field wildcat-dry (including temporarily abandoned well)	Dry and abandoned
34175201740000	174	M E Bowen	40.78758724	-83.33439431		836.6	2902	Dry & abandoned	1964-02-21	1964-02-11	1964-04-30		Texaco Inc	Precambrian	Vertical	Development well-dry (including temporarily abandoned well)	Dry and abandoned
34173202310000	231	Peek Lillian L	41.25483862	-83.66348982	698	689	2770	Dry & abandoned	1964-09-03	1964-08-27	1964-09-14	1964-09-14	Oneill Joseph I Jr	Precambrian	Vertical	Development well-dry (including temporarily abandoned well)	Dry and abandoned
34117200470000	47	A C Windbigler	40.69051025	-82.68135411	1398	1387.8	4891	Abandoned gas producer	1962-10-01	1962-09-21	1962-11-02	1970-12-04	Pan American	Granite	Vertical	Development well-gas	Abandoned gas
34101600180000	0018	Brown L C Brush Ridge	40.68625198	-83.16324865		951.4	2490	Dry & abandoned					Unknown	St Peter /Sd/	Vertical	Development well-dry (including temporarily abandoned well)	Dry and abandoned
34143200770000	77	V Haff	41.35427822	-82.91268114		643	3123	Dry & abandoned -gas shows	1960-01-01	1959-12-22	1960-11-17		East Ohio Gas Co The	Precambrian	Vertical	New field wildcat-dry (including temporarily abandoned well)	Dry and abandoned
34147202130000	213	Sendelbach Nancy M	41.15957747	-83.25538442	769	754.6	2610	Temporarily abandoned - oil	1979-08-30	1979-08-20	1979-10-10		A & S Energy LLC	Basement	Vertical	Development well-oil	Suspended undesignated
34011200710000		Hoelscher 1 Comm	40.50383221	-84.3944028		882.5	3067	Suspended well					West Ohio Gas Co	Unknown	Vertical	Suspended well	Suspended undesignated
34175202590000	259	Kuenzli C W & L M	40.82701647	-83.19026548	890	876	3149	Dry & abandoned	1982-11-05	1982-10-26	1982-11-21		Berea Oil & Gas Corp	Granite	Vertical	New field wildcat-dry (including temporarily abandoned well)	Dry and abandoned
34143202380000	238	Oil Liquid Disposal Inc	41.37332359	-82.98535588		603.7	2955	Saltwater disposal oil & gas operator	1980-11-18	1980-05-02	1980-11-26		Ohio Liquid Disposal	Basement	Vertical	Injection	Disposal
34069201390000	20139	Shidler James Swiw #2	41.32848285	-83.95923113	692	682.4	3375	Saltwater disposal	2005-02-17	2004-10-25	2005-04-03		Aurora Energy Ltd	Granite	Vertical	Injection	Disposal
34003636910000	3691	BP Chemical	40.71211442	-84.13041401	871	862.9	3409	Water injection					BP Amoco	Middle Run	Vertical	Injection	Water injector
34089254160000	5416	Dispennette Ralph & Opal	40.24431723	-82.47301732	1119	1102.4	4833	Oil producer	1990-11-29	1990-11-19	1991-09-08		Knox Energy Inc	Rome	Vertical	Development well-oil	Oil
34147202160000	216	Watson John W	41.15216046	-83.18375943	760	741.5	2796	Oil producer	1979-09-15	1979-09-05	1979-10-17		A & S Energy LLC	Precambrian	Vertical	Development well-oil	Oil
34043200070000	7	M P Sayler	41.3024566	-82.39852752		813.6	4424	Dry & abandoned -gas shows	1960-01-01	1959-12-22	1960-10-15		East Ohio Gas Co The	Granite Wash	Vertical	New field wildcat-dry (including temporarily abandoned well)	Dry and abandoned
34077202330000	233	Walcher/Gray	41.11851526	-82.56224856	970	954.7	4445	Dry & abandoned	1993-03-09	1993-02-27	1993-03-19		Ngo Development Corp	Basement	Vertical	New field wildcat-dry (including temporarily abandoned well)	Dry and abandoned
34063201400000	0140	Harris Bessie	40.93679708	-83.5126302	833	823.5	2798	Dry & abandoned	1964-05-25	1964-05-01	1964-06-06	2007-01-24	Cowen Michael T	Precambrian	Vertical	New field wildcat-dry (including temporarily abandoned well)	Dry and abandoned
34101200850000	0085	Parish L B & M D	40.61488288	-83.41895828		971.1	2985	Dry & abandoned	1964-10-08	1964-09-28	1964-12-04	1964-12-12	Unknown	Precambrian	Vertical	New field wildcat-dry (including temporarily abandoned well)	Dry and abandoned

17. Appendix 1C – Seismic Events

Earthquakes recorded by USGS within 100 miles of the Maple Project (USGS, 2024). (mw=moment magnitude scale, mwr=regional moment magnitude, mb=body wave magnitude, md=duration magnitude, lg=surface wave magnitude, mfa=mantle faulting assessment magnitude, mb_lg=combines both body wave magnitude and surface wave magnitude.)

Date	Latitude	Longitude	Depth	Magnitude	Magnitude Type	Place
7/14/2020	40.44030	-84.08650	9.64	1.80	ml	3 km W of Jackson Center, Ohio
3/13/2005	40.67000	-84.62000	5.00	2.20	mb_lg	2 km SE of Rockford, Ohio
4/22/2024	41.54950	-83.47510	9.47	2.30	mb_lg	4 km SSE of Walbridge, Ohio
7/14/2020	40.41650	-84.08760	9.78	2.30	mb_lg	Ohio
12/22/2022	41.10900	-83.45300	9.91	2.40	mb_lg	5 km E of Arcadia, Ohio
7/11/2022	41.81580	-83.51230	5.00	2.40	ml	5 km W of Luna Pier, Michigan
1/22/2021	40.72250	-84.14270	5.61	2.40	mb_lg	3 km SW of Lima, Ohio
4/3/2019	41.75320	-84.88450	5.00	2.40	ml	4 km WNW of Clear Lake, Indiana
4/26/2011	40.86000	-83.54000	5.00	2.40	mblg	4 km SSE of Mount Blanchard, Ohio
2/25/2010	41.22000	-83.29000	5.00	2.40	mblg	2 km S of Kansas, Ohio
1/2/2023	40.24450	-84.51333	8.62	2.43	md	3 km NW of Versailles, Ohio
3/18/2024	41.54910	-83.46890	5.61	2.50	mb_lg	4 km WSW of Millbury, Ohio
2/7/2016	41.65030	-82.89690	5.00	2.50	ml	6 km W of Put-in-Bay, Ohio
9/7/2012	41.86400	-83.07600	5.10	2.50	mblg	17 km ESE of Stony Point, Michigan
3/8/2010	42.16300	-83.07000	18.00	2.50	mblg	7 km ENE of Grosse Ile, Michigan
8/15/2006	40.71000	-84.11000	5.00	2.50	mblg	3 km NE of Fort Shawnee, Ohio
1/30/2004	40.67000	-84.65000	5.00	2.50	mblg	2 km S of Rockford, Ohio
6/4/1990	41.09800	-83.63800	5.00	2.50	mblg	4 km SSE of Van Buren, Ohio
1/14/1984	41.64500	-83.42700	5.00	2.50	md	4 km E of Oregon, Ohio
5/20/2023	41.55290	-83.48340	6.10	2.60	mb_lg	3 km SSE of Walbridge, Ohio
6/12/2015	40.95500	-84.76200	5.00	2.60	mb_lg	6 km NW of Convoy, Ohio
5/14/2010	41.39000	-83.30000	5.00	2.70	mblg	1 km ENE of Gibsonburg, Ohio
11/25/1998	41.07100	-82.40500	5.00	2.70	mblg	1 km SSW of New London, Ohio
9/30/2008	40.41000	-84.31000	5.00	2.80	mblg	5 km SW of Kettlersville, Ohio
4/12/2007	41.72200	-82.92400	5.00	2.80	mblg	11 km NW of Put-in-Bay, Ohio

Date	Latitude	Longitude	Depth	Magnitude	Magnitude Type	Place
5/12/2006	40.74000	-84.08000	5.00	2.80	mblg	2 km E of Lima, Ohio
12/29/2024	41.28030	-84.75650	9.48	2.90	mb_lg	1 km SSE of Hicksville, Ohio
12/9/2023	40.43220	-84.10840	6.79	2.90	mwr	5 km W of Jackson Center, Ohio
4/4/1994	40.40000	-84.40000	5.00	2.90	mblg	2 km WNW of Minster, Ohio
1/26/2012	41.57600	-85.49000	4.70	3.00	mblg	5 km NE of Topeka, Indiana
6/5/2011	41.03000	-82.08000	5.00	3.00	mblg	5 km W of Lodi, Ohio
4/17/1990	40.46000	-84.85200	5.00	3.00	mblg	8 km NW of Fort Recovery, Ohio
9/29/1974	41.23800	-83.36100	1.00	3.00	lg	6 km ESE of Risingsun, Ohio
8/17/1877	42.40000	-83.20000	0.00	3.00	mfa	Detroit area, Michigan
2/09/1882	40.40000	-84.20000	0.00	3.10	mfa	Near Anna, Ohio
8/21/2020	41.91250	-83.31790	9.20	3.20	mwr	2 km SSE of Detroit Beach, Michigan
8/20/1980	41.94100	-83.01000	5.00	3.20		19 km SSE of Amherstburg, Canada
6/17/1977	40.70700	-84.58200	5.00	3.20		5 km ENE of Rockford, Ohio
6/30/2015	42.14640	-85.04590	5.00	3.30	mb_lg	5 km NNE of Burlington, Michigan
4/20/2018	42.11810	-83.01500	2.70	3.40	mwr	Michigan
2/2/1976	41.96000	-82.67000	10.00	3.40	lg	11 km SSW of Leamington, Canada
9/30/1930	40.30000	-84.30000	0.00	4.20	fa	5 km E of Newport, Ohio
7/12/1986	40.53700	-84.37100	10.00	4.50	mb	1 km ESE of Saint Marys, Ohio
9/20/1931	40.42900	-84.27000	5.00	4.70	fa	1 km SSW of Kettlersville, Ohio
6/18/1875	40.20000	-84.00000	0.00	4.70	mfa	Western Ohio
9/19/1884	40.70000	-84.10000	0.00	4.80	mfa	Near Lima, Ohio
3/2/1937	40.48800	-84.27300	2.00	5.00	fa	3 km E of New Knoxville, Ohio
3/9/1937	40.47000	-84.28000	3.00	5.40	fa	3 km NNW of Kettlersville, Ohio

Earthquakes recorded by OhioSeis within 100 miles of the Maple Project [1]

Latitude	Longitude	Magnitude	Year	Month	Day	County
40.10000	-83.80000	3.50	1843	6	19	Champaign
40.20000	-83.00000	3.80	1873	1	4	Delaware
40.20000	-84.00000	4.70	1875	6	18	Champaign
40.40000	-84.20000	3.40	1876	6	0	Shelby
40.40000	-84.20000	3.10	1882	2	9	Shelby
41.35000	-82.10000	3.00	1883	1	5	Lorain
40.40000	-84.20000	2.90	1884	12	23	Shelby
40.40000	-84.20000	2.90	1889	9	0	Shelby
40.55000	-84.57000	3.80	1892	4	15	Mercer
40.30000	-84.20000	3.10	1896	3	15	Shelby
41.17000	-82.12000	3.30	1899	9	14	Lorain
39.80000	-83.90000	3.40	1925	3	27	Greene
40.40000	-84.20000	2.90	1925	10	0	Shelby
41.70000	-83.60000	3.40	1926	10	28	Lucas
41.70000	-83.60000	3.10	1926	10	28	Lucas
40.70000	-82.50000	3.10	1927	2	17	Richland
40.70000	-82.50000	2.50	1927	2	17	Richland
40.40000	-84.10000	3.00	1928	10	27	Shelby
40.40000	-84.20000	3.70	1929	3	8	Shelby
40.50000	-84.00000	3.20	1930	6	26	Auglaize
40.50000	-84.00000	3.10	1930	6	27	Auglaize
40.60000	-83.20000	3.10	1930	7	11	Marion
40.30000	-84.20000	2.90	1930	9	29	Shelby
40.30000	-84.30000	4.20	1930	9	30	Shelby
40.40000	-84.20000	3.00	1931	3	21	Shelby
40.40000	-84.00000	2.90	1931	4	1	Logan
40.43000	-84.27000	4.70	1931	9	20	Shelby
40.40000	-84.20000	2.90	1931	10	9	Shelby
40.40000	-84.20000	3.30	1933	2	23	Shelby
41.20000	-83.20000	3.10	1936	1	31	Seneca
41.20000	-83.20000	2.50	1936	1	31	Seneca
40.49000	-84.27000	4.90	1937	3	2	Auglaize
40.70000	-84.00000	3.20	1937	3	3	Allen
40.70000	-84.00000	2.90	1937	3	3	Allen
40.47000	-84.28000	5.40	1937	3	9	Shelby
40.70000	-84.00000	3.10	1937	4	23	Allen
40.70000	-84.00000	3.10	1937	4	27	Allen
40.70000	-84.00000	3.10	1937	5	2	Allen
40.40000	-84.00000	2.50	1939	3	18	Shelby

Latitude	Longitude	Magnitude	Year	Month	Day	County
40.40000	-84.00000	3.30	1939	3	18	Shelby
40.30000	-84.00000	3.10	1939	6	18	Logan
40.30000	-84.00000	2.50	1939	7	9	Logan
40.90000	-82.30000	3.10	1940	6	16	Ashland
40.90000	-82.30000	2.90	1940	7	28	Ashland
40.90000	-82.30000	2.90	1940	8	15	Ashland
40.90000	-82.30000	2.90	1940	8	20	Ashland
40.40000	-84.40000	4.10	1944	11	13	Auglaize
41.70000	-83.60000	2.90	1948	1	18	Lucas
39.80000	-84.20000	3.10	1950	4	20	Montgomery
41.70000	-83.60000	3.50	1953	6	12	Lucas
40.50000	-84.00000	3.70	1956	1	27	Logan
40.40000	-84.20000	3.70	1956	1	27	Shelby
41.20000	-83.30000	3.70	1961	2	22	Seneca
41.30000	-83.20000	3.30	1975	2	3	Sandusky
41.40000	-83.50000	2.50	1992	10	4	Wood
40.70000	-84.10000	4.80	1884	9	19	Allen
40.42000	-84.11000	0.90	1980	7	10	Shelby
40.43000	-84.09000	0.50	1980	9	26	Shelby
40.43000	-84.11000	1.20	1980	12	10	Shelby
40.42000	-84.10000	1.80	1981	1	4	Shelby
40.44000	-84.11000	1.80	1981	2	7	Shelby
41.05000	-84.32000	1.20	1981	3	15	Putnam
40.88000	-84.34000	0.80	1981	5	15	Putnam
40.42000	-84.10000	1.20	1981	5	19	Shelby
40.43000	-84.10000	1.20	1983	7	12	Shelby
41.59000	-84.39000	1.20	1983	9	30	Williams
40.43000	-84.10000	0.30	1983	11	4	Shelby
40.43000	-84.10000	0.70	1983	11	4	Shelby
41.70000	-83.50000	2.00	1983	12	7	Lucas
40.52000	-84.39000	1.40	1985	3	10	Auglaize
40.52000	-84.40000	1.70	1985	3	10	Auglaize
40.97000	-84.22000	1.50	1985	8	25	Putnam
40.43000	-84.18000	3.00	1968	7	26	Shelby
41.21000	-83.49000	3.00	1974	9	29	Wood
40.57000	-84.67000	3.30	1977	6	17	Mercer
39.80000	-83.75000	2.00	1980	10	4	Clark
40.43000	-84.10000	2.10	1983	7	5	Shelby
41.67000	-83.45000	2.60	1984	1	14	Lucas
40.55000	-84.39000	4.50	1986	7	12	Auglaize

Latitude	Longitude	Magnitude	Year	Month	Day	County
40.45000	-84.11000	2.20	1988	10	22	Shelby
41.08000	-83.51000	2.30	1990	6	4	Hancock
41.18000	-83.68000	2.00	1992	7	4	Wood
41.18000	-83.68000	2.00	1992	7	14	Wood
41.65000	-83.50000	2.00	1993	10	10	Lucas
41.40000	-83.50000	2.00	1993	11	9	Wood
40.40000	-84.00000	2.90	1994	4	4	Logan
40.80000	-82.68000	3.30	1995	1	12	Richland
41.02000	-82.54300	3.20	1998	11	25	Huron
41.01000	-82.55000	2.70	2001	7	26	Huron
40.67000	-84.62000	2.40	2004	1	30	Mercer
40.68000	-84.60000	2.20	2005	3	13	Mercer
40.74000	-84.08000	2.80	2006	5	12	Allen
40.71000	-84.11000	2.50	2006	8	15	Allen
41.71000	-82.93000	2.50	2007	4	12	Ottawa
41.75000	-82.90000	2.30	2007	4	24	Ottawa
41.73000	-82.22000	2.70	2007	10	18	Lorain
41.16000	-83.41000	2.90	2010	2	25	Seneca
40.41000	-84.31000	2.80	2008	9	30	Shelby
41.39000	-83.30000	2.60	2010	5	14	Sandusky
40.86000	-83.54000	2.40	2011	4	26	Hancock
41.03000	-82.08000	2.00	2011	6	5	Medina
41.86400	-83.07600	2.50	2012	9	7	Ottawa
40.94920	-84.74770	2.60	2015	6	12	Van wert
41.65030	-82.89690	2.50	2016	2	7	Ottawa
40.97720	-82.09490	2.20	2014	10	21	Wayne
40.72670	-84.14790	1.50	2015	1	10	Allen
40.71640	-84.15430	1.30	2019	10	20	Allen
40.64900	-83.84800	2.00	2020	6	30	Hardin
40.49100	-84.29100	0.30	2020	3	14	Auglaize
40.42100	-84.10900	2.50	2020	7	14	Shelby
40.43300	-84.10500	1.60	2020	7	14	Shelby
40.43750	-84.10170	1.44	2020	8	3	Shelby
40.43400	-84.11100	2.10	2021	1	15	Shelby
40.72900	-84.13500	2.50	2021	1	22	Allen
40.72300	-84.14500	2.00	2021	2	11	Allen
40.44100	-84.09700	1.90	2021	4	15	Shelby
40.43400	-84.09650	1.60	2021	7	16	Shelby
40.43450	-84.09580	1.70	2021	8	18	Shelby
40.70600	-83.01900	1.50	2022	9	24	Crawford

Latitude	Longitude	Magnitude	Year	Month	Day	County
41.11300	-83.43600	2.80	2022	12	22	Hancock
40.24000	-84.53600	2.20	2023	1	2	Darke
40.69700	84.09170	1.40	2023	3	15	Allen
41.56850	-83.48250	2.90	2023	5	20	Wood
41.06600	-84.34400	1.90	2023	10	1	Paulding
40.44130	-84.10470	3.10	2023	12	9	Shelby
41.56680	-83.48450	2.00	2024	3	18	Wood
41.55970	-83.47220	2.50	2024	4	22	Wood
41.02570	-3.79170	2.00	2024	5	4	Hancock
40.43200	-84.10100	1.40	2024	8	29	Shelby
41.36780	-83.89520	1.70	2024	9	27	Henry
41.53900	-83.48200	1.30	2024	12	18	Wood
41.31220	-84.78700	3.30	2024	12	29	Defiance
40.61000	-84.56700	2.10	2025	6	9	Mercer

[1] Depths are not available from OhioSeis data

18. Appendix 1D – Suitability of Selected Materials

The accompanying Zip File titled “Appendix 1D” includes information verifying the suitability of the selected materials. The files are too large to insert into this document.

This page intentionally left blank.